

**VIETNAM GENERAL CONFEDERATION OF LABOUR
TON DUC THANG UNIVERSITY
FACULTY OF ELECTRICAL & ELECTRONICS ENGINEERING**



NGUYEN THI PHUONG LOAN

**STUDY OF PHOSPHOR
CONFIGURATIONS FOR IMPROVING
COLOR QUALITY AND LUMINOUS
FLUX OF WHITE LIGHT LED**

**DOCTORAL DISSERTATION OF
ELECTRICAL ENGINEERING**

HO CHI MINH CITY, YEAR 2024

**VIETNAM GENERAL CONFEDERATION OF LABOUR
TON DUC THANG UNIVERSITY
FACULTY OF ELECTRICAL & ELECTRONICS
ENGINEERING**



NGUYEN THI PHUONG LOAN

**STUDY OF PHOSPHOR CONFIGURATIONS
FOR IMPROVING COLOR QUALITY AND
LUMINOUS FLUX OF WHITE LIGHT LED**

**DOCTORAL DISSERTATION OF
ELECTRICAL ENGINEERING**

Advised by

Dr. Nguyen Doan Quoc Anh

Dr. Nguyen Cong Trang

HO CHI MINH CITY, YEAR 2024

ACKNOWLEDGEMENT

I have learnt and acquired more useful information at Ton Duc Thang University from my research and studies, which will help me be better prepared to finish this dissertation. This presents another difficulty because I studied during an era of major outbreaks, such as COVID-19. Nonetheless, instructors and colleagues provided me with support, assistance, and direction to finish my research dissertation. First of all, I would want to express my gratitude to Drs. Nguyen Cong Trang and Nguyen Doan Quoc Anh for their assistance in helping me finish my dissertation. They gladly showed me the techniques for conducting thorough research and utilizing materials, in addition to providing me with appropriate guidance and suggestions throughout the process. Additionally, I would want to convey my profound gratitude to the professors at Ton Duc Thang University's Faculty of Electrical and Electronic Engineering, who have provided me with a wealth of useful and supplementary knowledge for my studies. I also want to express my gratitude to Ton Duc Thang University's Board of Directors and Training Department for setting up the right environment and greatly assisting me in my research and studies. We would also want to express our gratitude to Dr. Nguyen Quang Khoi of the University of Natural Sciences, who helped us to complete the white light LED experiment and provided constant support. Lastly, I would want to express my gratitude to my friends and family for their unwavering support and encouragement, which have given me the will and drive to finish the dissertation to the best of my ability. Thank you sincerely!

Ho Chi Minh city, 2024

Author

Nguyen Thi Phuong Loan

DECLARATION OF AUTHORSHIP

This dissertation was carried out at Ton Duc Thang University.

Advisor: Dr. Nguyen Doan Quoc Anh

Dr. Nguyen Cong Trang

This dissertation was defended at the Doctoral Dissertation Examination Committee held at Ton Duc Thang University on 22/12/2023 pursuant to Decision 4842/QĐ-TĐT on 13/12/2023

Members of the Doctoral Dissertation Examination Committee:

- | | |
|---|------------|
| 1. Assoc. Prof. Vo Ngoc Dieu, Ph.D | Chairman |
| 2. Assoc. Prof. Phan Thi Thanh Binh, Ph.D | Examiner 1 |
| 3. Assoc. Prof. Nguyen Van Hieu, Ph.D | Examiner 2 |
| 4. Ph.D. Dang Huu Phuc | Member |
| 5. Ph.D. Dinh Hoang Bach | Secretary |

Confirmation of the Chairman of the Doctoral Dissertation Examination Committee and the Dean of the faculty after receiving the modified dissertation (if any).

CHAIRMAN

.....

DEAN OF FACULTY

.....

DECLARATION OF AUTHORSHIP

I hereby declare that this thesis was carried out by myself under the guidance and supervision of Dr. Nguyen Doan Quoc Anh and Nguyen Cong Trang, and that the work contained in it and the results in it are true by the author and have not violated research ethics. The data and figures presented in this thesis are for analysis, comments, and evaluations from various resources in my own work and have been duly acknowledged in the reference part.

In addition, other comments, reviews, and data used by other authors and organizations have been acknowledged and explicitly cited.

I will take full responsibility for any fraud detected in my thesis or dissertation. Ton Duc Thang University is unrelated to any copyright infringement caused by my work (if any).

Ho Chi Minh City, day month year 2024

Author

(signature and full name)

Nguyen Thi Phuong Loan

STUDY OF PHOSPHOR CONFIGURATIONS FOR IMPROVING COLOR QUALITY AND LUMINOUS FLUX OF WHITE LIGHT LED.

ABSTRACT

Common lighting sources like incandescent and fluorescent lights have been increasingly replaced by solid state lighting technology, which offers excellent lighting efficiency and a green lighting environment. One of the best and most useful light sources in solid-state technology are light-emitting diodes, or LEDs. The range of applications for conventional LED devices is limited by their low color fidelity and good luminescence efficiency. In actuality, the color rendition must be beautiful and clean with high uniformity for the white light source to present the highest color quality. Because of this, the development of better LED structures has been the main goal in the manufacture of premium LED lighting. Two strategies are put forth in this dissertation in an effort to improve the quality of LED illumination. The first method uses three-layer remote phosphor configurations, with blue LED chips stimulating the green, red, and yellow phosphor films. By adding three distinct phosphor materials, the LED structure may produce white light with a wider spectrum, which will increase color rendering efficiency. Along with being compared to other distant phosphor structures, like single-film and dual-film remote configurations, the brightness of the three-layer remote structure is also studied. Additionally, a mathematical simulation utilizing the Lambert-Beer law supports the analysis of light transmission of multi-layer remote phosphor configurations. This simulation specifically looks at whether light energy is limited when light first passes through the phosphor layers and then is converted. The second approach uses scattering factors to control LED performance by adding scattering enhancement particles (SP) to traditional phosphor layers. Here, the scattering factors are tracked by changing the radius or concentration of particular particles. As auxiliary instruments,

Mie-scattering theory and simulation are used to examine how scattering affects the optical performance of LEDs and recommend suitable SP parameters. Additionally, the performances of the LED samples are tracked under various correlated color temperatures (CCT) ranging from 5600 K to 8500 K in both approaches. In this study, the Mie scattering theory is used to three software programs—Mie Calculator, Mie Spot, and Mie Scattering—to identify formulaic commonalities. This makes the problem more feasible to solve while running simulations to determine how much particle size affects scattering. It advances the quest for novel materials to increase scattering in order to raise the luminous flux and color quality of white light LEDs. SiO₂ is the suitable SP material, and the three-layer distant phosphor structure is more effective than the other configurations in boosting high flux and color rendition of the LED, according to the formula and experimental findings from these two approaches. The dissertation's conclusions can be a valuable and significant source of information when creating WLED packages with better white light quality. Lastly, an experiment utilizing a model in this study combines blue chips with other phosphor materials—yellow, red, and blue—to create white light with a configuration like the previously mentioned three-layer distant setup. In the first section of the study, simulate the best outcomes. The light source output from the white LED's three-layer construction is directly measured to verify the model. To compare the spectrum morphologies of various phosphor structures, the computed results—which included the lumen index, CRI index, CCT color temperature, and data output—were entered into an integrated meter and integrated with a computer. This experiment aims to show that it is possible to replicate changing the phosphor material and altering the LED's attributes while still getting accurate results. Green phosphor material will boost luminous flux; red phosphor material will increase CRI; and a three-layer phosphor remote structure will have a higher luminous flux than a single-layer phosphor remote structure in particular.

CONTENTS

LIST OF FIGURES	xii
LIST OF TABLES	xvii
ABBREVIATIONS	xviii
NOMENCLATURE	xx
CHAPTER 1. INTRODUCTION AND BACKGROUND	1
1.1 A rationale for this study	1
1.2 Objectives	3
1.3 Scope of the research.....	3
1.4 Research method	4
1.5 Proposed ideas.....	5
1.6 Contributions and study results of the dissertation	6
1.6.1 <i>Theory</i>	6
1.6.2 <i>Experiment</i>	7
1.7 The dissertation’s structure	8
CHAPTER 2. OVERVIEW	10
2.1 Basic Physics of LEDs	10
2.1.1 <i>Electrical and Optical Properties</i>	10
2.1.2 <i>Spectral energy distribution</i>	12
2.2 Literature review	14
2.3 Summary of the related domestic and international research of LED	16
2.4 Orientation.....	17

2.5	How to create white light	18
2.5.1	<i>Wavelength conversion method</i>	19
2.5.2	<i>Mixed three red, green, blue chip</i>	19
2.5.3	<i>Homoepitaxial Zn-Se method</i>	20
2.6	Common phosphor structures.....	21
2.6.1	<i>Conformal structure</i>	22
2.6.2	<i>In-cup structure</i>	22
2.6.3	<i>Remote structure</i>	23
2.7	Critical optical properties for evaluating the performance of a WLED...24	
2.7.1	<i>Color rendering index</i>	24
2.7.2	<i>Luminous performance</i>	25
2.7.3	<i>Correlated color temperature</i>	25
2.7.4	<i>CQS - Light Quality Scale</i>	26
2.7.5	<i>The color quality</i>	27
2.8	Summary	27
 CHAPTER 3. EXAMINATION OF MULTI-LAYER DISTANT PHOSPHOR STRUCTURES TO ENHANCE THE WHITE LED'S OPTICAL CHARACTERISTICS		
3.1	The three-layer remote phosphor structure	29
3.1.1	<i>Mathematical frameworks based on Lambert-Beer law for multi-layer remote phosphor structures</i>	29
3.1.2	<i>Summary of remote structure formula</i>	31
3.1.3	<i>Develop the mathematical formula for the triple-layer structure</i>	36

3.1.4	<i>The options in remote phosphor structure for better white LEDs color quality</i>	38
3.1.5	<i>Simulation detail</i>	39
3.1.6	<i>Results and discussion</i>	41
3.1.7	<i>Improving color quality and luminous flux of white LED utilizing triple- layer remote phosphor structure</i>	45
3.2	<i>Structure from distal convex with two layers of phosphor</i>	55
3.2.1	<i>Preparation of materials</i>	60
3.2.2	<i>Simulation</i>	61
3.2.3	<i>Calculations and discussion</i>	66
3.3	<i>Experiment for testing the simulation results</i>	71
3.3.1	<i>Introduction purpose and some notes on limitation of experimental conditions</i>	71
3.3.2	<i>Summary of some simulation results of different configuration</i>	71
3.3.3	<i>Introduction of used material in the experiment</i>	72
3.3.4	<i>Experiment results without using integrating sphere</i>	73
3.3.5	<i>Experiment results with using integrating sphere</i>	76
3.3.6	<i>Comments on obtained of experiment results and some results of the simulation for different configuration</i>	80
3.4	<i>Summary</i>	80
CHAPTER 4. RESEARCH ON SCATTERING ENHANCEMENT		
MATERIALS TO INCREASE THE OPTICAL		
CHARACTERISTICS OF LED LAMPS		
		81

4.1	MIE scattering theory for the approach using scattering enhancement particles	81
4.1.1	<i>Influences of different particle sizes on the light scattering properties</i>	81
4.1.2	<i>Scattering coefficients</i>	82
4.1.3	<i>Reduced scattering coefficient</i>	85
4.2	Scattering enhancement particles	92
4.2.1	<i>Scattering analysis</i>	93
4.2.2	<i>Computation and discussion</i>	96
4.2.3	<i>Simulation of results</i>	101
4.3	Using of green phosphor materials and scattering enhancement particles	110
4.3.1	<i>The role of green phosphor in the mixture</i>	110
4.3.2	<i>Simulation Results</i>	112
4.4	Using $Y_2O_3:Ho^{3+}$ and $ZnO:Bi^{3+}$ for enhancing color quality and luminous flux of WLEDs	119
4.4.1	<i>Preparation of phosphor materials</i>	120
4.4.2	<i>Scattering computation</i>	122
4.4.3	<i>Results and analysis</i>	127
4.5	Summary	135
CHAPTER 5. CONCLUSION AND FUTURE RESEARCH DIRECTIONS.....		
5.1	Conclusion	137

5.2 Future research directions.....	139
LIST OF PUBLICATIONS	140
REFERENCES	143
APPENDIX. SIMULATION PROGRESS	157

LIST OF FIGURES

Figure 1.1: Compare the lighting efficiency of LED lights with methods used from ancient times to the 21st century	2
Figure 2.1: Light-emitting P–N junction	11
Figure 2.2: Band diagram of a light-emitting P–N junction	11
Figure 2.3: LED spectral distribution	13
Figure 2.4: The most popular way to create white light today	18
Figure 2.5: Using Phosphor Conversion	19
Figure 2.6: How to create white light from mixing three colors RGB.....	20
Figure 2.7: Using white light chip.....	21
Figure 2.8: Conformal structure	22
Figure 2.9: In-cup structure.....	23
Figure 2.10: Remote structure.....	23
Figure 2.11: Color rendering index illustration.....	25
Figure 2.12: Illustration of color temperature	26
Figure 2.13: Illustration of the light quality ratio scale.....	26
Figure 3.1: Remote phosphor configuration.	31
Figure 3.2: (a) Schematic plot for a small section of phosphor layer (one-dimensional model) and (b) illustration of the boundary condition at $z=0$	31
Figure 3.3: Double-layer phosphor configuration.....	34
Figure 3.4: Three layer remote structure.....	36
Figure 3.5: Illustration of multi-layer phosphor structures of white LEDs: (a) Single-layer phosphor, DYRL (b) and DYGL (c), and (d) TL phosphor	38
Figure 3.6: YAG:Ce ³⁺ concentration corresponding to the remote structure.....	40
Figure 3.7: Emission spectra of the phosphor configurations.....	40
Figure 3.8: Color rendering indexes of the phosphor configurations	41

Figure 3.9: Color quality scale of phosphor configurations	43
Figure 3.10: Luminous efficiency of phosphor configurations.....	43
Figure 3.11: Correlated color temperature deviation (Δ CCT) of the remote phosphor configurations.....	44
Figure 3.12: Illustration of triple-layer remote phosphor configuration.....	47
Figure 3.13: CRI of phosphor structures.....	48
Figure 3.14: CQS of phosphor structures.....	49
Figure 3.15: Luminous flux of phosphor structures.....	50
Figure 3.16: YAG:Ce ³⁺ phosphor concentration in remote structure	50
Figure 3.17: D-CCT of remote phosphor structures	52
Figure 3.18: Emission spectra of phosphor configurations at CCTs difference	53
Figure 3.19: The remote structure model of 2 convex layers (a, b) and emission spectra of 2 types of yellow and red phosphors (c,d)	56
Figure 3.20: Modeling algorithm for an LED model.....	58
Figure 3.21: Experimental LIDC versus simulation for the Cree LED	59
Figure 3.22: Simulation model.....	61
Figure 3.23: Variation of phosphorus concentrations of RYC (a) and GYC (b) to keep average CCT.....	63
Figure 3.24: Emission spectra of RYC (a) and GYC (b)	65
Figure 3.25: Comparison of CRIs of red phosphor (a) and green phosphors (b).....	67
Figure 3.26: Comparison of CQSs of red phosphor (a) and green phosphors (b).....	68
Figure 3.27: Comparison of LF of red phosphors (a) and green phosphors	70
Figure 3.28: Some used material in the experiment.....	72
Figure 3.29: The experiment setup without using integrating sphere	73
Figure 3.30: Properties of configuration “Yellow” obtained from experiment	74
Figure 3.31: Properties of configuration “Yellow+Red” obtained from experiment.....	75
Figure 3.32: Comparison of spectra between YL and YRL structure	76

Figure 3.33: Experiment setup with using integrating sphere	77
Figure 3.34: Properties of configuration “Yellow+Red” obtained from experiment.....	77
Figure 3.35: Properties of configuration “Yellow+Green+Red” obtained from experiment.....	78
Figure 4.1: Effect of particle size on scattered rays (shows that scattered rays transmit more evenly in the phosphor layer in figure a than in figure b).....	82
Figure 4.2: (a)The particle with high scattering coefficient.(b)The particle with low scattering coefficient	83
Figure 4.3: (a).Simulation the scattering attenuation of large particle size.(b)Simulation the scattering attenuation of small particle size	85
Figure 4.4: Illustrate the attenuation of scattered energy between particles	86
Figure 4.5: Represent the scattering angle in a plane	88
Figure 4.6: The scattering angle of diferent paticles sizes	89
Figure 4.7: The relationship between scattering coefficientand scattering angle	90
Figure 4.8: Computation of scattering coefficient, anisotropic scattering and reduced scattering coefficient of the SEPs at 455 nm.....	94
Figure 4.9: Computation of scattering coefficient, anisotropic scattering and reduced scattering coefficient of the SEPs at 595nm.....	95
Figure 4.10: Angular scattering amplitudes of different SEPs.....	96
Figure 4.11: (a) Photograph of WLEDs sample, (b) parameter of WLEDs, (c) illustration of 2D WLEDs model, and (d) the simulated WLEDs model.	97
Figure 4.12: Comparison of CCT deviation of pc-LEDs using different SEPs.....	99
Figure 4.13: Comparison of LF using different SEPs: (a) CaCO ₃ , (b) CaF ₂ ,(c) SiO ₂ , and (d) TiO ₂	100
Figure 4.14: Simmulation 4 SEPs on Mie Scattering Calculator software.....	101
Figure 4.15: Simulation scattering coefficient of 4 SEPs on Mie Simulator software .	103

Figure 4.16: Simulation reduce scattering coefficient of 4 SEPs on Mie simulator software	104
Figure 4.17: Simulation scattering angle of 4 SEPs on Mie Simulator software	105
Figure 4.18: The affected of 4 SEPs to output parameters DCCT and luminous efficiency	106
Figure 4.19: Simulation of Lumen and D-CCT from 5000 K- 8000 K of SiO ₂ particle	109
Figure 4.20: Simulation results of %Ratio.....	112
Figure 4.21: Simulation results of CCTs.....	113
Figure 4.22: Simulation results of Luminous flux	115
Figure 4.23: Simulation results of spectrum	116
Figure 4.24: Simulation results of CRI	117
Figure 4.25: Simulation results of CQS	118
Figure 4.26: Illustration of multi-layer remote structures and associated parameters.	120
Figure 4.27: Concentration YAG: Ce ³⁺ phosphor at different correlated color temperatures	121
Figure 4.28: Scattering coefficient of ZnO:Bi ³⁺ phosphor at wavelengths 453 nm, 555 nm and 680 nm.....	124
Figure 4.29: Anisotropic scattering of ZnO:Bi ³⁺ phosphor at wavelengths 453 nm, 555 nm and 680 nm.....	125
Figure 4.30: Reduced scattering coefficient of ZnO:Bi ³⁺ phosphors at wavelengths of 453 nm, 555 nm and 680 nm.....	126
Figure 4.31: Angular scattering magnitude of ZnO:Bi ³⁺ phosphors at wavelengths of 453 nm, 555 nm and 680 nm.....	127
Figure 4.32: Emission spectrum image of phosphor remote structures.....	129
Figure 4.33: CRI and CQS indices of structures with different correlation temperatures	130

Figure 4.34: Luminous flux and color temperature deviation of different structures..132

LIST OF TABLES

Table 3.1: Composition of phosphor LaAsO ₄ : Eu ³⁺	60
Table 3.2: Composition of yellow phosphor YAG: Ce ³⁺	61
Table 3.3: Actual WLED parameters	62
Table 3.4: Comparison of CRI and LF between YL and YRL structure	71
Table 3.5: Comparison of CRI and LF between YRL and YGRL structures.....	72
Table 3.6: Comparison between configuration of “Yellow” and “Yellow+Red”	76
Table 3.7: Comparison between configuration of “Yellow+Red” and “Yellow+Green+Red”	79
Table 4.1: Analysis the influence of SiO ₂ particle size on the scattering coefficient	84
Table 4.2: Relationship between scattering coefficient and.....	87
Table 4.3: The parameters of scattering enhancement particles	92
Table 4.4: Optical parameters of each particles in the mixture.....	110
Table 4.5: Correlation between G-P particle size and color quality	111

ABBREVIATIONS

CCT	Correlated Color Temperature
CIE	International Commission on Illumination
COB	Chip on Board
CQS	Color Quality Scale
CRI	Color Rendering Index
CDRP	Concave Dual-Remote Phosphor Structure
DIP	Dual In-line Package
DL	Dual Layer Structure
DP	Double Phosphor
FC	Flip-Chip
FDTD	Finite-Difference Time-Domain
FWHM	Full-Width Half-Maximum
FDRD	Flat Dual-Remote Phosphor
Gas	Gallium and Arsenide
G-P	Green Phosphor
LCDs	Liquid Crystal Displays
LED	Light Emitting Diode
LIDC	Light intensity distribution curve
MCOB	Multiple Chips on Board
MCCOB	Multiple Chips and Cups on Board
NUV	Near Ultra Violet
PL	Photoluminescence Emission
PLE	Photoluminescence Excitation
RGB	Red-Green-Blue

SCOB	Stereoscopic Chips on Board
Sic	Silica and Carbon
SMD	Surface Mounted Diode
SEP	Scattering Enhance Particle
TL	Triple Layer Structure
W-LEDs	White Light-Emitting Diode
YAG: Ce	$Y_3Al_5O_{12}: Ce$
Y-P	Yellow Phosphor
YL	Yellow structure (Single Structure)
YGL	Yellow-Green Layer Structure (Dual-layer)
YRL	Yellow-Red Layer Structure (Dual-layer)
YGRL	Yellow-Green-Red Layer Structure (Triple-layer)

NOMENCLATURE

S_1, S_2	Angular scattering amplitude
$W_{silicone\ glue}$	Ingredients of silicone glue
$W_{YAG:Ce}$	Y yellow phosphorus composition
I_0	Incoming light ray energy
μ_{ext}	Attenuation coefficient
L	Phosphorus layer thickness
N_r	Intensity of particle distribution
I	Incoming ray energy
C_{ext}	Attenuated cross-section
a_n	Expansion coefficient with even symmetry
b_n	Expansion coefficient with odd symmetry
D	Phosphorus particle diameter
m	Refractive index
x	Size parameter
θ	angular displacement
λ	Wavelength
$\psi_n(x) \xi_n(x)$	Riccati-Bessel function
NCC	Norm cross-correlation

CHAPTER 1. INTRODUCTION AND BACKGROUND

1.1 A rationale for this study

Researchers found that, in 2012, lighting accounted for one of the highest percentages of power usage (17 percent) in the US alone (Liu & Xiaoping, 2011). Because of its low energy usage, the LED has been seen as a new generation of lighting technology in this circumstance. LEDs are four times more efficient than CFLs and fifteen times more efficient than filament bulbs. It doesn't contain hazardous mercury and uses less energy than fluorescent lamps. Furthermore, LEDs have a longer lifespan than incandescent bulbs—roughly thirty times longer. A lot of LED bulbs may last up to 25,000 hours, which is 17 years if they are used for 4 hours a day. Liu and associates, (2008). The initial cost of LEDs is usually higher than that of conventional bulb types. But the cost has been steadily declining, and it should soon be at a price point that is often used in developing nations. Their quality of life can be enhanced by the usage of LED lighting.

The development of high-quality white LEDs that may be used for many lighting applications is receiving a lot of attention due to the growing demand for sustainable lighting applications. Particularly, the luminous efficacy and uniformity of white light have grown in significance. The correlated color temperature deviation is used to analyze the white-light color uniformity dynamic. The light white color is more uniform the lower the color temperature fluctuation, and vice versa (Chen et al., 2013). The emitted luminous flux diminishes when the color temperature variation (Δ CCT) can only be decreased by approximately 200 K to 450 K. Thus, an essential goal for LED application is to improve color uniformity (Δ CCT is lowered by more than 450 K) while maintaining consistent luminous efficiency of the LED.

The development of a higher-standard WLED is a multi-objective problem that needs to be resolved. It is necessary for the device to have a high temperature, steady CQS, and strong CRI without significantly compromising the output lumen. Nevertheless, in real-world

scenarios, LED packages face constraints such as rising CRI, falling lumen efficiency (LE), or reaching high output lumens even while CRI or CQS are unstable. Furthermore, if an excessively high current is used, the output will decrease rapidly. Poor color quality and performance result from an LED chip's CRI only reaching a value of 80 Ra at high light current, with an LE value of roughly 150 Lm/W. The main objective of this dissertation is to provide novel strategies to get around the restrictions and improve the performance of the WLED packages in light of the previously described shortcomings in LED optical capabilities.

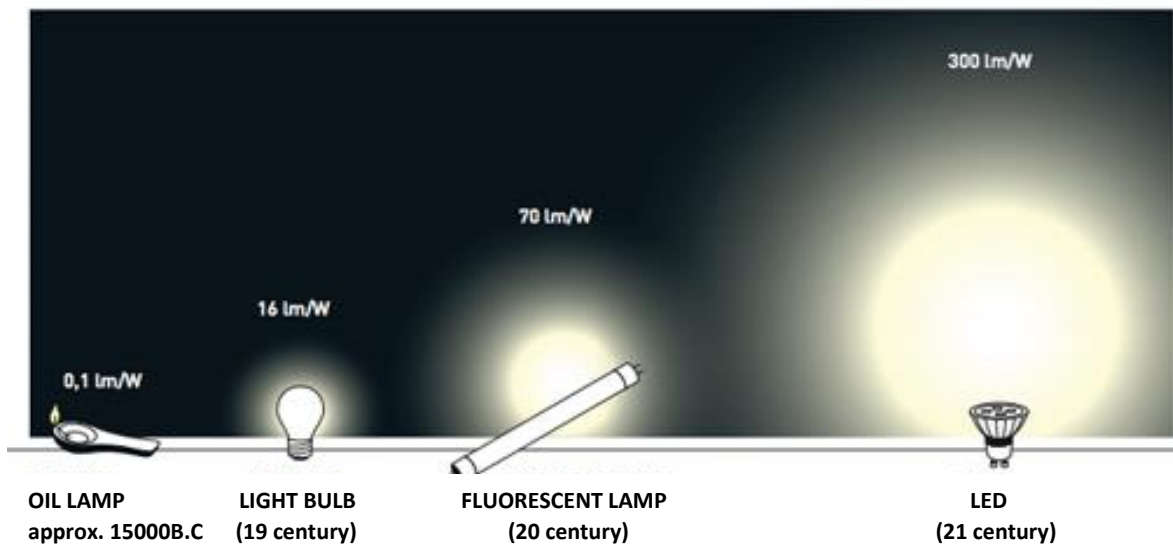


Figure 1.1: Compare the lighting efficiency of LED lights with methods used from ancient times to the 21st century

A development in lighting is depicted in Figure 1.1. Initially, oil lamps were utilized for lighting, a rather inefficient form of lighting. The 19th century saw the birth of LIGHT BULB. But the efficiency is limited to 160 Lm/W. With the invention of the fluorescent lamp in the tenth century, luminous efficiency reached 170 Lm/W. As LED lights were available in the 21st century, lighting technology reached a new milestone when luminescent efficiency reached 300 Lm/W. The invention of solid-state lighting technology led to its progressive improvement. This dissertation also shows enhancements in the white LED lighting performance with the recommended

approaches, which are found in international journal contributions (Loan et al., 2022). These enhancements include higher luminescent efficiency, an improved color rendering index, and increased color uniformity.

1.2 Objectives

In Vietnam, developments on high-standard WLED structures have not been thoroughly researched. There are various factors to assess a high-quality LED, notably including color quality index, luminescence efficiency (LE), color uniformity, color rendering index (CRI), and color quality scale (CQS). Hence, the major dissertation objective is to improve these factors for LED lighting in order to overcome the limitations in their applications. Particularly, the thesis demonstrates two different approaches: one is to combine the scattering particles with the phosphor compound to induce the scattering factor for greater blue-light utilization; and the other is to study a novel multi-layer remote phosphor structure for white LEDs to achieve enhancement color quality and light flux efficiency.

1.3 Scope of the research

The performance of LEDs is influenced by various factors, such as the driving current, the luminescent materials' synthesis, the temperature of the experiment environments, the concentration and/or particle size of the phosphors, etc. Besides, means of measurement, computation, and simulation lead to variances in the research results.

Therefore, the scope of the research in this thesis is limited to the following factors to serve certain objectives. The concentration and particle size of the phosphor and scattering particles, the number of phosphor layers in the remote structure, and the correlated color temperature are critical factors in the LED performance assessment. In terms of research approaches, Mie-scattering theory-based simulation and LightTools

software are employed, which will be further demonstrated in the research method section. Besides, the dissertation researches blue-pumped multi-chip LED instead of the other LED chip types such as laser, ultraviolet, or near-ultraviolet.

On the other hand, this thesis does not cover the Raman scattering, the in-depth study of the phosphor characteristics and morphologies, and the other factors affecting light emission in LED packages. Thus, future research will concentrate on such factors, combined with the proposed solutions in this thesis, to explore the novel structure and/or luminescent materials for the development of white LEDs.

1.4 Research method

The dissertation employs a multi-disciplinary approach, combining both qualitative and quantitative methods, to research the topic. Particularly, the dissertation used data collected from other online public works, including international journals, books, and conference papers, for the establishment of the simulation basis and the comparison with achieved findings of the dissertations. Then simulation, experiment, and testing based on principles of physics and mathematics were applied to further demonstrate the factors determining the performance of white LEDs. Here, the Lambert-Beer law, Mie-scattering theory, and LightTools software are the primary media of this dissertation methodology work.

The dissertation work on phosphor-converted white LED as this type of LED is more feasible to tailor the spectral emission bands. The remote phosphor structure consisting a gap between the phosphor films and LED chips is utilized for simulation and experiment. The simulation parameters of LED package between tests are mostly the same, the variables are the metrics of phosphor layers, such as phosphor concentrations, the number of phosphor layers, and the volume of dopants in the phosphor layers, as demonstrated further in Chapters 3 and 4. The optical properties of the simulated LED are measured. The measurement of LED output is performed with 9

LED chips, having a peak emission of around 465 nm. In this way, it is possible to make specific conclusion about the influence of the varied parameters, supporting the contributions of the dissertation in the field.

Simulations are conducted on the same LED design model corresponding to the identified LED type. The simulation model incorporates precise optical properties of the LED package, with most of the input parameters held constant. A critical aspect of these simulations involves comparing the power spectral distributions of the simulated and measured phosphor-converted LEDs. The simplicity of the investigation method is maintained by altering as few LED parameters as possible during simulations, thereby enhancing the reliability of the conclusions drawn from the validation process. Successful validation of the simulation tool provides a foundation for potential optimization of the white LED parameters, offering the prospect of significantly reducing the number of experiments required for further advancements in LED technology.

1.5 Proposed ideas

Realizing the drawbacks of white LEDs and limitations of studies in the literature review, the dissertation proposed two approaches to overcome such difficulties. The first idea is to build a multi-layer remote phosphor structure, comprising the yellow, green, and/or red phosphors, to enrich the converted color emission for the white LED. This approach aims to determining the suitable remote phosphor structures for specific goals of lighting applications. In addition, the efficiency of the proposed multi-layer phosphor structure, in comparison with the traditional single-layer remote structure, is proved by a mathematical formula based on Lambert-Beer law and experiment results.

An alternative method involves incorporating scattering enhancement elements to regulate the dispersion of the phosphor conversion layers. To perform the second method, we use the commercial software LightTools 9.0 in conjunction with Mie

scattering simulation software. This combination allows us to create a light scattering simulation that incorporates several types of scattering particles. In addition, the Mie Plot software is employed to identify similarities within the Mie scattering formula. The simulation is used to identify and choose the most appropriate scattering particle, which is then utilized as the scattering center for the phosphor layer. Furthermore, an examination is conducted of additional elements that impact the scattering efficiency of the phosphor layer, such as the size and concentration of the phosphor particles being used. The determination of optimal scattering particles and phosphor materials to enhance the luminosity and color rendering efficiency of LEDs can be achieved by considering their size and concentration.

Each method has proven the effectiveness in improving specific properties of LED lighting. The findings demonstrate that it is possible to obtain high color rendition performance while reducing an insignificant amount of lumen output. Though there are a lot of rooms for further investigations and modifications, this dissertation contributes to paving a solid path to overcome the limitations of conventional WLED configurations.

1.6 Contributions and study results of the dissertation

1.6.1 Theory

The theory underpinning the efficient application of white-light LEDs has been streamlined and made clearer thanks to the dissertation. A proposal for optimizing the new structure to meet the requirements of various fields' applications is based on a review of the advantages and disadvantages of conventional white-light LED structures. Furthermore, Lambert's formula confirmed the dissertation by showing that the novel distant structure of white light LEDs has improved luminous flux.

The dissertation suggested that manufacturing costs can be significantly reduced by producing white light for LEDs utilizing blue chips with YAG: Ce³⁺ yellow phosphor material rather than by combining different types of phosphorus. Moreover, this method

enables the enhancement of the optical characteristics of white light LEDs in a manner that is both feasible and achievable.

The dissertation uses a Mie scattering calculator and Mie spot software to uncover formula similarities, which furthers the systematization of Mie scattering theory in LightTools 9.0 commercial software simulation. It replicates parameters like particle size and concentration that affect light flux and color uniformity. The thesis has also altered the overall perception of the conventional LED structure, which needs to be modified in order to be improved with the new structure—the remote structure—in order to increase LED device light performance.

1.6.2 Experiment

Recent studies and data on LED products that are marketed have been cited in this dissertation. Furthermore, present LED structure in combination with phosphor materials to enhance luminescence and other materials to enhance white light LED color uniformity have been researched. The study's findings are a useful resource for LED producers.

By combining phosphor powders with silicon, heating the mixture to 150 degrees, and letting it dry for five minutes, this dissertation conducted basic experiments using red, yellow, and green phosphor materials based on the findings of the analysis of the acknowledged contributions. These substances are mixed with blue chips that have a maximum power of 10 mW to 300 mW and are sold by Cree.

Consequently, the only pattern identified by the research findings when testing with the three-layer distant structure is that adding red phosphor enhances CRI and CQS, while adding green phosphor enhances white light LED photosynthesis.

1.7 The dissertation's structure

With the major objectives of increasing the luminous efficiency and color quality of WLED, my dissertation includes the following core chapters:

- *Chapter 1: Introduction and background* – This chapter introduces the primary rationale and objectives of the dissertation. In addition, it presents the scope of work, proposed ideas, research method, a summary of the dissertation's results and contributions, and how this dissertation is structured.
- *Chapter 2: Overview* – The chapter goes over the basis of LED, the research and investigation of domestic and abroad situations, the methods of generating white light, types of WLED's phosphor structures, and the essential optical factors for assessing the WLED quality. The purpose of this chapter is to provide the general understanding and foundation of the dissertation.
- *Chapter 3: Examination of multi-layer distant phosphor structures to enhance the white LED's optical characteristics* - This chapter highlights the strategy for utilizing multi-layer remote phosphor structures to improve LED performances. First, it presents a mathematical framework for analyzing the performance of multi-layer distant phosphor structures based on the Lambert-Beer law. Subsequently, the three-layer remote phosphor structures and various multi-layer remote phosphor structures are proved by modeling, experimentation, debate, and comparison.
- *Chapter 4: Research on scattering enhancement materials to increase the optical characteristics of LED lamps* - This chapter details the study conducted on controlling the phosphor layer's scattering factor through the use of various scattering enhancement particles. We describe the Mie-scattering theory, which simulates the impact of luminescent particles on WLED performance. This

chapter also covers the choice of the best dispersing particles and how to combine the chosen particles with green phosphor.

- *Chapter 5: Conclusion and future research directions* – This chapter summarizes the notable achievements of the two proposed approaches and shows the future works based on the findings of this dissertation.

CHAPTER 2. OVERVIEW

2.1 Basic Physics of LEDs

With a forward polarization voltage, the light-emitting diode (LED) is a p-n junction where holes are sprayed into the n-side and electrons are sprayed on the p-side. In the empty space, these minority particles merge with the majority particles. Recombination with radiation is the process of recombination in direct semiconductor materials. Thermal energy is the primary form of released energy in indirect semiconductor materials, where luminescence efficiency is very low.

2.1.1 Electrical and Optical Properties

Overall, the photoelectric effect is being referred to. LEDs has the characteristics of being semiconductor P-N junction diodes. Figure 2.1 illustrates the combination of a P-type and an N-type semiconductor to form a P-N junction. Homotopic refers to the junction formed when both the N-type and P-type regions are composed of same semiconductor material. Conversely, the junction is denoted as a heterojunction when the N-type and P-type regions are composed of different semiconductor materials. Upon the establishment of a P-N junction, electrons from the N-type region diffuse into the P-type region.

When a hole and a free electron make touch, they undergo recombination and disappear. The N-type region is doped with positively charged ions, whereas the P-type region is doped with negatively charged ions for each electron-hole pair that recombines. The formation of an increasing electric field over the depletion zone impedes and finally halts the process of recombination as it progresses and more ions are generated (Liu & Xiaoping, 2011). During forward voltage, electrons are transferred from the N area to the P region, whereas holes are transferred from the P region to the N region. Light emission occurs as a result of the combination of electrons and holes. A P-N junction, unlike a resistor, has a significantly non-linear relationship between current and voltage.

As a result, it is frequently used as a rectifier. LEDs exhibit the typical properties of a P-N junction, such as forward conduction, reverse cut-off, and breakdown. Furthermore, LEDs demonstrate light-emitting characteristics under particular circumstances.

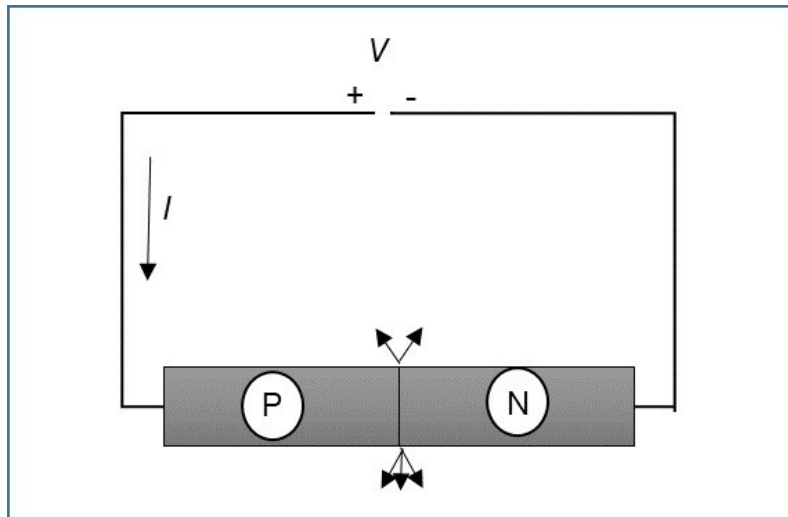


Figure 2.1: Light-emitting P–N junction

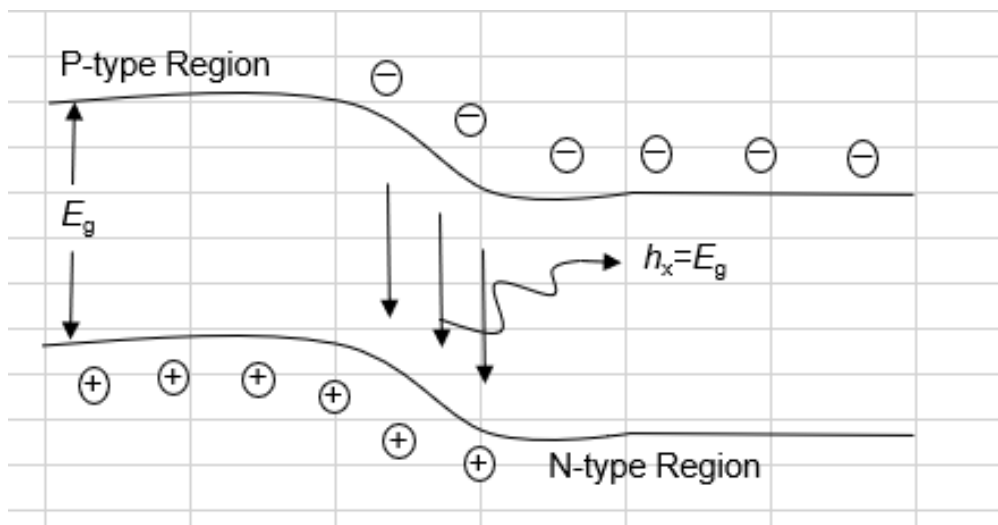


Figure 2.2: Band diagram of a light-emitting P–N junction

Figure 2.2 illustrates that the injected electron can either directly combine with the hole to emit light within the LED or first capture the hole through the radiative recombination center to emit light. A non-radiative recombination center, located near the intermediate level between the conduction band and valence band, captures electrons in addition to emitting recombination light. The light-emitting diode (LED) is a p-n junction that functions by applying a forward polarization voltage and introducing electrons to the p-side and holes to the n-side. Within the vacant region, these minority particles amalgamate with the majority particles. Recombination with radiation refers to the recombination process that occurs in direct semiconductor materials. Indirect semiconductor materials exhibit a relatively poor luminescence efficiency, mostly releasing thermal energy. Subsequently, these electrons combine with holes, resulting in the emission of energy that falls short of producing visible light. An increase in the ratio of electrons undergoing radiative recombination to those undergoing non-radiative recombination leads to a higher optical quantum efficiency. Recombination light emission occurs only in the diffusion zone between the P-type and N-type areas, within a few microns of the P-N junction. Light's peak wavelength (λ) is related to the band-gap energy (E_g) of semiconductor material in light emission zones. This can be written as $\lambda = 1240/E_g$ (nm), where E_g is measured in electron volts (eV). Both theory and practice confirm this relationship. To generate visible light, the semiconductor material's bandgap (E_g) must fall between 3.26 eV and 1.63 eV.

2.1.2 Spectral energy distribution

The distribution of radiation energy throughout a spectrum within a particular range of radiation wavelengths is referred to as the spectral energy distribution. This is so because, as opposed to releasing a single wavelength, a light-emitting diode emits a variety of wavelengths. In addition, the wavelength affects the LED's simultaneous changes in luminous intensity and optical power output. In Figure 2.3, a spectral

distribution curve is shown. Relevant chromaticity parameters are ascertained when the curve is constructed, including the dominant wavelength and color purity of the device. A number of parameters, including the kind, structure, and thickness of the epitaxial layer as well as doping impurities in the compound semiconductor employed in its manufacture, affect the spectral distribution of LEDs. But it has nothing to do with the shape and packing of the device (Liu & Xiaoping, 2011).

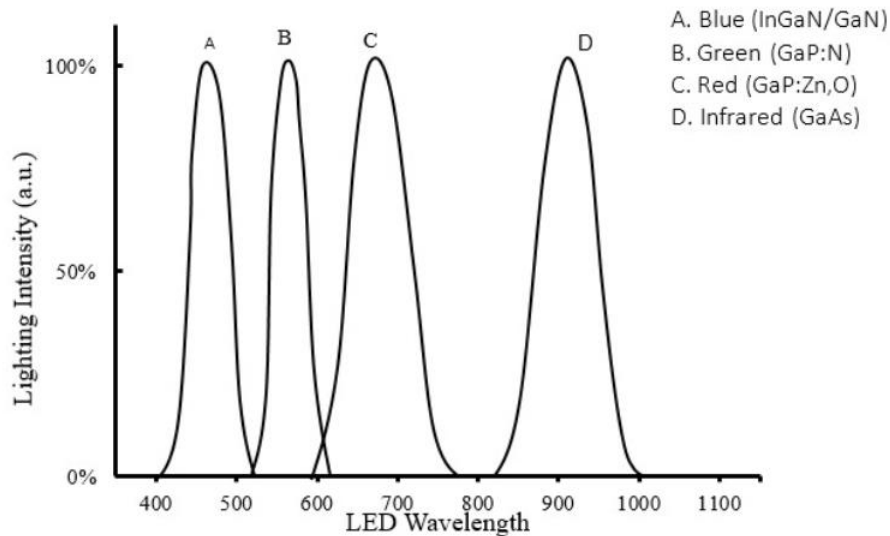


Figure 2.3: LED spectral distribution

This type of LED chip can be categorized into two groups based on the location of the electrodes. The first group consists of chips with electrodes on both sides, including indium-gallium nitrogen grown on silicon carbide substrates, gallium phosphide, gallium aluminum-arsenide, and gallium-arsenide-phosphide chips. The second group consists of chips with electrodes on the same side, such as epitaxial materials surrounding sapphire substrates. The substrate, which requires isolation, dictates the positioning of the positive and negative electrodes on the same side. Semiconductor components essentially make up LED lights. Different materials yield unique color changes when used in LED light sources. The LED chip has semiconductor components that generate

white light. Several materials determine the range of colors that white LED light can produce. Studies on white LED light can modify its visual features to meet people's fundamental requirements. This is the rationale behind it.

2.2 Literature review

White light-emitting diodes (WLEDs) with phosphorus conversion are a potential light source due to their compact size, great energy efficiency, affordability, and color stability (Le et al., 2019). According to Josh and Cauwerts (2018), WLED uses the color complementarity concept, combining blue light from blue chips with yellow light from phosphorus. Solid-state lighting may benefit from the usage of WLEDs, although their luminous effect needs to be improved (Wang et al., 2010). A blue-emitting InGaN-based LED chip with YAG:Ce³⁺ yellow phosphors acting as a color conversion layer is now used in the majority of commercial WLEDs. However, because of the phosphor layer's low conversion efficiency and the absence of red-energy components, this type of WLED exhibits low-uniformity chromaticity and rendering performance. Generally speaking, the most popular technique for producing white light is to apply phosphor coating to blue chips. This procedure involves mixing phosphorus powder with transparent encapsulating resin and dispersing it across the phosphorus package. This approach does not result in high-quality WLED, while making it simple to regulate the phosphor layer's thickness and saving a lot of money (David et al., 2015 and Cheng et al., 2012). Thus, the appropriate coating technique may be applied in its place. According to Yu et al. (2019), this technique produces angular homogeneity of correlated color temperature (CCT) by distributing colors equally. However, the backscattering effect lowers the luminous efficiency of WLED with an appropriate phosphor structure. By separating chips and phosphorus layers, earlier research has illustrated the idea of phosphorus structure remotely to reduce backscattering and improve the luminous effect (Zhong et al., 2012 & Lai et al., 2014). Additionally, polymer hemispherical shell lenses with inside phosphor coating are introduced, which can boost the extraction effectiveness

due to the reflecting structure inside enhanced light extraction (Smet & Hansel, 2015). Oh et al. (2012) developed an alternate solution that involves an embedded structure with an air gap. This approach has the potential to improve luminous efficiency by reflecting light downward. The findings demonstrate that the WLED structures have a direct impact on the lumens at the output.

In efforts to address drawbacks in WLEDs, in 2019, the perovskite downconverters were proposed by (Peifen et al., 2019) to achieve the tunable white LED. Though the enhancement in color rendering was notable, the fabrication process of this perovskite-downconverter based LED is costly as it involves the complexity of driver circuit and packaging procedure. Previously, to enhance the red energy in the white light emission, the alternative approach called Red-Green-Blue (RGB) was introduced (Muthu et al., 2002). This method utilized the combination of three LEDs with distinct emission color: red, green, and blue. By adjusting the drive current for each LED, the tunable-color-temperature white light could be produced.

However, the packaging process of this LED type is complex, difficult to control, and ultimately increasing the production cost. In the meantime, an alternative approach to enhance the conversion of phosphorescent layer was reported in a work of (Li et al., 2021). They developed composite ceramics of (Ce, Gd):YAG- Al_2O_3 to achieve the high brightness for the LED (Li et al., 2021). In their study, the scattering is factor is the key momentum. However, their study did not discuss the color quality with the proposed composites, and that the luminosity of the composite is dependent on the sintering temperature makes it complex to applied and may induce the cost of fabrication. As the price of LEDs has been reducing overtime, it is essential to figure out the new approach to enhance the LED performance while fulfilling the cost-saving requirement for production.

2.3 Summary of the related domestic and international research of LED

- Domestically

With outstanding features, LED lights have gradually become familiar and widely used in the field of projection and are gradually replacing traditional lighting methods. It is the continuous developments in performance, durability, energy savings, size as well as environmental friendliness that have allowed LEDs to be used in indoor lighting, decoration, backlighting applications to expand to other areas with harsher operating conditions such as outdoor lighting, street and tunnel lighting. Along with the current situation of Vietnam in the group of 20 developing countries consuming the most electricity, in which the electricity consumption for lighting needs accounts for 25 %, it promises to give the LED lighting sector many opportunities for development and expansion. To supply this sector, Vietnam currently has about 200 enterprises producing and trading LED lights, but the limitations of technology, price and quality hinder the development. Because of the potential, the increasing demand for LEDs and the existing difficulties, the research to produce LEDs with high quality and reasonable price is an inevitable result. The core of LED research aims at comparing the quality of LEDs of different manufacturing methods and finding the most optimal option, while helping domestic manufacturers master the design and technology of production and thereby create branded products, quality and prestige, avoiding the case of copying poor quality products.

Although there have been many studies aimed at improving the lighting quality of LEDs, the majority of studies stop at finding problems and do not go into solutions, or offer solutions to improve one aspect without considering other factors, or lack of comparisons between choices to highlight strengths and weaknesses. For these reasons, the applicability and reliability of these studies are limited, growing the need for studies that can offer thoroughly analyzed problems and solutions.

- Internationally

With the situation of energy scarcity, and the current environmental movement, the application of LEDs in lighting applications is more replicated than ever. Realizing that traditional LED models with a phosphor layer and a chip structure are no longer suitable for modern lighting needs due to the low color rendering index (CRI), there are currently many scientific studies focusing on changing the external structure and internal components of LEDs to achieve higher lighting efficiency. Many studies have reported on experimental results that can improve the quality of LEDs at a certain level, including the solution to combine light-emitting diodes with phosphors, equip more phosphor layers for LED models, how to spray phosphor coating on chips, etc.

2.4 Orientation

- As the introduction stated, there are numerous restrictions with regard to luminescence efficiency and color quality with the current simple structure LED. Thus, optimizing the two aforementioned components is the thesis' primary objective. A few items need to be clarified, which are as follows:
Examine the phosphor structure of LEDs that emit white light.
- Discuss the benefits and drawbacks of each kind of structure.
- Bring up a potential structural orientation.
- Replicate the decision made for that structural exam.
- More research on how other material particles can be scattered to boost the luminous flux of LED white light sources.
- Research on how particle size affects white light LED luminosity. The best size for a scattering particle should be chosen to maximize luminous flux.
- When adding scattering particles and structural components, simulate the experiment.

Following the aforementioned introduction, the topic would want to provide an overview of some of the following contents:

2.5 How to create white light

The current standard structure for LEDs is the conformal structure, as seen in Figure 2.8. The LED creates white light by combining the blue chip and the yellow phosphor layer. As a result, the LED chip is considered the fundamental component of the LED.

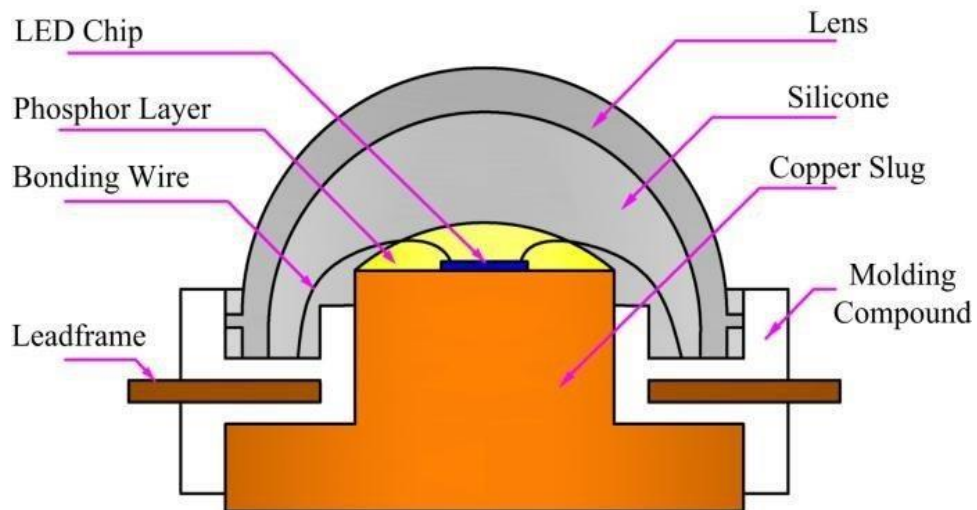


Figure 2.4: The most popular way to create white light today

Currently, the most widely used technique for creating white light involves the application of a thin coating of yellow phosphor onto the blue chip (Figure 2.4). The combination of the blue chip's light and the yellow phosphor material produces white light. White light can be generated through various means.

2.5.1 Wavelength conversion method

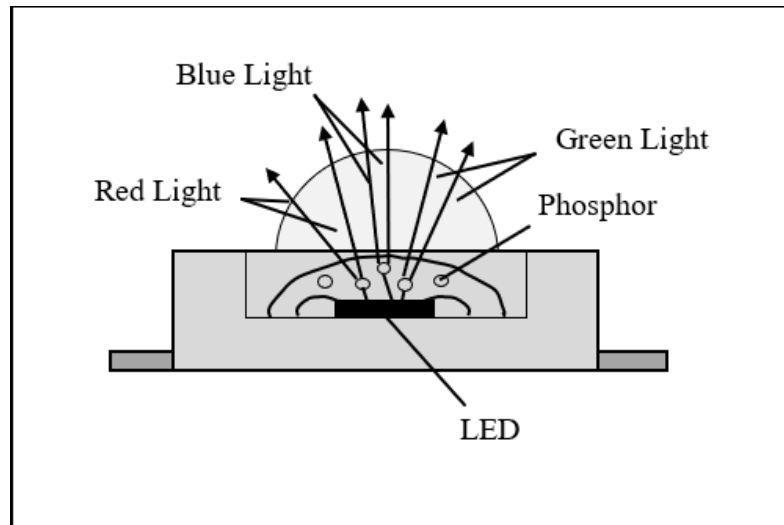


Figure 2.5: Using Phosphor Conversion

In the two techniques that will be discussed in the upcoming chapters of this dissertation, this methodology will be applied. As seen in Figure 2.5, white light is created when the blue chip's light interacts with the yellow phosphor above. But one drawback of this approach is that it can result in the yellow ring phenomena. Consequently, the two methods this dissertation presents will address that constraint and enhance the white light's quality.

2.5.2 Mixed three red, green, blue chip

The American Lighting Association states that blending single-color chips into three colors—green, red, and blue—will result in white light (Figure 2.6). The lifespan of the LED, however, degrades quickly due to the variation in each single-color chip's lifetime. Numerous investigations and advancements have been made using this methodology.

Furthermore, it is more complicated to modify the package of three single-color chips than it is to modify the phosphor components in order to convert wavelength. This dissertation will therefore not make use of this technique for creating white light

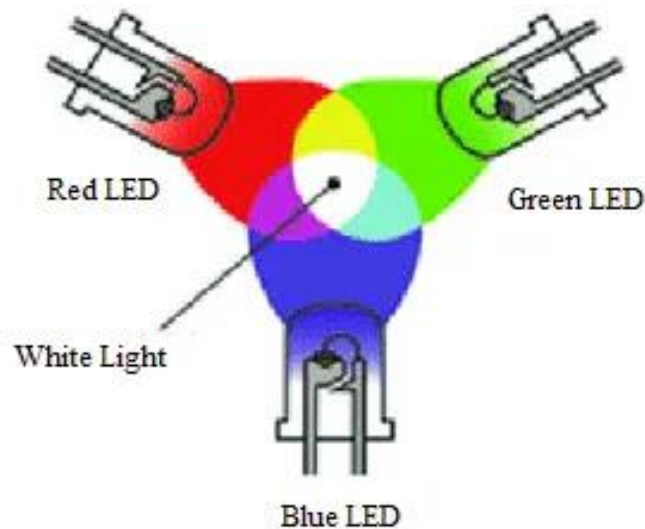


Figure 2.6: How to create white light from mixing three colors RGB

2.5.3 Homoepitaxial Zn-Se method

Based on Zn-Se, this technique was developed by a Japanese LED company. To provide blue light, they implanted blue LEDs using coaxial technology (Figure 2.7). Whereas only blue and yellow light is released, they are released in the active zone. Because phosphorus was not utilized, the combined light's white color and spectrum are similar to those of UV and phosphor-converted LEDs, but with a larger output of white light. In theory, the wavelength conversion approach to manufacture a single LED yields a lower luminous efficiency than the dithering approach. It is more important to combine several LEDs with the correct brightness, though.

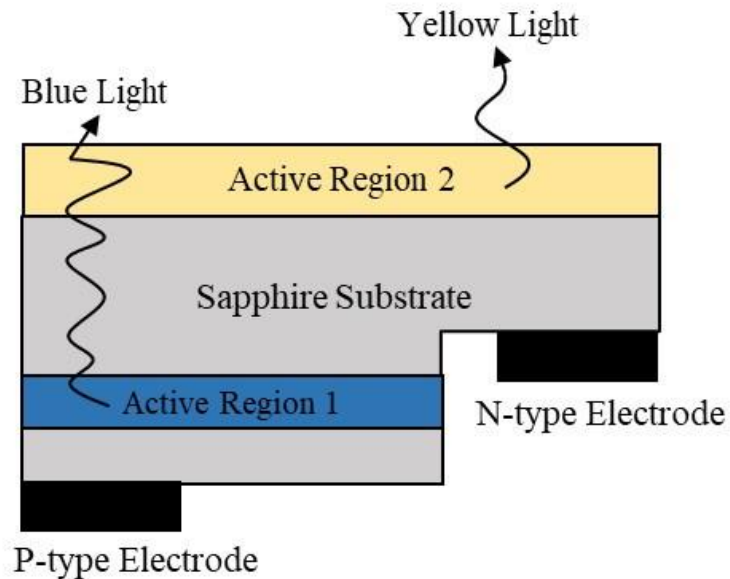


Figure 2.7: Using white light chip

Whereas color-blend lights have a more intricate LED architecture and a more significant lamp size, conventional and simple white LEDs all have a compact design that can be matched in any configuration.

Furthermore, the color-mixed white light of an LED bulb undergoes a metamorphosis after a certain amount of use due to the significantly varied attenuation time of these lights. As a result, neither the producer nor the supplier of LED lights uses this technology.

2.6 Common phosphor structures

Numerous novel investigations on phosphorus structures have been conducted thus far. Entering the LED's yellow phosphor layer from the inside is still the primary way of implementation, nevertheless.

2.6.1 Conformal structure

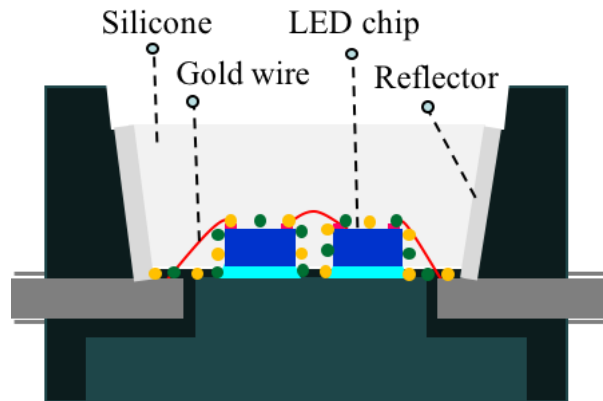


Figure 2.8: Conformal structure

According to Figure 2.8, this is both the initial and standard construction of LED. This construction consists of a thin sheet of yellow phosphor, a few millimeters thick, applied to a blue chip. This structure has the benefits of high economic efficiency and ease of implementation. Its structure does not, however, have the same color quality or luminous flux as other illumination sources. Not only that, but LEDs have a short lifespan and can easily overheat when utilized for extended periods of time.

2.6.2 In-cup structure

On the blue chip with this arrangement in Figure 2.9, the yellow phosphor layer is firmly and densely covered (Ying & Chien, 2015). Improved luminous flux is one of this structure's benefits; low color quality and implementation challenges are its drawbacks. Using this technique, the phosphor concentration mixing plays a key role in determining the LEDs' luminosity. Phosphorus scattering particles are enhanced, which causes this structure to grow quickly.

However, the response time is longer because the phosphor particles are mixed together with the silicone gel, so the scattering of the particles occurs more slowly.

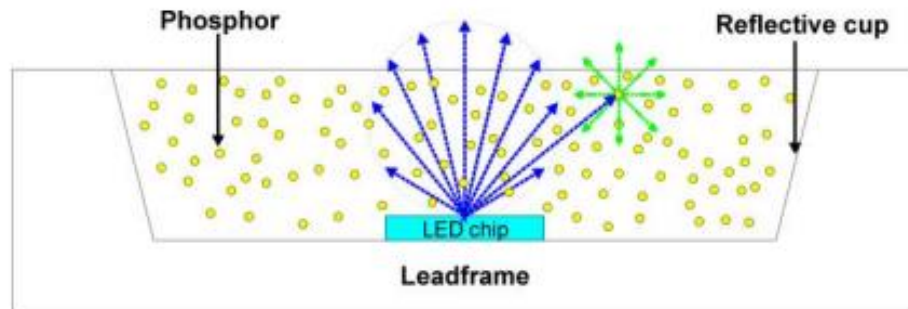


Figure 2.9: In-cup structure

2.6.3 Remote structure

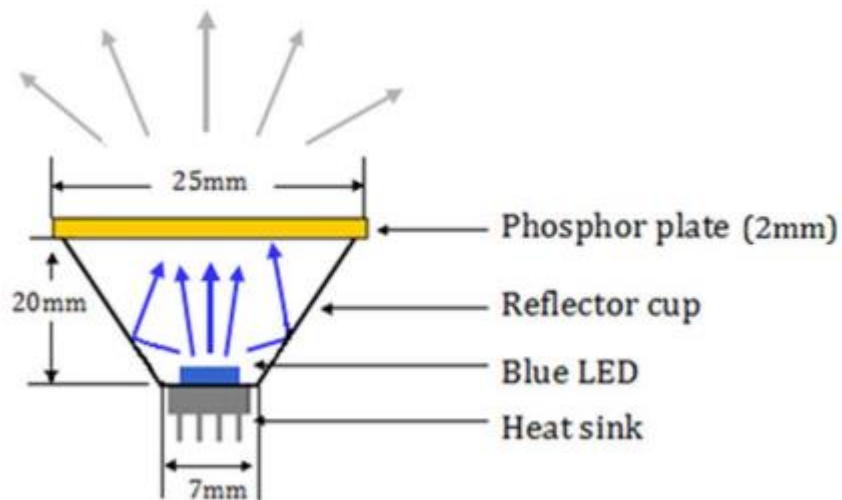


Figure 2.10: Remote structure

A schematic of these remote-phosphor-based WLEDs shows the InGaN blue LED, which gives off light at a peak wavelength of 450 nm; the reflector cup, which is 20 mm tall and has a reflectance greater than 0.96 because it has BaSO₄ painted on the inside; and the phosphor plate sample, which is 2 mm thick and 25 mm across. Figure 2.10 illustrates the structure.

The blue LED is attached to the tip of a cone-shaped reflector in Figure 2.10 (Dang et al., 2015). The yellow phosphor is covered by this structure quite a distance from the blue chip. There has also been research on the various spacing between phosphor layers and LED chips. The benefit of this structure is that it offers acceptable color quality; the drawback is that the luminous flux is subpar. White light is produced when the energy from the blue LED chip is reflected on the cup's two sides and then dispersed throughout the yellow phosphor layer. Compared to the conformal structure and the in-cup structure, this bright structure is superior. But low red-light energy results in low-quality color.

As a result, additional research is needed to determine whether of these two key aims may be achieved by using this structure:

Continue researching multi-layer structures of phosphorus.

- Act out the exam to find the best structure.
- Simulate and explain science using math and software.

The usage of remote structures is crucial to achieving the study's main objective, which is to improve the LEDs' color quality and luminescence efficiency. This is reinforced by the structures mentioned above. Previous investigations demonstrating the phosphorus structures are presented in the next chapter, however there are still some issues to be resolved.

2.7 Critical optical properties for evaluating the performance of a WLED

2.7.1 Color rendering index

The illuminance quality of the light source is precisely reflected by the Color Rendering Index, or CRI for short. CRI ratings vary amongst different light sources. The more exact the color of the lighted object reflected by the light source, the higher the CRI. According to Figure 2.11, a picture is clearer and more beautiful the higher its color rendering index.

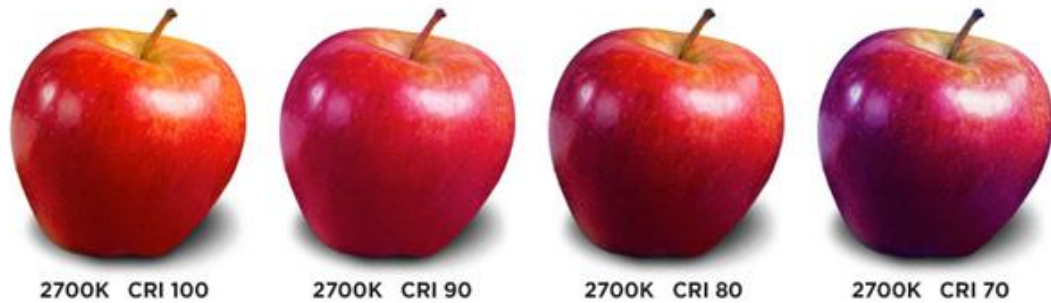


Figure 2.11: Color rendering index illustration

2.7.2 Luminous performance

LEDs use luminescence efficiency (LE) as a metric to quantify their luminous efficiency. The value is denoted in lumens per watt (Lm/W). There is an inverse link between the CRI index and the luminous efficiency of LEDs. An LED's luminous efficiency increases as its CRI decreases. Consequently, it is necessary to achieve a harmonious equilibrium between these two indications during the production of LED lights. LEDs with a luminous efficiency greater than 100 Lm/W and a Color Rendering Index (CRI) higher than 75 Ra are the most effective in producing high-quality illumination. These LEDs accurately reproduce the color of the object being illuminated while also being energy-efficient.

2.7.3 Correlated color temperature

The abbreviation CCT stands for color-correlated temperature, which represents the light color temperature (Figure 2.12). The color temperature of LEDs typically ranges from 2500 K to 6700 K. The color temperature of the LED also affects the CRI. An LED with a correlated color temperature (CCT) ranging from 4500 K to 6500 K will possess a greater color rendering index (CRI) compared to an LED with a CCT of 2000 K.



Figure 2.12: Illustration of color temperature

2.7.4 CQS - Light Quality Scale

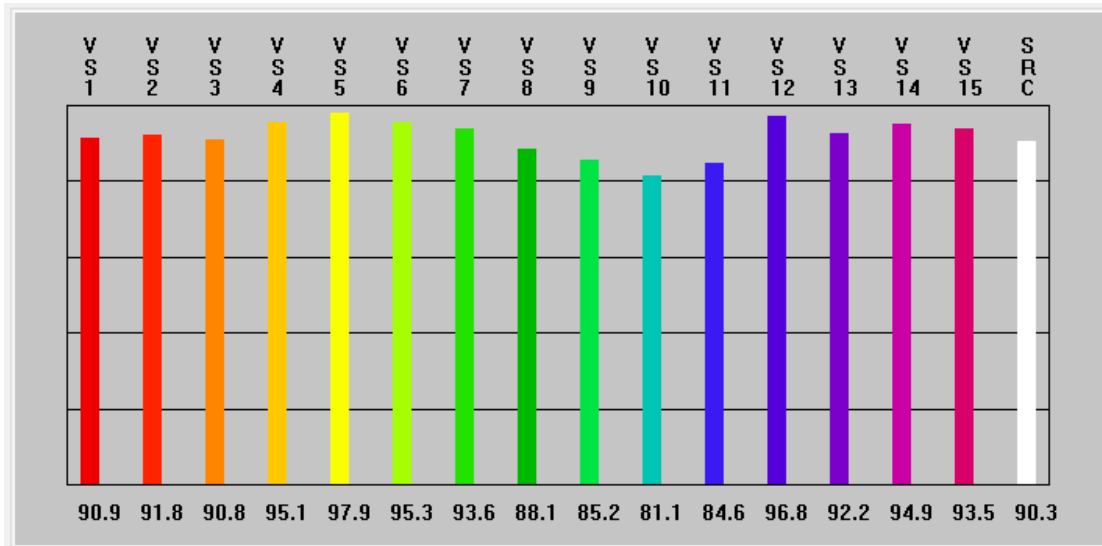


Figure 2.13: Illustration of the light quality ratio scale

It is also a metric that measures the quality of light. However, unlike CRI, CQS is calculated as the mean value of R1 and R15. The parameter is considered in the ultraviolet and infrared color bands R9 to R15 (Figure 2.13). When assessing the quality of light, these elements are considered. In general, the Color Quality Scale (CQS) is somewhat lower than the Color Rendering Index (CRI), and it is challenging to achieve a 100 percent CQS due to the difficulties of increasing the value of R9, which represents

the red color factor that enhances infrared light. In order to enhance the R9 value of the lamp, manufacturers must utilize cutting-edge LED chip technology to accurately reproduce the red hue in the light.

2.7.5 The color quality

Color temperature deviation (D-CCT), luminous flux, and color rendering index (CRI & CQS) are the three main parts of color quality. Every color has a unique spectrum and color temperature. The LED can emit light in a wide variety of directions. Moreover, the color quality is also influenced significantly by various LED components. For instance, different luminescence efficiencies can be found in the same LED with the same power. In conclusion, at least two of the three previously listed criteria—CRI, CQS, and LE—must be met in order to determine whether the quality of WLED is ideal. This dissertation's main objective is to investigate how to use appropriate distant phosphor structures and scattering particles to meet the aforementioned requirements.

2.8 Summary

A variety of white light generation techniques are presented in this chapter, each with pros and cons of their own. The blue chip and the yellow phosphorus-coated substance are used in this dissertation's method of producing light. A white light source is produced when the blue chip's light and the transmitted blue light merge once the blue light travels through the yellow phosphor material and turns into yellow light. But because there aren't any green or red LEDs, the resulting white light is chilly and has poor color quality. Additionally, studies showed that red light energy is more important than green light energy for improving color rendition. As such, research concentrating on the integration of red phosphorus elements into the structure of LED packages has garnered a great deal of attention in an effort to produce white light that is well balanced. Enhancing the ideal properties of white light-emitting diodes (WLEDs) is a promising application of this technique. Furthermore, a number of research structures are

introduced and the optical characteristics of WLED are explored. Each of the phosphor structures discussed has advantages and disadvantages of its own, and each optical feature has a distinct purpose. Long-term use is not recommended for the standard conformal construction due to its low luminous efficiency, poor color rendering index, and yellow ring phenomena. Images displayed in color are less accurate because to the in-cup structure's low color rendering index and increased light flux. With a relatively steady color rendering index, the remote structure has the largest luminous flux. In order to maximize the luminous flux, CRI, CQS, and color uniformity of WLED, the distant structure is therefore suggested as a study goal.

CHAPTER 3. EXAMINATION OF MULTI-LAYER DISTANT PHOSPHOR STRUCTURES TO ENHANCE THE WHITE LED'S OPTICAL CHARACTERISTICS

3.1 The three-layer remote phosphor structure

3.1.1 Mathematical frameworks based on Lambert-Beer law for multi-layer remote phosphor structures

This law was created in collaboration with three scientists: August Beer (1825–1863), Johann Heinrich Lambert (1728–1777), and Pierre Bouguer (1698–1758). It is predicated on the absorption of electromagnetic radiation by a solution. The optical attenuation of a particular material, the concentration of the solution in that substance, and the distance over which the energy travels are all factors in the Beer-Lambert law that directly impact the energy loss process. Energy that is metabolized is also equally impacted by the absorption coefficient, which can be written as:

$$A = \varepsilon lc \quad (3.1)$$

where ε is the attenuating species' molar attenuation coefficient, also known as their absorptivity, and A is their absorbance. Where c is the concentration of the attenuating species and l is the optical path length in centimeters. The relationship between the transmittance T of the material sample, its optical depth τ , and its absorbance A can be defined as follows:

$$T = \frac{\Phi_e^t}{\Phi_e^i} = e^{-\tau} = 10^{-A} \quad (3.2)$$

Where:

Φ_e^t : The radiant flux that material sample transmits is denoted

Φ_e^i : The radiant flux received by the material sample is denoted

Respectively, according to the definitions of attenuation cross section and molar attenuation coefficient, The Beer-Lambert law can be expressed in the following manner:

$$T = e^{-\int_0^l \mu(z) dz} = 10^{-\int_0^l \mu(z) dz} \quad (3.3)$$

Content of the legislation Beer-Lambert can be summed up as follows: variables like the quantitative concentration of solution C in the material or the attenuation coefficient (Napierian) μ , $\mu_{10} = \frac{\mu}{\ln 10}$ of each material can alter the energy transferred across layers of phosphor materials. What is the amount in question, and how is it expressed? It is as follows:

$$\mu(z) = \sum_{i=1}^N \mu_i(z) = \sum_{i=1}^N \sigma_i n_i(z) \quad (3.4)$$

$$\mu_{10}(z) = \sum_{i=1}^N \mu_{10,i}(z) = \sum_{i=1}^N \varepsilon_i c_i(z) \quad (3.5)$$

If attenuation is uniform, these relations take the following form:

$$T = e^{-\mu l} = 10^{-\mu_{10} l} \quad (3.6)$$

Or equivalently:

$$\tau = \mu l \quad (3.7)$$

$$A = \mu_{10} l \quad (3.8)$$

When the attenuation coefficient does not change with z , as is frequently the case, an integral need not be performed and the law can be expressed as follows:

$$I(z) = I_0 e^{-\mu z} \quad (3.9)$$

The absorption coefficient α or scattering, which results in greater scattering attenuation with larger particle sizes and vice versa, also contributes to the energy loss. Consequently, the size of the particles within material areas affects how much energy is exchanged between them.

3.1.2 Summary of remote structure formula

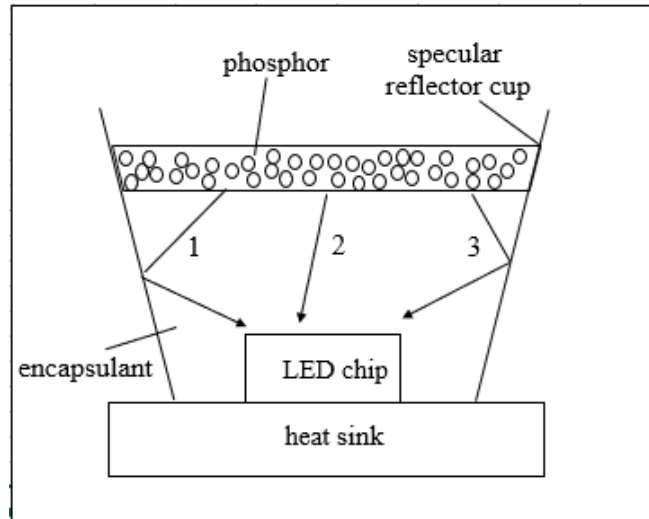


Figure 3.1: Remote phosphor configuration.

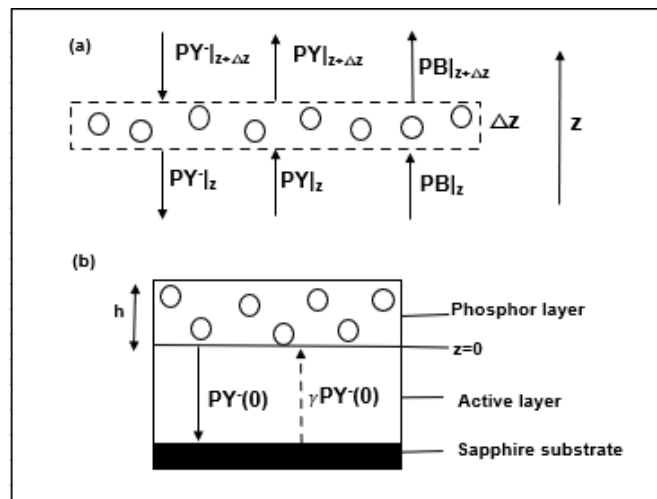


Figure 3.2: (a) Schematic plot for a small section of phosphor layer (one-dimensional model) and (b) illustration of the boundary condition at $z=0$

The energy contained in blue light that is produced by the blue chip and absorbed by yellow phosphor materials is lost when the phosphor transforms the blue light into yellow light (Yang et al., 2011). An example of this can be seen in Figure 3.2a, where

blue light is attenuated in this material layer because the horizontal sand surface of a thick phosphor layer absorbs its energy. The Lambert-Beer law states that the amount of energy lost is proportionate to the intensity of the blue light input. When energy from the blue light coming from the blue chip combines with the yellow light produced by the yellow phosphor layer, white light is produced. Here, the yellow phosphor layer and green energy will be combined to convert a portion of the yellow energy. The light that the blue chip emits will increase the luminous flux in comparison to the light that is isolated from it. Nevertheless, the converted yellow light energy travels in the opposite direction from the direction prescribed by the law of straight light propagation, which results in the yellow ring phenomenon in the LED. The blue light intensity in Figure 3.2 is denoted by PB , the clear yellow light intensity in the z -direction by PY , and the yellow light in the opposite direction by PY^- . The energy balance is used to obtain the following three equations:

$$PB|_{z+\Delta z} - PB|_z = -\alpha_B \times \Delta z \times PB|_z \quad (3.10)$$

$$PY|_{z+\Delta z} - PY|_z = -\alpha_Y \times \Delta z \times PY|_z + \frac{1}{2}\beta \times \Delta z \times PB|_z \quad (3.11)$$

$$PY^-|_z - PY^-|_{z+\Delta z} = -\alpha_Y \times \Delta z \times PY^-|_{z+\Delta z} + \frac{1}{2}\beta \times \Delta z \times PB|_{z+\Delta z} \quad (3.12)$$

The energy loss portions of blue and yellow light during their propagation in the phosphor layer are described by the parameters α_B and α_Y , respectively, while the conversion coefficient for blue light converting to yellow is represented by β . The phosphor particle volume fraction (γ) in the phosphor layer determines its properties, α_B , α_Y , and β . When Δz approaches zero, equations (3.10)–(3.12) become:

$$\frac{dPB}{dz} = -\alpha_B \times PB \quad (3.13)$$

$$\frac{dPY}{dz} = -\alpha_Y \times PY + \frac{1}{2}\beta \times PB \quad (3.14)$$

$$\frac{dPY^-}{dz} = \alpha_Y \times PY^- - \frac{1}{2}\beta \times PB \quad (3.15)$$

A schematic representation of the flip-chip construction of an LED chip with a phosphor material with a layer thickness of h may be found in Figure 3.2b. The light intensity from the blue LED, denoted by PB_0 , is the energy of blue light (PB) at $z=0$. Yellow light's PY^- energy, which is moving in the negative z -direction, is equal to zero at $z=h$. The yellow light intensity from the phosphor layer to the active layer is PY^- at $z = 0$, or $PY^-(0)$, assuming that there is no energy loss in the substrate. With a yellow light reflection coefficient of γ , some of the energy of yellow light that reaches the bottom boundary of the phosphor layer is reflected back into the phosphor layer. From this, the boundary condition ($PY(z = 0) = \gamma PY^-(0)$) may be obtained. (scitation.aip.org). The solutions to equations (3.13) through (3.15) can then be derived by further assuming that α_B , α_Y , and β are all constant. The PB , PY , and PY^- at $z = h$ is thus represented as:

$$PB = PB_0 \times e^{-\alpha_B h} \quad (3.16)$$

$$PY = \frac{1}{2} \frac{\beta \times PB_0}{\alpha_Y - \alpha_B} [e^{-\alpha_B h} - e^{-\alpha_Y h}] + \frac{1}{2} \frac{\gamma \times \beta \times PB_0}{\alpha_Y + \alpha_B} [e^{-\alpha_B h} - e^{-\alpha_B h - 2\alpha_Y h}] \quad (3.17)$$

$$PY^- = \frac{1}{2} \frac{\beta \times PB_0}{\alpha_Y + \alpha_B} [e^{-\alpha_B h} - e^{-\alpha_B h - 2\alpha_Y h}] \quad (3.18)$$

Since the light that is transferred secondary is smaller than the light that is communicated directly, $\gamma = 0$. Equation 3.17 therefore becomes:

$$PY = \frac{1}{2} \frac{\beta \times PB_0}{\alpha_Y - \alpha_B} (e^{-\alpha_B h} - e^{-\alpha_Y h}) \quad (3.19)$$

The thickness is represented by the subscript "1" when it is $2h$ (Figure 3.3), in which case equations (3.16) and (3.19) become:

$$PB_1 = PB_0 \times e^{-2\alpha_{B1} h} \quad (3.20)$$

$$PY_1 = \frac{1}{2} \frac{\beta_1 \times PB_0}{\alpha_{B1} - \alpha_{Y1}} (e^{-2\alpha_{Y1} h} - e^{-2\alpha_{B1} h}) \quad (3.21)$$

The package is referred to as a "2" subscript when it is a double-layer phosphor structure (Figure 3.3) with a thickness of h for each layer. In particular, the energy will be reflected back to the LED chip once it has passed through the first layer. The luminous flux is negatively impacted by this occurrence. Hence, the transition energy to the second layer can increase with thickness, and at some point it can retain backscattering as the transition energy to the second layer increases and the transition energy adds up to the second layer. Backscattering is stopped from absorbing back into the LED chip by the first layer if it occurs.

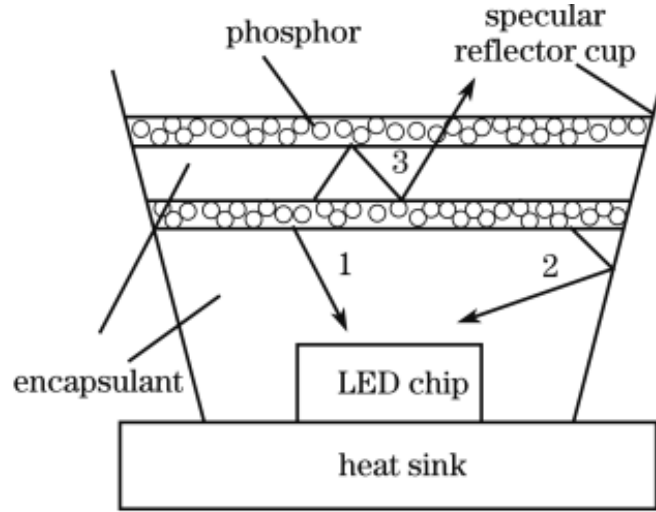


Figure 3.3: Double-layer phosphor configuration.

$$PB_2 = PB_0 \times e^{-\alpha_{B2}h} \times e^{-\alpha_{B2}h} = PB_0 \times e^{-2\alpha_{B2}h} \quad (3.22)$$

$$\begin{aligned} PY_2 &= \frac{1}{2} \frac{\beta_2 \times PB_0}{\alpha_{B2} - \alpha_{Y2}} (e^{-\alpha_{Y2}h} - e^{-\alpha_{B2}h}) \times e^{-\alpha_{Y2}h} \\ &\quad + \frac{1}{2} \frac{\beta_2 \times PB_0 \times e^{-\alpha_{B2}h}}{\alpha_{B2} - \alpha_{Y2}} \times (e^{-\alpha_{Y2}h} - e^{-\alpha_{B2}h}) \\ &= \frac{1}{2} \frac{\beta_2 \times PB_0}{\alpha_{B2} - \alpha_{Y2}} \times (e^{-2\alpha_{Y2}h} - e^{-2\alpha_{B2}h}) \end{aligned} \quad (3.23)$$

The magnitude of the transmitted blue light varies:

$$PB_2 - PB_1 = PB_0 \times (e^{-2\alpha_{B2}h} - e^{-2\alpha_{B1}h}) \quad (3.24)$$

The magnitude of the transmitted blue light varies:

$$PY_2 - PY_1 = \frac{1}{2} \frac{\beta_2 \times PB_0}{\alpha_{B2} - \alpha_{Y2}} \times (e^{-2\alpha_{Y2}h} - e^{-2\alpha_{B2}h}) - \frac{1}{2} \frac{\beta_1 \times PB_0}{\alpha_{B1} - \alpha_{Y1}} \times (e^{-2\alpha_{Y1}h} - e^{-2\alpha_{B1}h}) \quad (3.25)$$

The parameters α_B , α_Y , and " β " are all affected in the same way by the thickness h and the particle density ρ_v . Thus, when thickness increases, α_B climbs dramatically whereas α_Y grows very little and approaches zero. The conversion coefficient β is growing because of the steady increase in yellow transmitted light that occurs with the growth of α_B . Consequently, $\alpha_{B2} < \alpha_{B1}$, $\beta_2 < \beta_1$ and α_{Y1} is near α_{Y2} ($\alpha_{Y2} < \alpha_{Y1}$). With $\frac{\beta_1}{\alpha_{B1}} < \frac{\beta_2}{\alpha_{B2}}$ and α_Y significantly smaller than α_B , the following can be deduced:

Therefore, the equation 3.25 becomes:

$$PY_2 - PY_1 > \frac{1}{2} \frac{\beta_1 \times PB}{\alpha_{B1} - \alpha_{Y1}} \times (e^{-2\alpha_{B1}h} - e^{-2\alpha_{B2}h}) \quad (3.26)$$

The entire change in transmitted light is:

$$(PB_2 - PB_1) + (PY_2 - PY_1) > PB_0 (e^{-2\alpha_{B2}h} - e^{-2\alpha_{B1}h}) \times \left(1 - \frac{1}{2} \frac{\beta_1}{\alpha_{B1} - \alpha_{Y1}}\right) \quad (3.27)$$

α_{B1} is significantly greater than α_{Y1} and β_1 under the same ρ_v and thickness h . Consequently,

$$\frac{1}{2} \frac{\beta_1}{\alpha_{B1} - \alpha_{Y1}} < \frac{1}{2}$$

Therefore,

$$(PB_2 - PB_1) + (PY_2 - PY_1) > \frac{1}{2} PB_0 [e^{-2\alpha_{B2}h} - e^{-2\alpha_{B1}h}] \quad (3.28)$$

Equation 3.28's right side is positive when $\alpha_{B2} < \alpha_{B1}$. The double-layer phosphor structure becomes more efficient:

$$\frac{(PB_2 + PY_2) - (PB_1 + PY_1)}{(PB_1 + PY_1)} > \frac{e^{-2\alpha_{B2}h} - e^{-2\alpha_{B1}h}}{e^{-2\alpha_{Y1}h} - e^{-2\alpha_{B1}h}} > 0 \quad (3.29)$$

It is evident from these calculations that the new three-layer multiplication model is probably a wise course of development.

3.1.3 Develop the mathematical formula for the triple-layer structure

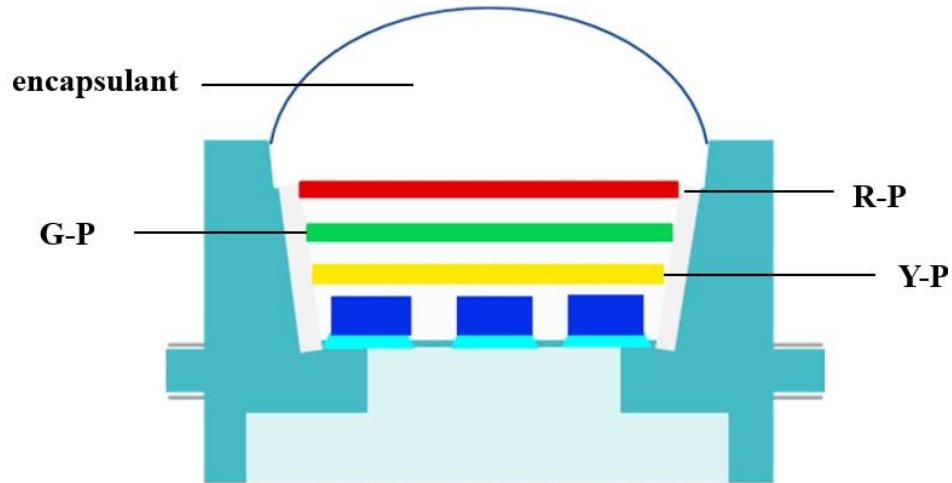


Figure 3.4: Three layers remote structure

Figure 3.4 visualizes the three-layer remote structure. Each of the phosphor layer is clearly indicated by phosphor color in the figure: the first layer is the yellow phosphorus material, the second is green phosphorus material, and the last one is the red phosphorus material. Each layer is 0.8 mm apart, and the phosphor material is mixed with silicon according to formula 4.4. Note that, there are various types of green phosphorus materials or red phosphorus materials with unique luminescence properties including absorption and emission characteristics.

Thus, in all previous studies, the enhancement of green-light or red-light spectral energy depends on the selected type of phosphor material in the conversion layer of the LED package. Based on the formulas of single-layer and two-layer structure above, the mathematical expressions for the three-layer remote structure can be demonstrated from Equations 3.30-3.32.

$$PB_3 = PB_0 e^{-\alpha_{B_2} \frac{2h}{3}} e^{-\alpha_{B_2} \frac{2h}{3}} e^{-\alpha_{B_2} \frac{2h}{3}} = PB_0 e^{-2\alpha_{B_2} h} \quad (3.30)$$

$$\begin{aligned} PY_3' &= \frac{1}{2} \frac{\beta_3 PB_0 e^{-\alpha_{Y_3} \frac{2h}{3}}}{\alpha_{B_3} - \alpha_{Y_3}} \left[e^{-\alpha_{Y_3} \frac{2h}{3}} - e^{-\alpha_{B_3} \frac{2h}{3}} \right] \\ &+ \frac{1}{2} \frac{\beta_3 PB_0 e^{-\alpha_{B_3} \frac{2h}{3}}}{\alpha_{B_3} - \alpha_{Y_3}} \left[e^{-\alpha_{Y_3} \frac{2h}{3}} - e^{-\alpha_{B_3} \frac{2h}{3}} \right] \\ &= \frac{1}{2} \frac{\beta_3 PB_0}{\alpha_{B_3} - \alpha_{Y_3}} \left[e^{-\alpha_{Y_3} \frac{4h}{3}} - e^{-2\alpha_{B_3} \frac{4h}{3}} \right] \end{aligned} \quad (3.31)$$

$$\begin{aligned} PY_3 &= PY_3' e^{-\alpha_{Y_3} \frac{2h}{3}} + \frac{1}{2} \frac{\beta_3 PB_0 e^{-2\alpha_{B_3} \frac{4h}{3}}}{\alpha_{B_3} - \alpha_{Y_3}} \left[e^{-\alpha_{Y_3} \frac{2h}{3}} - e^{-\alpha_{B_3} \frac{2h}{3}} \right] \\ &= \frac{1}{2} \frac{\beta_3 PB_0 e^{-\alpha_{Y_3} \frac{2h}{3}}}{\alpha_{B_3} - \alpha_{Y_3}} \left[e^{-\alpha_{Y_3} \frac{4h}{3}} - e^{-\alpha_{B_3} \frac{4h}{3}} \right] \\ &+ \frac{1}{2} \frac{\beta_3 PB_0 e^{-\alpha_{B_3} \frac{4h}{3}}}{\alpha_{B_3} - \alpha_{Y_3}} \left[e^{-\alpha_{Y_3} \frac{2h}{3}} - e^{-\alpha_{B_3} \frac{2h}{3}} \right] \\ PY_3 &= \frac{1}{2} \frac{\beta_3 PB_0}{\alpha_{B_3} - \alpha_{Y_3}} \left[e^{-\alpha_{Y_3} h} - e^{-2\alpha_{B_3} h} \right] \end{aligned} \quad (3.32)$$

Additionally, a structure with three layers of phosphor coating on the blue chip is believed to be represented by the index "3". The energy communicated after going through two layers of phosphor material is represented by equation 3.31. As of right now, the third layer of phosphor coating has greatly increased luminous performance. Given that each layer has a lag thickness of $h/3$, the created structure is referred to as a three-layer distant structure in this instance. Equation 3.33 demonstrates that employing three layers results in an output energy that is even more than that of a two-layer structure:

$$\frac{(PB_3 - PY_3) - (PB_2 + PY_2)}{PB_2 + PY_2} > \frac{e^{-2\alpha_{B_3} h} - e^{-2\alpha_{B_2} h}}{e^{-2\alpha_{Y_3} h} - e^{-2\alpha_{B_2} h}} > 0 \quad (3.33)$$

3.1.4 The options in remote phosphor structure for better white LEDs color quality

Compared to WLEDs with conformal or dispensing coating, WLED configurations with distant phosphor layers exhibit superior luminescence performance and are widely used in contemporary products. More research is necessary to achieve the difficult goal of controlling the chromatic performance of lighting fixtures made of distant phosphor materials. In an effort to enhance color quality, multi-layer phosphor setups with gaps between the layers have been inspired by this. Manufacturers of LED devices using many phosphor materials can benefit from the dissertation's findings in selecting the best configuration for optical performance. A 6500 K CCT WLED is the simulated model that was utilized in the studies. The triple-layer construction is more advantageous in terms of color quality and light output, according to the results. Furthermore, a significant decrease in color deviation is seen, indicating an improvement in chromatic stability in WLEDs with three phosphor layers. This work provides a useful method and information to make improved WLEDs through experimental results that are validated by the Mie-scattering theory.

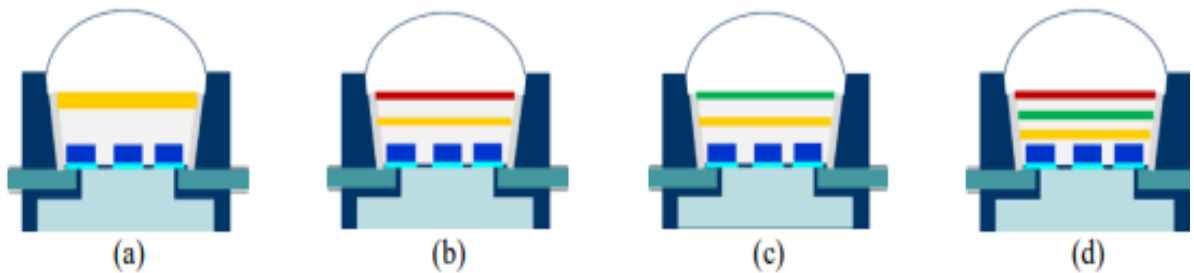


Figure 3.5: Illustration of multi-layer phosphor structures of white LEDs: (a) Single-layer phosphor, DYRL (b) and DYGL (c), and (d) TL phosphor

3.1.5 Simulation detail

WLED employs nine LED chips internally in this study. The peak power of 1.16 W is emitted by each blue chip at its highest wavelength. The conventional configuration (Y) with a layer of YAG:Ce³⁺ yellow phosphor on an LED chip is shown in Figure 3.5a. The two levels of the distant phosphorus (YR) structure are shown in Figure 3.5b: the yellow YAG:Ce³⁺ phosphorus layer is located below the red phosphorus layer. Located above the LED chip depicted in Figure 3.5c is another distant phosphorus (YG) structure with two layers of green phosphorus (Ce,Tb) MgAl₁₁O₁₉:Ce:Tb. The unique three-layer distant structure is depicted in Figure 3.5d. The two other phosphorus layers are separated by green phosphorus (Ce,Tb)MgAl₁₁O₁₉:Ce:Tb. Multiple phosphor layers are intended to fill up the red-light deficiency and green gap in the produced white light, improving color rendition and luminous flux.

Specifically, the green radiation energy of WLED emitted from the structure is enhanced by the use of the green phosphorus material (Ce,Tb)MgAl₁₁O₁₉:Ce:Tb. Next, to improve the CRI and CQS at the WLED output, more red energy is added using the red phosphorus material. The effects of LiAl₅O₈:Fe³⁺ on the optical characteristics of WLED in relation to the total phosphorus content in the distant structure are explained in depth in this work. For the dissertation, the phosphorus LiAl₅O₈:Fe³⁺ and phosphorus (Ce,Tb)MgAl₁₁O₁₉:Ce:Tb were chosen due to their excellent thermal uniformity and good quantum performance.

The phosphorus particle diameters are approximately 14.5 μm on average, according to results from earlier studies. Every phosphorous layer in the distant structure has a predefined density at a level of 0.08 mm. The YAG:Ce³⁺ concentration needs to be adjusted in order to stabilize the mean correlated color temperature (ACCT), an important indication.

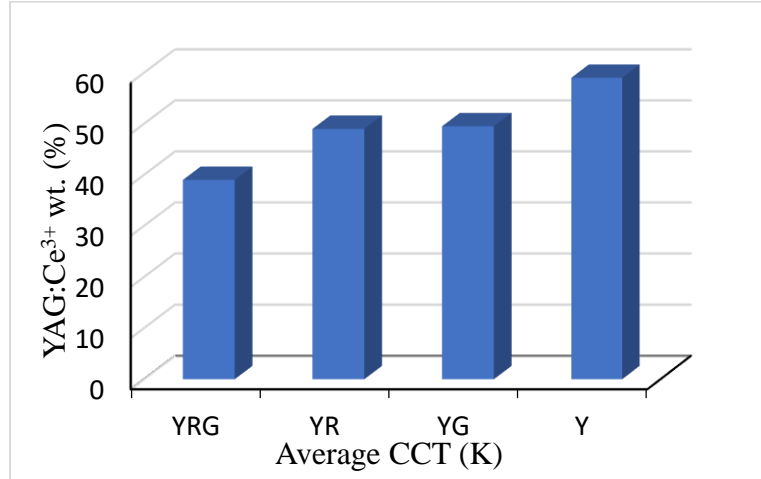


Figure 3.6: YAG:Ce³⁺ concentration corresponding to the remote structure

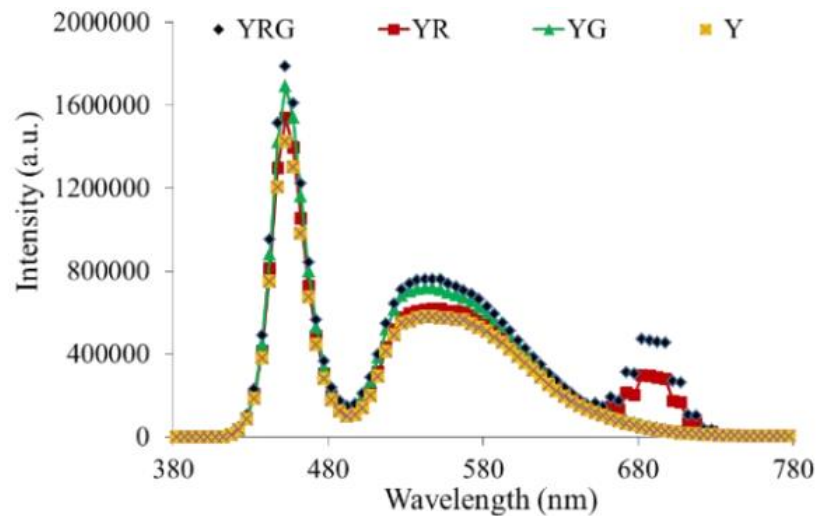


Figure 3.7: Emission spectra of the phosphor configurations

Figure 3.6 displays the proportion of YAG phosphorus releasing yellow YAG:Ce³⁺ in each remote phosphor configuration (Loan & Anh, 2020). The phosphorus structure Y has the maximum concentration of yellow phosphorus, whereas the YRG structure has the lowest concentration, as demonstrated by the difference in the proportion of YAG:Ce³⁺ phosphorus among the phosphorus structures in Figure 3.6.

The observed variations in the emission spectra of distant phosphor structures are clearly discernible, as illustrated in Figure 3.7. A structure's minimal emission spectrum is indicated by the Y structure with the lowest intensity index among the others. The YRG structure, on the other hand, emits the most, with a spectrum that spans 380 to 780 nm. The spectral intensity of YG is higher than that of YR between 400 and 500 nm; hence, the YG emission spectrum is larger than that of YR. The intensity of the YG and YR structures is dependent on the wavelength range. YG's color rendering in this emission spectrum is less successful than YR's, however, because YR has a higher intensity in the 650–750 nm region

3.1.6 Results and discussion

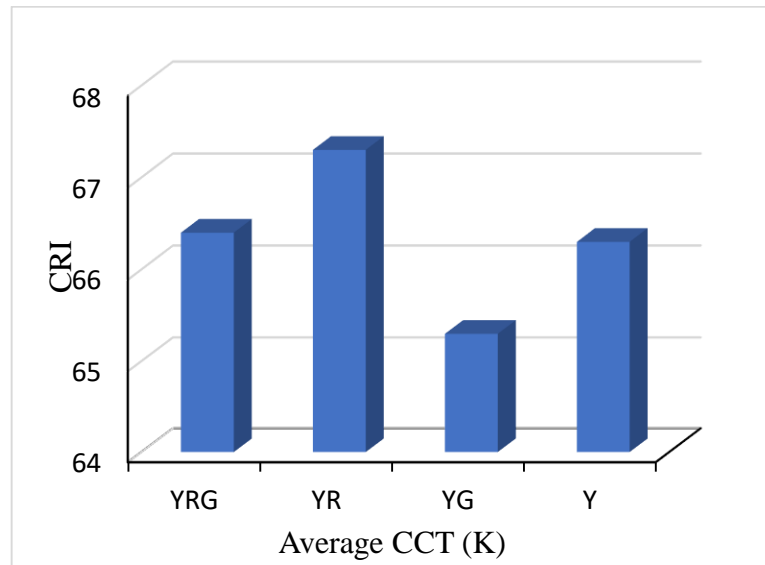


Figure 3.8: Color rendering indexes of the phosphor configurations

The color rendering index (CRI) for each lighting setup is measured and shown in Figure 3.8. It is evident that the maximum CRI is achieved by the YR structure. Regarding the enhancement of CRI in distant phosphor structures, this is a significant finding. The YR structure can accomplish this objective even if managing the CRI in

high ACCT is quite challenging. A higher color rendering index (CRI) is attained by the YR structure with the red phosphor layer, which supplies the structure with more red particles. In terms of attained CRI, YRG structure comes in second. The YG structure produces the lowest CRI, in contrast. With CRI as the primary objective, this conclusion indicates that the best course of action is to apply the YR structure to the serial manufacturing of WLEDs. Although the CRI is a well-liked quality indicator, it is insufficient to determine a lighting device's performance on its own.

In recent study, the CQS has emerged and been used for quality assessment. It looks at three features: color coordination, observer choice, and CRI. CQS appears to be an important factor and is thought to be the most important indicator to assess color quality after all three parameters have been covered. The configurations' CQS values were computed and shown in Figure 3.9. Since the chromatic lights of yellow, red, and green are more evenly balanced in the YRG structure, CQS peaks there as well, if CRI is highest in the YR structure.

The excellent chromatic performance of WLEDs is guaranteed by the high CQS value. However, the Y structure offers excellent value for the lumen output. In contrast to other structures, it has a lower CQS and finds it difficult to control the chromatic attribute of emitted light because it lacks chromatic sources.

Owing to its comparatively low cost and simpler production procedure than other designs, the Y structure remains a good manufacturing structure even with its color quality issue. The YRG structure is an ideal match for WLEDs with high requirements for color quality, as demonstrated by the results shown in Figure 3.9 (Loan & Anh, 2020).

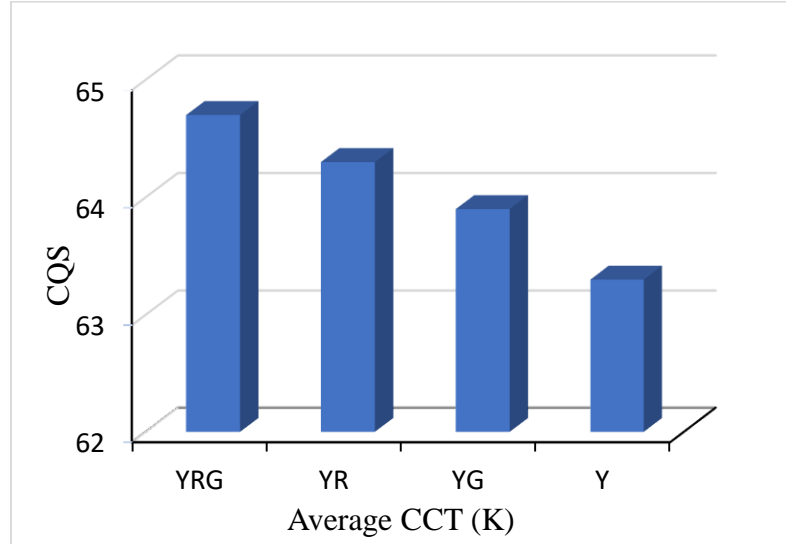


Figure 3.9: Color quality scale of phosphor configurations

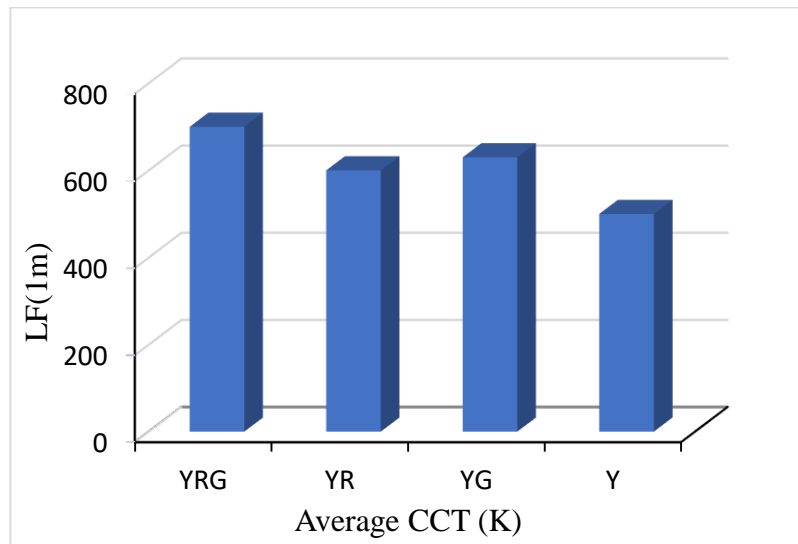


Figure 3.10: Luminous efficiency of phosphor configurations

But how does the improved color quality impact the luminous flux? The prior question was addressed by means of a comparative analysis between the initial and secondary layers. Section 3.1.3 contains the mathematical formula for calculating the

blue and yellow light produced by WLEDs with two phosphor layers. The findings offer important insights into WLED processes and enhancing techniques.

The Y structure in Figure 3.10 has the least quantity of light released among the structures, based on the graph. On the other hand, the luminous flux achieved by the YRG structure is the largest. Since YRG structures have the best color quality, this answers all the problems regarding their effect on the luminous flux. However, the luminous flux intensity of the YG structures is noticeably higher, though still slightly lower than that of the YRG structures. The inclusion of phosphor (Ce,Tb) to $\text{MgAl}_{11}\text{O}_{19}:\text{Ce}:\text{Tb}$ materials, which raises the emission intensity throughout the wavelength range of 500–600 nm to bridge the “green gap,” is responsible for the two structures' increased luminosity.

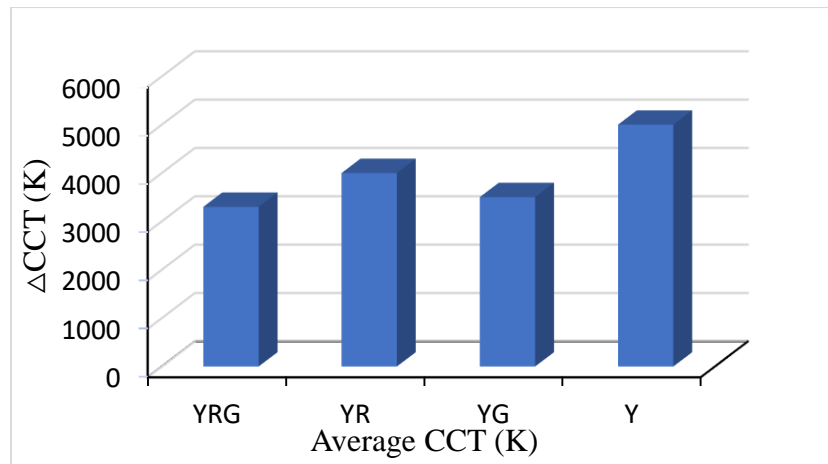


Figure 3.11: Correlated color temperature deviation (ΔCCT) of the remote phosphor configurations

In addition to other factors, color consistency is another one that might be disregarded when determining the hue of light. Some have suggested using phosphorus particles that increase the scattering effect, like TiO_2 , ZnO , or an appropriate coating

technique, as a way to improve color uniformity. The color quality can be enhanced, but when the suggested techniques are used, lumen output will drop.

Thus, increasing the amount of red phosphor and phosphorus $\text{MgAl}_{11}\text{O}_{19}:(\text{Ce},\text{Tb})$ will improve the color performance of WLED. The primary cause of this is that LED chips' reabsorbed backscattering lowers their light output. The resultant color divergence in structures is seen in Figure 3.11. It's evident that the Y structure has the highest color deviation value, while the YRG structure has the lowest. The better the color homogeneity, the lower the color deviation. These findings suggest that, as compared to a single-layer construction, a multi-layer structure is more effective at reducing color variation for improved LED color uniformity. The explanation is that WLED scattering is improved due to the additional phosphor layers in the YRG structure's enhanced scattering capabilities, which also improve color uniformity. In conclusion, YRG structures outperform single-class Y structures in terms of luminescence efficiency and color uniformity (Loan & Anh, 2020).

3.1.7 Improving color quality and luminous flux of white LED utilizing triple-layer remote phosphor structure

In order to achieve a more pleasing luminous appearance, the traditional distant construction frequently uses a space between the LED chip and phosphor layer; however, it has trouble maintaining sufficient color quality. In order to improve the luminescence performance or color quality of WLEDs, multi-layer distant structures are studied in this research. It is found that, as compared to traditional structures, the two-layer and three-layer structures improve LED quality more effectively. Here, luminous efficiency (LE), color uniformity, color rendering index (CRI), and color quality scale (CQS) are the WLED quality indices. LED color temperatures of 5600 K and 8500 K were used in the studies in this dissertation. The findings show that, in comparison to alternative remote-layer architectures, WLED with three layers of phosphors has superior CRI, CQS, LE,

and significantly smaller color deviation. Notably, more color consistency in white light is a result of a lower color deviation. To validate these results, the Mie scattering theory is applied (Loan & Anh, 2020). While great work has been done to increase luminous flux, not enough attention has been paid to other optical qualities. For instance, studies have been conducted on the impact of phosphor layer spacing on luminous flux in concave double-layer remote phosphorus structures (CDRP) and flat double-layer remote phosphorus structures (FDRP). This study showed that FDRP had superior luminous efficiency, and it also recommended the ideal distance. In order to maximize light output, the separation between the phosphorus layers in the remote triple-layer phosphorus structure was also examined. Moreover, the investigation of $\text{SrBaSiO}_4:\text{Eu}^{2+}$ particles for regulating WLED green light output with appropriate phosphor packets was also highlighted. On the other hand, increasing the luminous effect depends on the concentration and density of phosphor. The amount of light lost as a result of reabsorption increases with phosphorus concentration.

According to Quintero et al. (2012) and Linhares et al. (2009), WLEDs with low CCT and inadequate luminous performance have this impact. Though not all of them are discussed, there may be ways to enhance WLED's optical characteristics. As a result, this dissertation can be very important in selecting the right multi-layer distant structures for WLED uses.

To determine the increased luminous flux, the structure of a WLED with multiple phosphor layers was fitted with the remote phosphor profile proposed in this dissertation. The lighting outcomes were then compared with those of alternative structures. Green and red phosphor layers are merged to produce a triple-layer structure that has just formed (Figure 3.12).

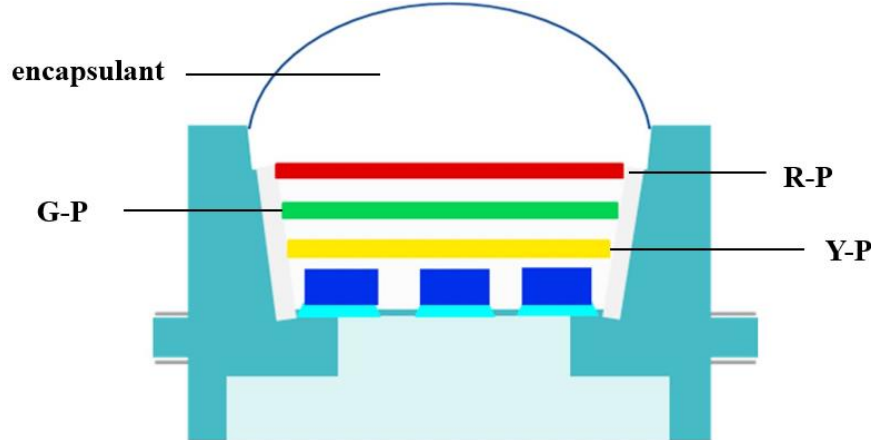


Figure 3.12: Illustration of triple-layer remote phosphor configuration

Color rendering index (CRI), color quality scale (CQS), and color uniformity are examples of optical attributes from these two remote phosphor profiles that have never been simulated and compared before. When there are two layers of phosphorus, a yellow phosphorus film is positioned beneath either a red or green phosphorus layer (Trang et al., 2019 & Price et al., 2012).

The red phosphor film is the top layer in a three-layer phosphorus structure, with yellow phosphorus located beneath the green phosphor sheet. Keeping CRI high at high color temperatures without significantly affecting LE is a primary difficulty in this dissertation.

The dissertation examined a three-layer distant structure with a tested correlation color temperature of up to 8500 K in order to address this difficulty. $\text{Sr}_w\text{F}_x\text{B}_y\text{O}_z: \text{Eu}^{2+}$, Sm^{2+} , and $\text{SrBaSiO}_4:\text{Eu}^{2+}$ phosphor are the red phosphor materials employed in this test. The YR (yellow-red) two-layer structure has the highest CRI value, according to the simulation findings, with the YRG having the second-best CRI value.

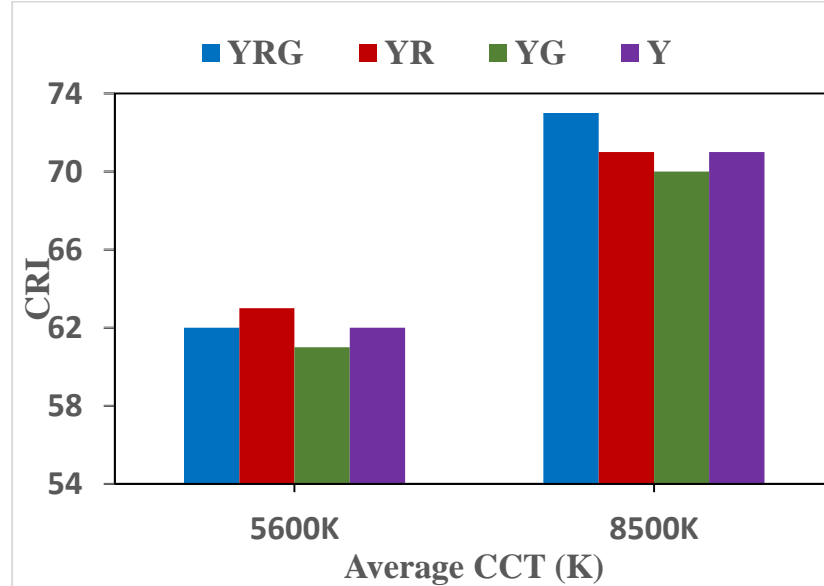


Figure 3.13: CRI of phosphor structures

As shown in Figure 3.13, the CRI values of three-layer and other two-layer structures are investigated at 5600 K and 8500 K to validate such findings. The data in this figure exhibit a pattern that is consistent with the simulation results, indicating that the YR structure is advised for maximizing the LED's CRI value.

This dissertation adds the CQS as an additional criterion for determining the ideal level of WLED, in addition to the CRI. The CQS assessment incorporates a broader set of criteria, as illustrated in Chapter 2, making it more accurate in assessing color fidelity. A great combination for assessing WLED reliability is the CQS in conjunction with the CRI criterion. Figure 3.14 illustrates how CQS findings are gathered and compared amongst distant structures.

Specifically, (and at a different position from earlier research) Figure 3.14 shows the CQS results of remote buildings at two temperatures (5600 K and 8500 K). In contrast to the CRI, the CQS values exhibit a different pattern, ranking the YR structure second and the three-layer YRG structure first. This outcome is consistent with the

simulation as well. Put differently, it is found that the YRG structure is the best way to get noticeably better color fidelity and rendition.

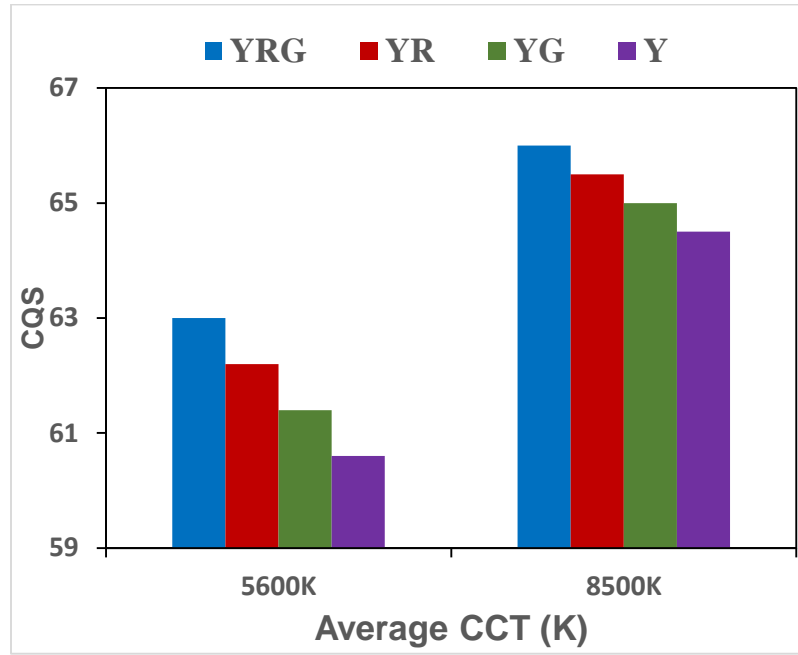


Figure 3.14: CQS of phosphor structures

Furthermore, for every distant phosphor structure in Figures 3.13 and 3.14, the CRI and CQS rise with a higher tested CCT (8500 K). This is a significant finding that shows how well the tested structures' color rendering quality is managed at elevated temperatures. It is possible to pursue this new line of inquiry in the future. This study can be a useful resource for companies who produce high-power LED lights.

As per the established Lambert-Beer law, the luminous flux of the three-layer remote structure is greater than that of the two-layer and single-layer structures. By passing the energy from the LED chip via a layer of yellow phosphor material mixed with silicon to create white light energy, the output energy of the current LED is raised even further. Consequently, with a multi-layer construction as opposed to a single-layer remote structure, the transmission power improves more noticeably

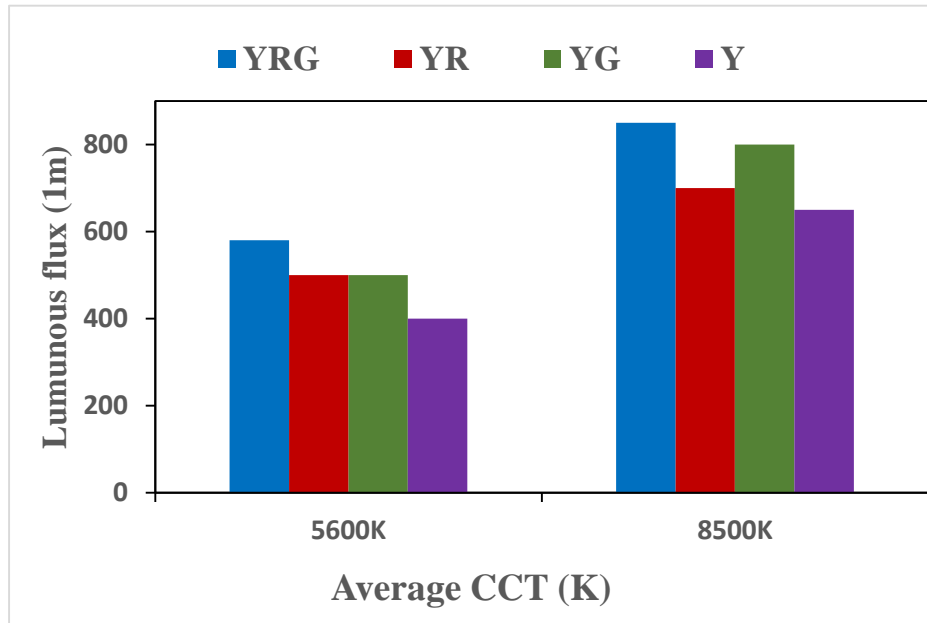


Figure 3.15: Luminous flux of phosphor structures

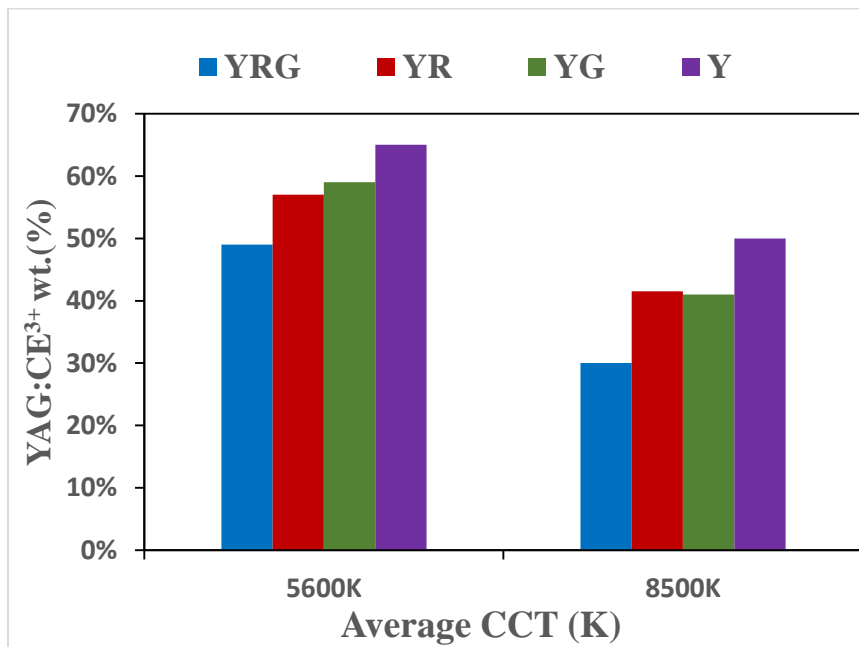


Figure 3.16: YAG:Ce³⁺ phosphor concentration in remote structure

Figure 3.15 shows the measured light output of the constructed LED's distant structures. All other things being equal, the single-layer yellow remote structure has the lowest luminous flux results. According to the data, the three-layer structure made of red, green, and yellow phosphor materials is the one with the lightest flux. An excellent substitute for the three-layer structure is the two-layer yellow-green structure, as the green phosphor is crucial in augmenting the brightness of the distant structure. Its luminous flux is larger than the other two configurations and only slightly lower than the YRG structure, particularly when evaluated at a higher color temperature (Figure 3.16). Consequently, the YRG three-layer structure with the lowest YAG:Ce³⁺ concentration can significantly improve blue-light conversion and lessen backscattered light, improving white LED overall in terms of color rendering and luminous performances, particularly at high CCT (8500 K). This is further evidence that the three-layer distant structure is the best option through experimental modeling. Furthermore, an additional technique is employed to enhance the luminosity flux, which capitalizes on the dispersing properties of specific particles like SiO₂, CaCO₃, TiO₂, and CaF₂ when paired with an appropriate phosphorus structure (Hanh et al., 2020). Later in the following chapter, this strategy will be covered. The phosphor layer structure can be broken by high temperatures due to a change in phosphor concentration, even if using this method can boost the luminous flux. This will ultimately affect the color uniformity. In order to attain the improvement without disrupting the phosphor layer structure, multi-layer architectures can be used. Furthermore, between the two-layer and three-layer architectures, the latter is better at maximizing light flow while minimizing backscatter, which has an impact on color quality. Based on the simulation results, it appears that the three-layer structure is the best option for maintaining color consistency. Still, more elements are required in light of white-light LEDs' ideal characteristics. The pictures are simulations created using the specialized program Lighttools 9.0, and the elements are

shown afterwards. A smaller color deviation corresponds to a stronger color uniformity in the color-deviation analysis, which provides access to the color uniformity.

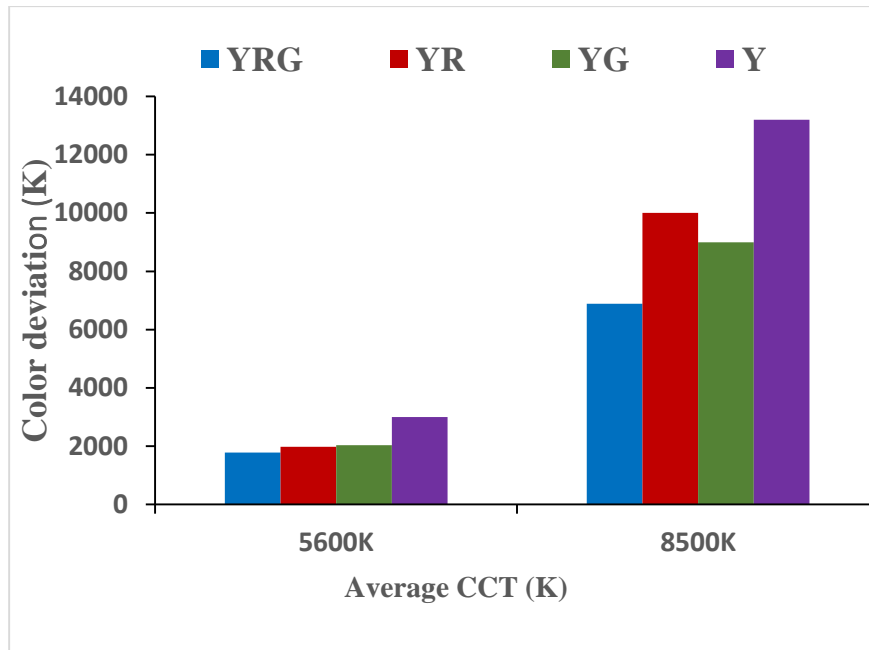


Figure 3.17: D-CCT of remote phosphor structures

Figure 3.17 depicts this evaluation using various distant structures at the two tested CCTs (5600 K and 8500 K). According to Loan and Anh (2020), the three-layer structure has the best color consistency or to put it another way, the least color deviation. Enhancing color homogeneity is possible with the three-layer structure. The rationale is that it produces white light first by amplifying internal scattering. Enhancing the scattering leads to improvements in the distribution, combination, and conversion of light by various phosphor materials. As a result, color balance in light emission is attained, improving the white light's color consistency. However, there is disagreement over whether adding more than three phosphor layers to an LED is a wise choice for enhancing its characteristics. Stronger scattering is observed with an increase of phosphor layers. On the other hand, because of the deterioration of the light emission-

color balance and the reduction of incident light energy, intense scattering might result in a decrease in luminous flux and degrade color uniformity. The emission spectra for distant phosphor structures clearly shows a difference.

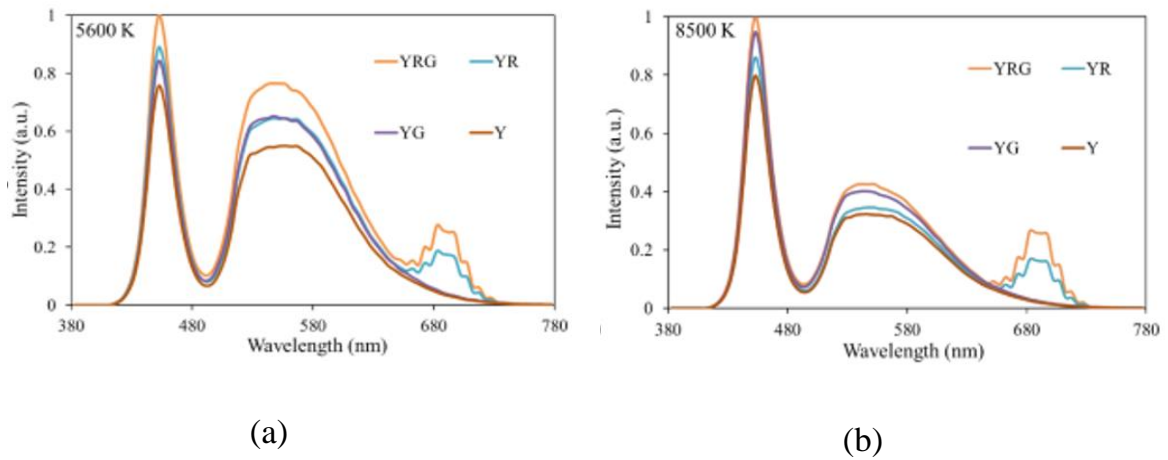


Figure 3.18: Emission spectra of phosphor configurations at CCTs difference

The emitter spectrum of the Y structure shows the weakest intensity, indicating that it exhibits the lowest light flux among the three distant phosphor structures at two ACCTs. On the other hand, the YRG structure displays the greatest spectral intensity within the wavelength range of 380 to 780 nm. Due to the higher spectral intensity of the YG structure compared to the YR structure in the 400–500 nm wavelength region, it is possible that the YG structure has a larger luminous flux than the YR structure (Figure 3.18a). However, the YR structure exhibits greater spectral intensity between 650 and 750 nm compared to the YG structure. This characteristic may contribute to the YR structure having a higher color rendering index than the YG structure (Loan & Anh, 2020). Consequently, selecting a phosphor structure with more than three layers will negatively impact color quality and luminous flux. Green phosphor is the most crucial component in this dissertation to alter the output luminous flux. Lambert Beer's law states that the backscattering property will diminish in the case of adding a layer of green

phosphor because yellow energy will be converted to green. The greatest light flux will be produced if this phosphor's concentration is suitably raised in conjunction with yellow phosphor. However, the red phosphor is the essential component for the excellent color quality. As a result, the goal of this dissertation is to maximize output luminous flux, guarantee consistent color uniformity, and improve output color quality over earlier research. Furthermore, it is shown that the phosphor structures' spectrum energy indicates how effective the three-layer structure is in comparison to the other ones. The enhancements obtained with a three-layer remote phosphor structure can be further illustrated by examining the emission wavelength and intensity of each remote structure in Figure 3.18. The YR and YRG structures in Figure 3.18 exhibit three distinct emission bands with wavelengths of roughly 450–480 nm, 500–600 nm, and 650–700 nm. Two emission bands are visible in the Y (single-layer) structure and the YG structure, which are located at 500–600 nm and 450–480 nm, respectively. The blue LEDs and the green/yellow phosphor layer are the source of the 450–480 nm and 500–600 nm bands, respectively. With regard to YR and YRG structures, the 650–700 nm band most likely formed from the red phosphor layer; these images are simulations of results from the specialized program Lighttools 9.0. Regardless of CCT values, it can be easily observed that the YRG structure has the strongest transmission power intensity, indicating that the LED that uses the YRG three-layer structure has the highest lumen output (Figure 3.18b). As an illustration of the Y structure's lower lumen output, the scenario with the lowest transmission intensity is seen. In addition, the transmittance intensity at higher CCT remains constant in the blue-light zone but decreases in the longer wavelength bands between two CCT points. Nevertheless, when the CCT point rises, the YG structure's transmission band intensity improves and surpasses that of the YR structure, suggesting that it is better suited for use in high-CCT LEDs in order to attain notable lumen efficiency.

3.2 Structure from distal convex with two layers of phosphor

For the purpose of enhancing WLEDs' optical characteristics at high temperatures, the DP structure was investigated in 2021. The outcomes demonstrated once more that a considerable change in CQS occurred when red phosphorus was added to the CRI. Furthermore, Beer-Lambert's rule and the Mie theory provide mathematical confirmation of this result (Loan & Anh, 2021).

Furthermore, the arrangement and structure of the phosphor layer influence the generated luminous flux (Wang et al., 2016). Certain issues arising from reverse-polarized light in the preceding investigation were resolved by the matching phosphor layer's distance factor. This facilitates the process of enhancing WLED's color quality (Zhang et al., 2017).

Furthermore, this shift is vividly displayed by a phosphor structure that resembles an inverted lens (Lin et al., 2015). New avenues for solid-body illumination technology research have been made possible by the two-layer telescoping architecture. It has never been simple in simulation to design a two-layer convex distant arrangement.

However, scientists are constantly willing to take on new challenges and lead the way in refining this convex structure, such as choosing the best simulation results. Its mention stems from the fact that convex or concave features associated with reflections on surfaces are used in physics to explain optical phenomena. T

his physical characteristic enables convex constructions to serve their intended purpose. The convex reflective surface increases energy emission outward, which significantly increases and brightens the light flux of LEDs. It is required to take into account additional parameters like CRI and CQS in order to assess whether or not this structure is optimum. We'll talk about all of this in the next part.

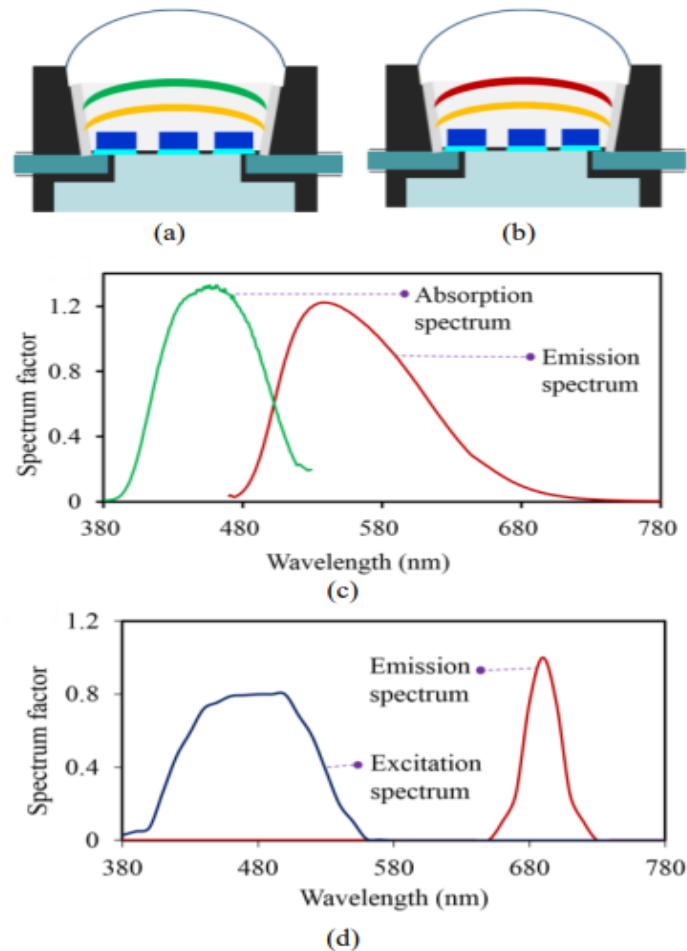


Figure 3.19: The remote structure model of 2 convex layers (a, b) and emission spectra of 2 types of yellow and red phosphors (c,d)

The correlation between CCT and emission spectra is depicted in Figure 3.19d. The LF has changed at the high temperature of 8500 K because to red phosphor participation. Models based on real WLED goods that have been tested at extreme temperatures and stability. The goal is to verify the validity of the simulation and reality by using the *NCC* cross-correlation approach (Equation 3.34). Furthermore, the elements that significantly affect the optical properties of the WLED were coupled with the commercial software LightTools. This outcome is meant to serve as a guide for manufacturers when producing WLED in accordance with their needs, which differ significantly.

Before building a workable structural model for the LED, a number of measurements were made in order to determine the geometric parameters. Next, by simulating the LED with a million beams, the widely used Monte Carlo ray tracing method was used to find the Light Intensity Distribution Curve (LIDC). After that, a careful model of the LED optical system was created by evaluating how closely the experimental and simulated LIDCs (light intensity distribution curves) matched each other. The normalized cross-correlation (NCC), which may be mathematically stated as follows (Sun et al., 2006), was used to quantify this evaluation.

$$NCC = \frac{\sum_x \sum_y (A_{xy} - \bar{A})(B_{xy} - \bar{B})}{\left[\sum_x \sum_y (A_{xy} - \bar{A})^2 \sum_x \sum_y (B_{xy} - \bar{B})^2 \right]^{1/2}} \quad (3.34)$$

In Equation 3.34, A_{xy} and B_{xy} denote the intensity or irradiance values for the simulation (A) and experimental (B) data, respectively. The negation of the negation of A , denoted as $(A\bar{\bar{}})$, is equivalent to A . The symbol \bar{B} represents the average value of A (or B) over the x-y plane. As seen in Figure 3.20 (Wang et al., 2008), the modeling algorithm for an LED changes the scattering properties and refractive indices of different packaging materials used in the LED, like phosphor, polymer, silicone, and more. The flowchart algorithm Figure 3.20 below is used to evaluate simulated LEDs by specialized software Lightools with actual measured LED values. LightTools is commercial software that simulates optical objects such as glass, LED, materials, scattering. In particular, LightTools is highly regarded for accurately simulating LEDs with multiple declared inputs as mentioned on page 61. In this study, the LEDs used had 9 LED chips, called multi-chip LEDs. The power of each LED chip is 1.16 W. These LED chips are coated on top of a phosphorus mixture with a thickness of 0.08 mm. Ascertaining that the simulation model is accurate is the first important task to do before performing additional particle simulations.

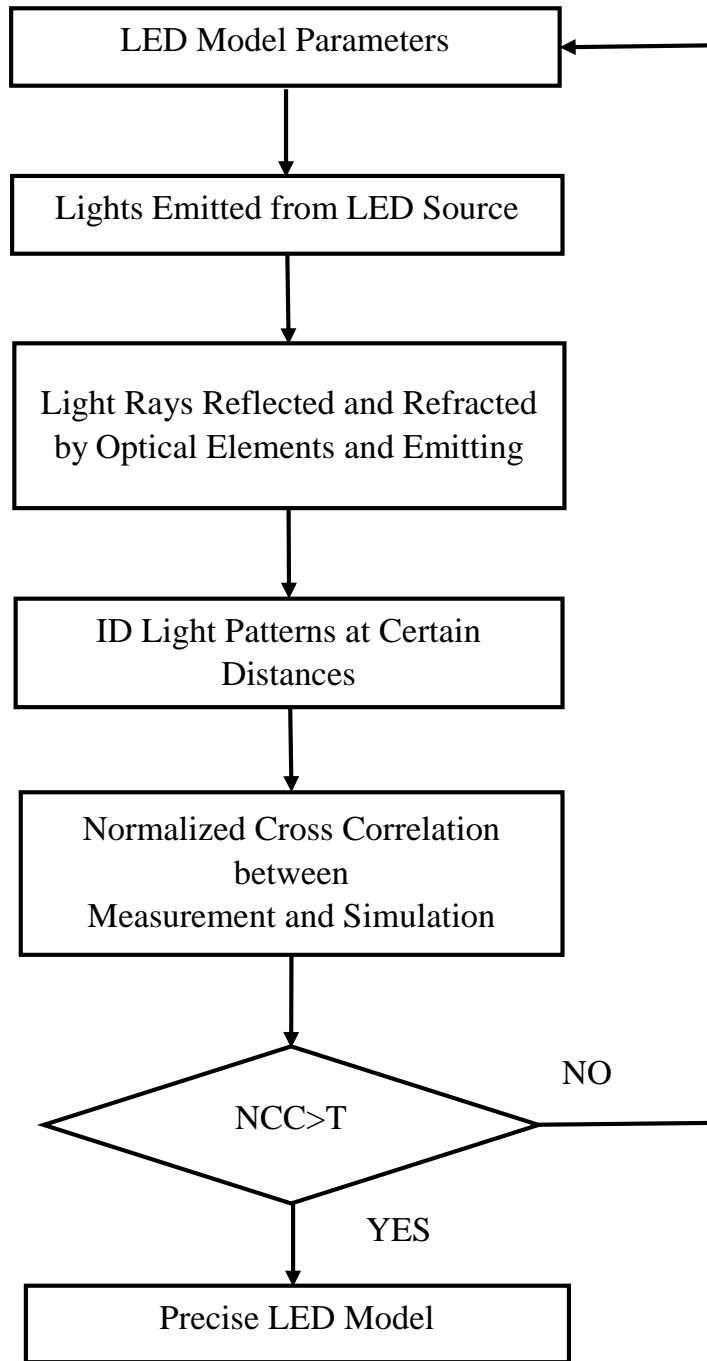


Figure 3.20: Modeling algorithm for an LED model

The rated cross-correlation (*NCC*) expression is applied to compare the similarity between the simulation model and the actual LED. These adjustments were iteratively

performed until the Normalized Cross-Correlation (*NCC*) reached a high value of 97.6 %, as depicted in Figure 3.21 (Liu & Xiaoping, 2011).

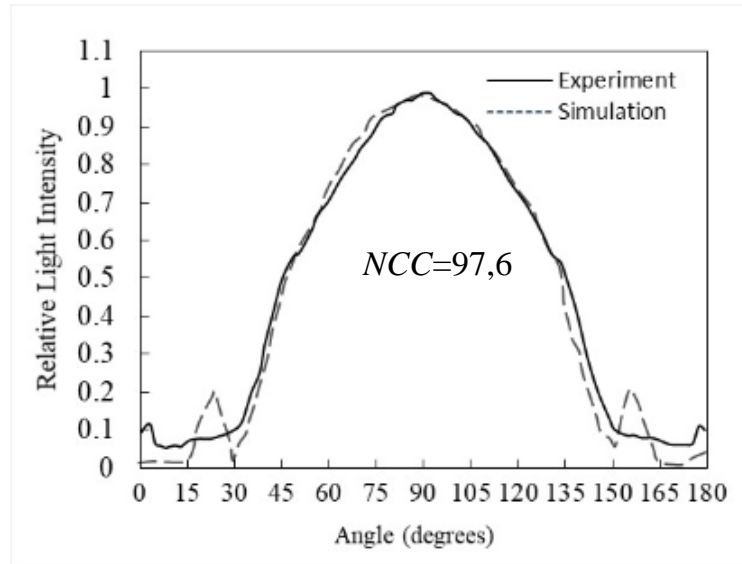


Figure 3.21: Experimental LIDC versus simulation for the Cree LED

See Figure 3.20 for the steps involved. The study begins by entering the specific LED's specifications, including its material, maximum power consumption, absorption and emission spectra, and current. Proceed with the simulation by replacing the original structure with layers of phosphor material coated in it. What is the light's value that the LED source simulation emits? Subsequently, input the reflecting and refractive indicators of the simulation's substance. The amount, which has the silicon layer in the center, determines the separation between the layers of material. Everything is done in simulation.

The measured characteristics from actual LEDs will then be compared with the outcomes of the simulation. Using the initial spectral form and the simulated spectrum as comparison points, Equation 3.34 compares the observed genuine current and the LED's simulated current. Achieving 97.6% for the *NCC* indicates that the simulation was run correctly.

It is necessary to repeat the refractive index, reflection, absorption spectroscopy index, and emission spectroscopy until the permitted *NCC* value is attained if the simulation step from a different material is not carried out (Liu & Xiaoping, 2011).

After the simulation results are processed, the spectrum measured from the actual genuine LED is compared in Figure 3.21. When the *NCC* value approaches the permissible level of compatibility, as demonstrated in Figure 3.21, the simulation is considered successful. Simulated LEDs are now practically as useful as actual LEDs. For the successful creation of white-light LEDs based on simulated phosphor parameter values, this is the initial stage. T

The majority of the real-life comparisons with the simulation outcomes were 99.5 percent among all the simulated articles in this study when *NCC* was analyzed. *NCC* is thus a practical component for conducting simulations in situations when the real LED has not yet been manufactured, merely at the research stage, offering significant benefits to producers who wish to produce white light LEDs with a wide range of applications.

3.2.1 Preparation of materials

As part of the study, simulations were used to prepare the composition of red phosphorus, comprising processes like calcination, dispersion, drying, and calcination twice to generate red phosphor with an emission peak between 1,785 and 2,149 eV (Loan & Anh, 2021).

Table 3.1: Composition of phosphor LaAsO₄: Eu³⁺

Ingredient	Mole (%)	By weight(g)
La ₂ O ₃	95 of (La)	155
Eu ₂ O ₃	5 of (Eu)	8,8
As ₂ O ₃	100 of (Au)	75

Table 3.2: Composition of yellow phosphor YAG: Ce³⁺

Ingredient	Mole (%)	By weight(g)
Y ₂ O ₃	100 of (Y)	108
Bi ₂ O ₃	0,1 of (Bi)	0,230
CaF ₂	2,5	1,95

When added to the YAG: Ce³⁺ yellow phosphor mixture, the components of the phosphorus material particle LaAsO₄: Eu³⁺ are described in Tables 3.1 and 3.2. The weights of the particles are equivalent to the material just enough—not too much nor too little supply. Everything needs to be thoroughly combined, and then dried at 1500 °C (Loan & Anh, 2021).

3.2.2 Simulation

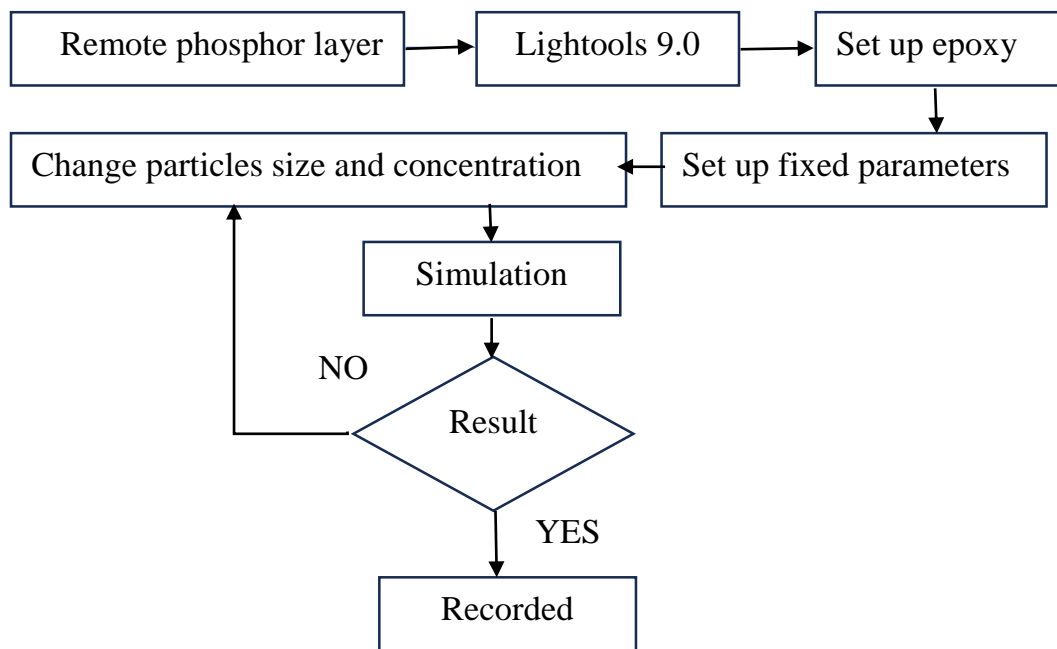
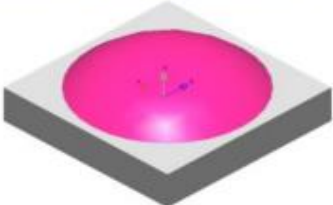
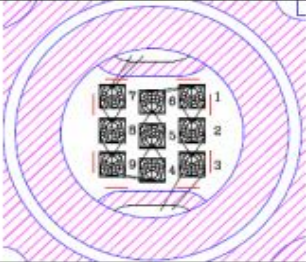
**Figure 3.22: Simulation model**

Figure 3.22 shows the flowchart of the simulation process for the LED in this dissertation. As seen on page 57, the LED's physical input parameters are fixed.

Next, the smallest value is first chosen in order to alter the concentration and particle size of a specific phosphor material.

Clicking the simulate button initiates the simulation when the inputs have been selected. The luminous flux index, correlated color temperature (CCT), color rendering index (CRI), color temperature deviation (DCCT), and spectral shape are the results that are displayed on the screen.

Table 3.3: Actual WLED parameters

LED vender	<i>Epistar</i>
LED chip	<i>V45H</i>
Voltage (V)	<i>3.5~3.6</i>
Peak Wavelength (nm)	<i>453</i>
Power (mW)	<i>320~340</i>
Lead frame	<i>4.7mm Jentech Size-S</i>
Die attach	<i>Sumitomo I295SA</i>
Actual sample	
Simulated sample	
Bonding diagram	

The processing is done using the trial-and-error method, which is carried out repeatedly to obtain the optimal results. If this result is satisfied, choose it; if not, change the concentration and particle size to continue simulating until the optimal result is chosen. At that point, the process is stopped. Models that are based on real WLED items that have been tested at high temperatures. The goal is to verify the dependability of simulation and reality by attempting the *NCC* cross-correlation method. Furthermore, the elements influencing the optical properties of the WLED were ascertained by using the commercial software LightTools. The appendix contains information on the practice simulation. The LightTools software's parameters, genuine LED images, and simulated LEDs are listed in Table 3.3.

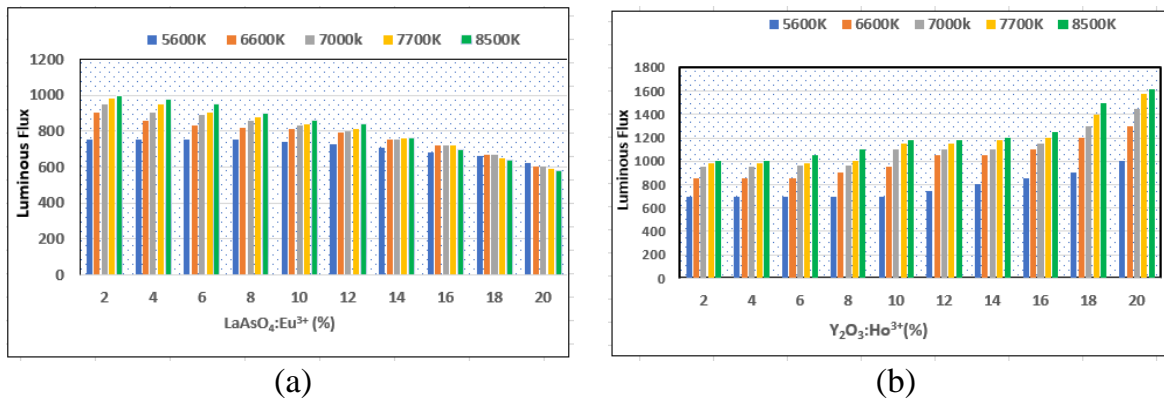


Figure 3.23: Variation of phosphorus concentrations of RYC (a) and GYC (b) to keep average CCT

Figure 3.23 depicts the luminous flux of the two convex double-layer remote phosphor structures with varying concentration of red phosphor and green phosphor. The outcome of raising the concentration of red phosphor from 0 % to 20 % is shown in Figure 3.23a; the concentration of yellow phosphor YAG: Ce³⁺ falls from 40 % to 2 %. The 20 % red color concentration in this study is the expected outcome, as red concentrations over this point sharply reduce CQS (albeit they do greatly enhance light

flux).

In contrast to earlier research, the use of the red phosphor in LED designs appears to stabilize luminous flux output while enhancing color quality. This indicates that the concentration of yellow phosphor, YAG:Ce^{3+} , must be kept to a minimum because an excessive rise in this concentration significantly reduces light flux. Energy transfer at the LED output is impacted by the phosphor particles' diminished energy scattering effect. Yellow phosphorus dropped from 18 % to 2 % as the concentration of red phosphorus rose from 10 % to 20 %. In this investigation, 20 % of the red phosphor concentration is the optimum option since 2 % of the yellow phosphor concentration greatly affects the light flux output. In a prior investigation conducted by Loan and Anh, 2020, an 8 % variation in yellow phosphor concentration led to a considerable reduction in light flux. The red phosphor, $\text{CaGa}_2\text{S}_4:\text{Mn}^{2+}$, was utilized at a concentration of 24 %, while yellow phosphor was at 8 %. In summary, the red phosphor is the best choice in this investigation. The consequences of raising the concentration of green phosphor, from 0 % to 20 % are shown in Figure 3.23b. This causes the concentration of yellow phosphor, YAG:Ce^{3+} , to fall from 40 % to 20 %. The selected outcome for this investigation is a 2 % concentration of green phosphor. The CRI tends to drop when the $\text{Y}_2\text{O}_3:\text{Ho}^{3+}$ concentration rises over this threshold.

The goal of this research is to stabilize CRI while raising the luminous flux. The energy scattering of the green phosphor, in combination with the energy of the yellow phosphor material, tends to increase significantly with increasing amounts of this material. Energy dispersion increases significantly as a result. This highlights even more how the best option is to have the highest possible concentration of green phosphor. In conclusion, Figure 3.23's simulations using Lightool 9.0 demonstrate that the blue phosphorus material $\text{Y}_2\text{O}_3:\text{Ho}^{3+}$ significantly enhances white light LEDs' capacity to create more light. The luminous flux remains unchanged when the red phosphorus substance, is added. However, the concentration of yellow phosphor, YAG:Ce^{3+} , falls

from 20 % to 2 % as the concentration of green phosphorus, increases from 10 % to 20 %. Since a greater concentration of yellow phosphor has a substantial impact on color consistency, a greater difference in the concentration of yellow phosphor (YAG:Ce³⁺) is preferred. A 20 % concentration of phosphor (YPO₄:Ce³⁺, Tb³⁺) was employed in a prior work by Hanh, Loan, and Anh (2020), along with an 8 % concentration of yellow phosphor (YAG:Ce³⁺), which only produced a 6 % change in yellow phosphor concentration. In summary, the study concludes that the 20 % concentration of green phosphor is the most appropriate.

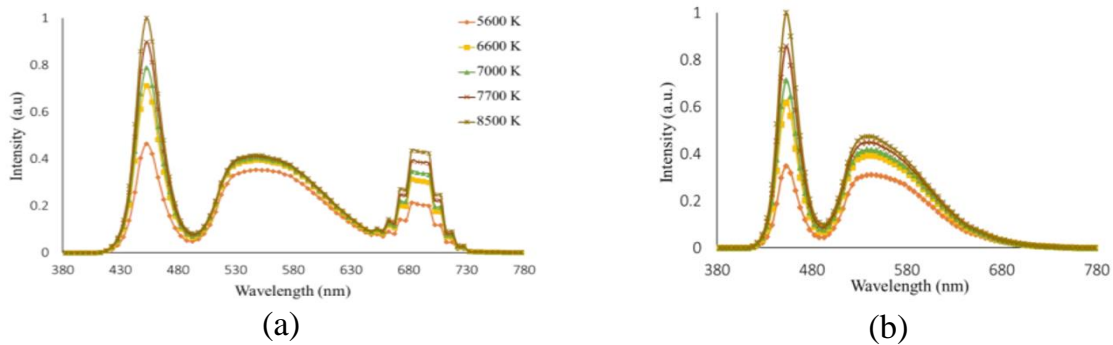


Figure 3.24: . Emission spectra of RYC (a) and GYC (b)

Figure 3.24 clearly illustrates how red phosphorus concentrations impact the WLED spectrum. When comparing the red-yellow arrangement to the structure with the green phosphor, three distinct locations show an increase in spectrum emission. Figure 3.24b illustrates how the spectral bands of 420 nm–480 nm and 500 nm–640 nm grow in intensity as the Y₂O₃:Ho³⁺ concentration rises. Stated differently, the increase in emission spectra in these two regions indicates an improvement in luminous flux. Moreover, an increase in internal blue light scattering events is caused by Y₂O₃:Ho³⁺, indicating an increase in phosphor scattering inside LEDs that improves the copper color.

Concurrently, as LaAsO₄:Eu³⁺ grows the rise in emission spectra in conjunction with the color temperature increase is another outcome that can be seen in Figure 3.24a.

Put differently, improved emission spectra are the consequence of greater color temperatures. Better color and optical quality can therefore be attained. Since it might be challenging to regulate the quality of WLEDs at high temperatures, this result is crucial for reference in the fabrication of LEDs using $\text{LaAsO}_4:\text{Eu}^{3+}$ phosphor.

The study concludes, in summary, that the high color temperature (8500 K) WLEDs can achieve more consistent color performance when they use the red phosphor. The construction can be chosen based on the specifications provided by the manufacturers. It is okay to have a slight reduction in lumen output if they wish to create WLEDs with excellent color fidelity (Loan & Anh, 2021).

3.2.3 Calculations and discussion

In contrast to earlier research, the optical characteristics of WLED were assessed most closely for materials containing red and green phosphorus. The CRI and CQS trends will increase significantly if the red phosphorus material is layered on top of the yellow and green phosphorus $\text{YAG}:\text{Ce}^{3+}$ layers. This is because the red phosphorus will increase the energy of red light, giving the hues a more uniform appearance. By improving dispersed particles, the phosphorus $\text{Y}_2\text{O}_3:\text{Ho}^{3+}$ substance greatly boosts energy metabolism. Everything will be examined in light of the outcomes of the images below. This work aims to illustrate how red phosphorus can be used to enhance color consistency and green phosphorus can be used to increase luminous flux. The optical characteristics of WLED were assessed most rigorously for materials containing red and green phosphorus, similar to earlier research. The CRI and CQS trends will increase significantly if the red phosphorus material is layered on top of the yellow and green phosphorus $\text{YAG}:\text{Ce}^{3+}$ layers. This is because the red phosphorus will increase the energy of red light, giving the hues a more uniform appearance. The scattered particles are improved by green phosphorus material, which dramatically increases energy metabolism. Everything will be examined in light of the outcomes of the images below.

This research aims to illustrate how luminous flux can be enhanced by using green phosphorus and color uniformity can be improved by using red phosphorus.

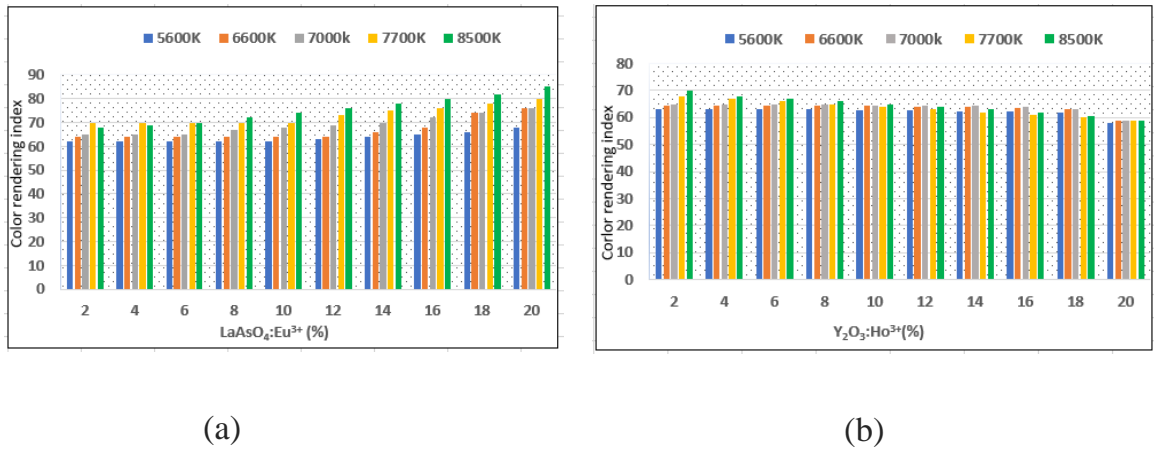


Figure 3.25: Comparison of CRIs of red phosphor (a) and green phosphors (b)

The color rendering index (CRI) comparison between the green and red phosphor materials is shown in Figure 3.25. The results imply that color quality at high temperatures stays constant as red phosphor concentration rises (see Figure 3.25a). Conversely, a little drop in CRI occurs when the concentration of green phosphor rises in tandem with the associated color temperature (CCT) (Figure 3.25b). At a phosphor concentration of 2 %, CRI can get a 60 Ra level. CRI can get a rating of 80 Ra at 20 %. It is obvious that there is a significant difference—up to 20 %. LaAsO₄:Eu³⁺ phosphor can therefore be used to improve CRI.

In summary, Figure 3.25 shows quite clearly that the properties of the green phosphor material are not conducive to improving the color rendering index. Meanwhile, the red phosphorus promotes the improvement in CRI significantly. These findings show that using red phosphor to raise the CRI and green phosphor to raise the output brightness of LEDs with a remote configuration works really well. With the obtained information, the dissertation contributes to enriching the reference for manufacturers seeking optimal improvements for white LED lighting. However, the emitted luminous flux needs to be

considered to determine the appropriate red phosphor concentration. As the concentration of selected red phosphor gradually increases to 10 %, the concentration of yellow phosphor also increases. Due to increased scattering within the phosphor layer, coupled with the higher concentration, the luminous flux results may decrease. This outcome will be further analyzed below.

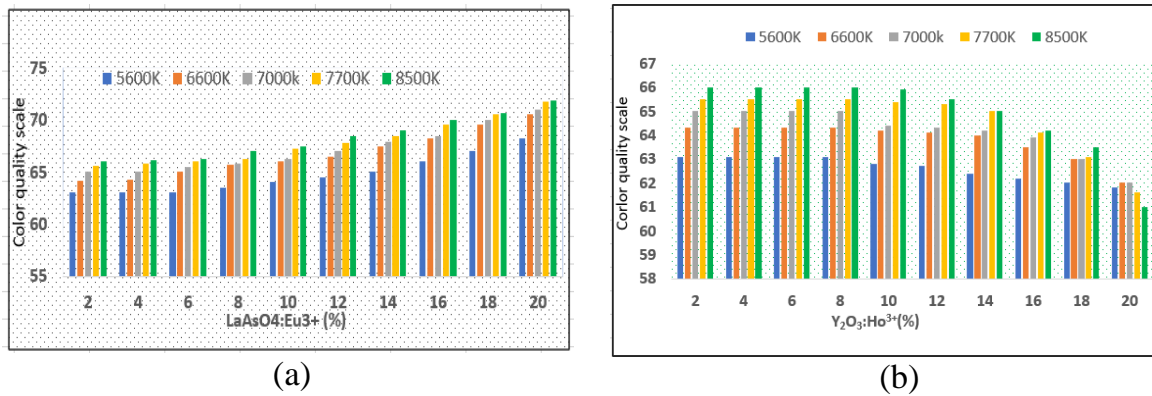


Figure 3.26: Comparison of CQSs of red phosphor (a) and green phosphors (b)

Figure 3.26 illustrates the CQS parameter of the remote-phosphor LEDs at different red and green phosphor concentrations, ranging from 2 % to 20 %.

The data in Figure 3.26a shows an increasing CQS value with a higher red phosphor concentration, indicating the efficiency of using LaAsO₄:Eu³⁺ to achieve the color fidelity of the remote phosphor configuration for white LED. This also serves as an essential reference for manufacturing companies aiming to improve CQS. Additionally, when compared with the results of Liem, Loan, and Tran (2023), the phosphorus LaAsO₄:Eu³⁺ delivers a higher CQS than the LaO_F:Eu³⁺ when monitored under high-CCT conditions.

Particularly, the CQS value reaches 73 Ra with 20 % phosphor LaAsO₄:Eu³⁺, while the application of phosphor LaO_F:Eu³⁺ with the same concentration achieves a CQS of 70 Ra (Liem, Loan & Tran, 2023).

Figure 3.26b depicts the results of the color quality index when adding green phosphor material to the phosphor blend. It is observed that the concentration of the phosphor $\text{Y}_2\text{O}_3:\text{Ho}^{3+}$ has increased from 0 % to 20 %. In this experiment, 20 % was chosen as the stopping point because when the phosphor $\text{Y}_2\text{O}_3:\text{Ho}^{3+}$ concentration exceeded 20 %, there was a significant decrease in color fidelity.

With a 2 % concentration of the phosphor $\text{Y}_2\text{O}_3:\text{Ho}^{3+}$, CQS can reach 66 Ra. With 20 %, CQS can decrease to 61 Ra. These indexes show a significant difference between $\text{Y}_2\text{O}_3:\text{Ho}^{3+}$ phosphor and $\text{LaAsO}_4:\text{Eu}^{3+}$ phosphor.

Thus, the former phosphor cannot be used to improve CQS. This finding is different from those in previous studies that applied green phosphor to LED structures with various correlated color temperatures (CCT) ranging from 5600 K to 8500 K, signifying practical applications of this dissertation.

It can be noted that CQS decreases with the concentration of $\text{Y}_2\text{O}_3:\text{Ho}^{3+}$ phosphor at any CCT, indicating the potential for its application in white LED lights. The increase in green light within the phosphor layer leads to a more pronounced color variation, and the color quality of CQS decreases.

However, the luminous flux needs to be considered to determine the appropriate percentage of concentration. When the concentration of $\text{Y}_2\text{O}_3:\text{Ho}^{3+}$ increases gradually to 10 %, the concentration of yellow phosphor decreases. As the scattering process occurs repeatedly within the phosphor layer, together with the increased concentration, the luminous flux potentially increases.

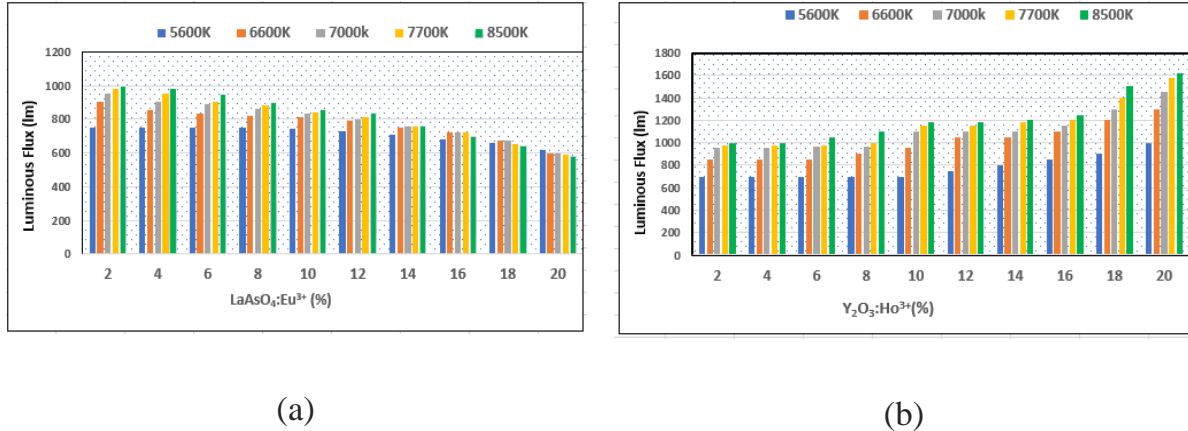


Figure 3.27: Comparison of LF of red phosphors (a) and green phosphors (b) of remote structure

In Figure 3.27, you can see how well the phosphor material LaAsO₄:Eu³⁺ and the phosphor material Y₂O₃:Ho³⁺ work together as a mixed phosphor blend. Selecting a 2 % concentration of the phosphor LaAsO₄:Eu³⁺ results in the best outcome (see Figure 3.27a). This means that a 2 % concentration of the phosphor LaAsO₄:Eu³⁺ will give off the lightest from the red-yellow remote phosphor structure. As discussed earlier, increasing the phosphor LaAsO₄:Eu³⁺ concentration significantly contributes to improving the Color Rendering Index (CRI) and Color Quality Scale (CQS) but does not increase luminous efficacy. Conversely, the phosphor material Y₂O₃:Ho³⁺ at the highest concentration is chosen to achieve optimal luminous efficacy, as shown in Figure 3.27b. In a previous study by Hanh, Loan, and Anh (2020), the phosphor material NaYF₄:Er³⁺Yb³⁺ was utilized and achieved a maximum luminous efficacy of 1000 Lm. However, in this dissertation, the luminous efficacy reaches 1600 Lm when using phosphorus Y₂O₃:Ho³⁺, 600 Lm greater than when using the reported NaYF₄:Er³⁺Yb³⁺ phosphor. This result is valuable for manufacturers aiming to enhance the luminous efficacy of white LED lighting.

3.3 Experiment for testing the simulation results

3.3.1 Introduction purpose and some notes on limitation of experimental conditions

It is important to confirm the simulation result by experiment. However, due to some limitation on finance and facility, so it is not possible to do the experiment as same as simulation. With my best effort, some related experiment has been conducted.

In this section, some experiments which are suitable to currently conditions Vietnam are conducted to test the result in simulation which including behavior of luminous flux, and CRI at the similar value of CCT.

3.3.2 Summary of some simulation results of different configuration

For convenience in follow content, firstly a summary of some simulation results in previous sections of different configuration are summarized in follow Tables 3.4 and Table 3.5

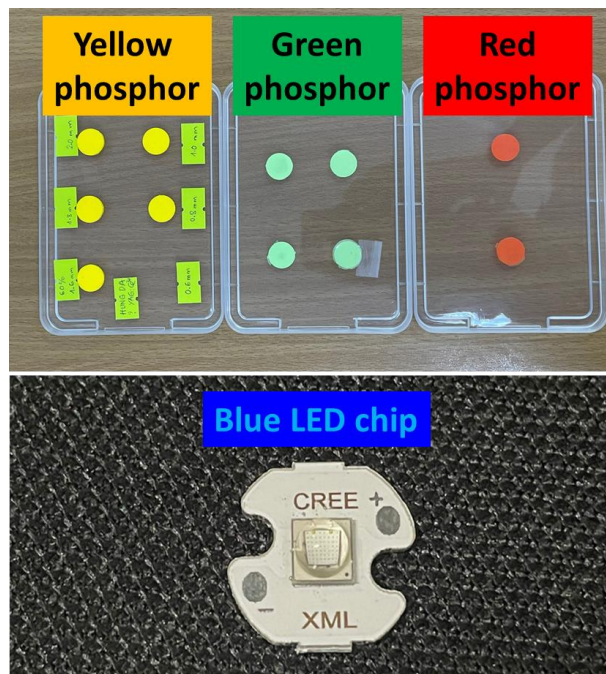
Table 3.4: Comparison of CRI and LF between YL and YRL structure

Structure/configuration	CRI	Luminous Flux (Φ)	Note on behavior/change
Yellow	CRI	Φ	Configuration “Yellow+Red” showed a higher CRI, lower flux than configuration yellow
Yellow+Red	CRI +	$\Phi -$	

Table 3.5: Comparison of CRI and LF between YRL and YGRL structures

Structure/configuration	CRI	Luminous Flux (Φ)	Note on behavior/change
Yellow+Red	CRI	Φ	Configuration “Yellow +Green+Red” showed a lower CRI, higher flux than configuration “yellow+Red”
Yellow+Green+Red	CRI -	$\Phi +$	

3.3.3 Introduction of used material in the experiment

**Figure 3.28: Some used material in the experiment**

In the experiment, different kind of phosphor includes yellow phosphor powder (YAG: Ce^{3+}), red phosphor, and green phosphor are utilized. The blue chip is used as an excitation sources. These used material in the experiment are shown in the Figure 3.28

3.3.4 Experiment results without using integrating sphere

Results from an experiment conducted without the use of an integrating sphere are shown in this section. Since the lab did not have an integrating sphere when this experiment was performed, it was set up as Figure 3.29 illustrates.

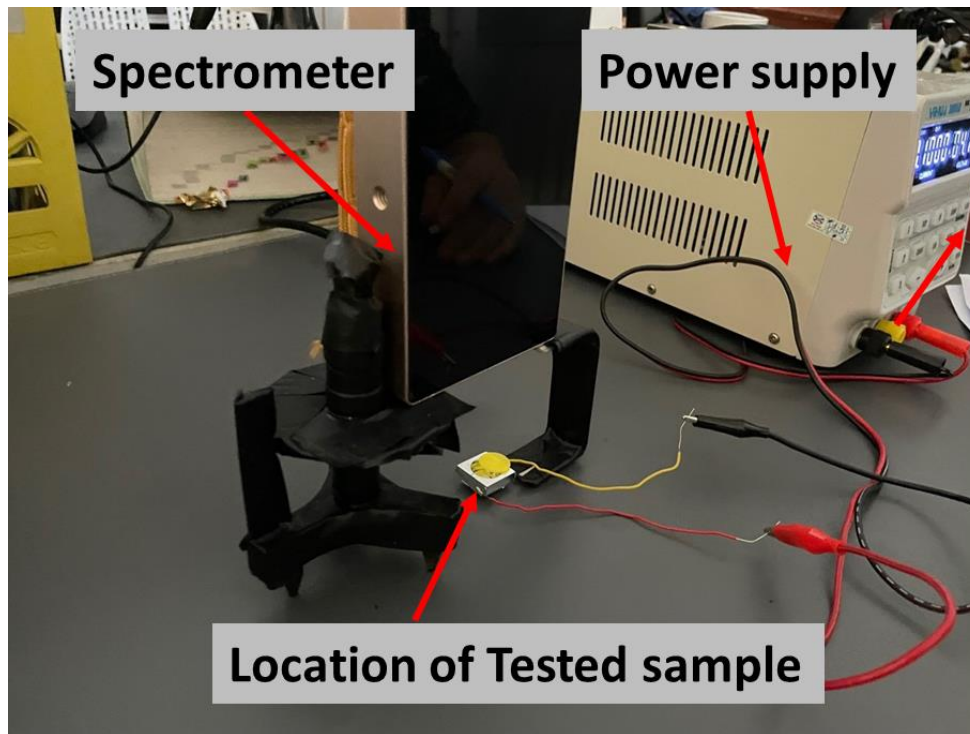


Figure 3.29: The experiment setup without using integrating sphere

The experiment to compare two configurations of "Yellow+Red" and "Yellow" is carried out based on the arrangement without the use of an integrating sphere. Figures 3.30 and 3.31 present the findings.

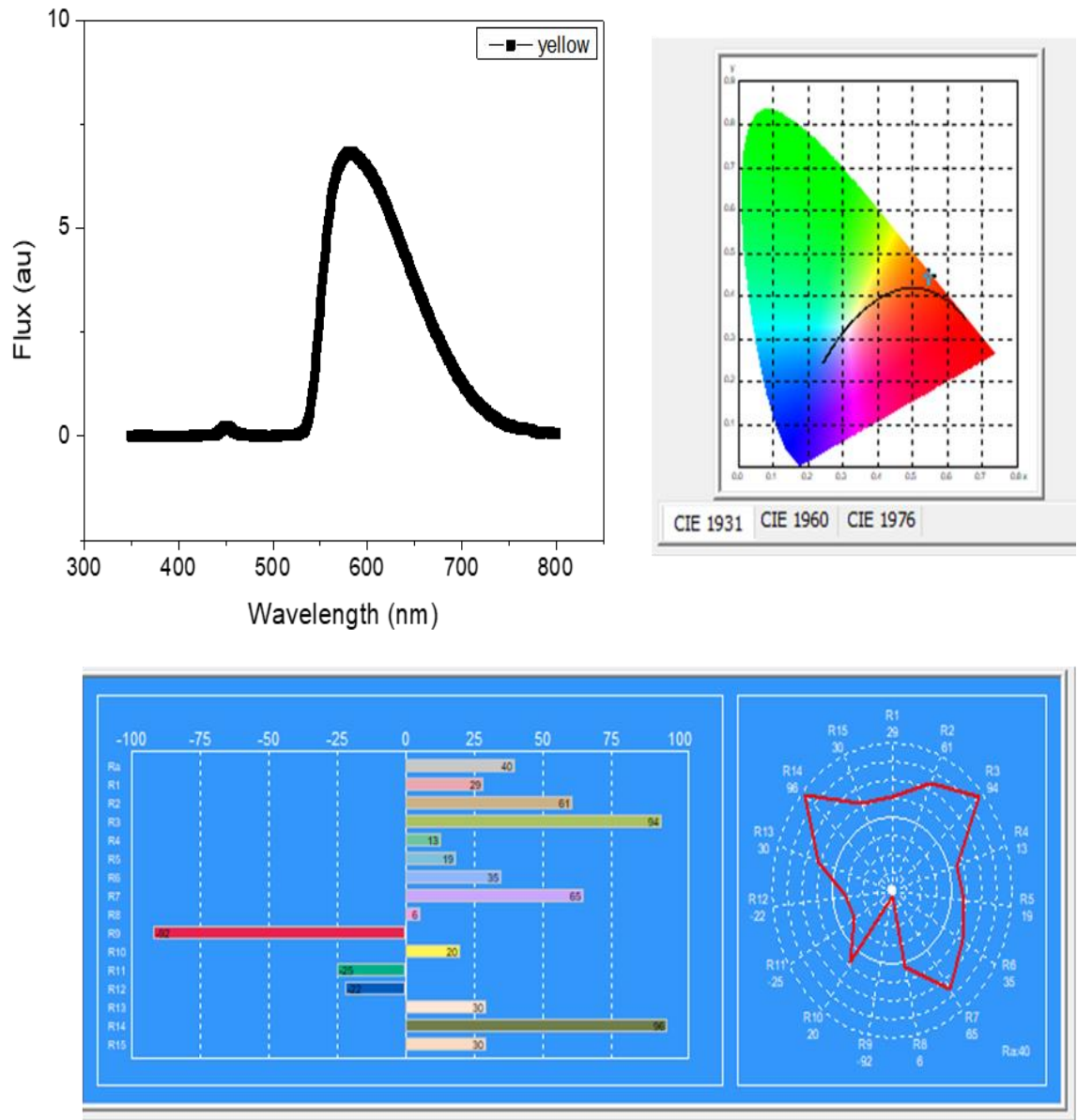


Figure 3.30: Properties of configuration "Yellow" obtained from experiment

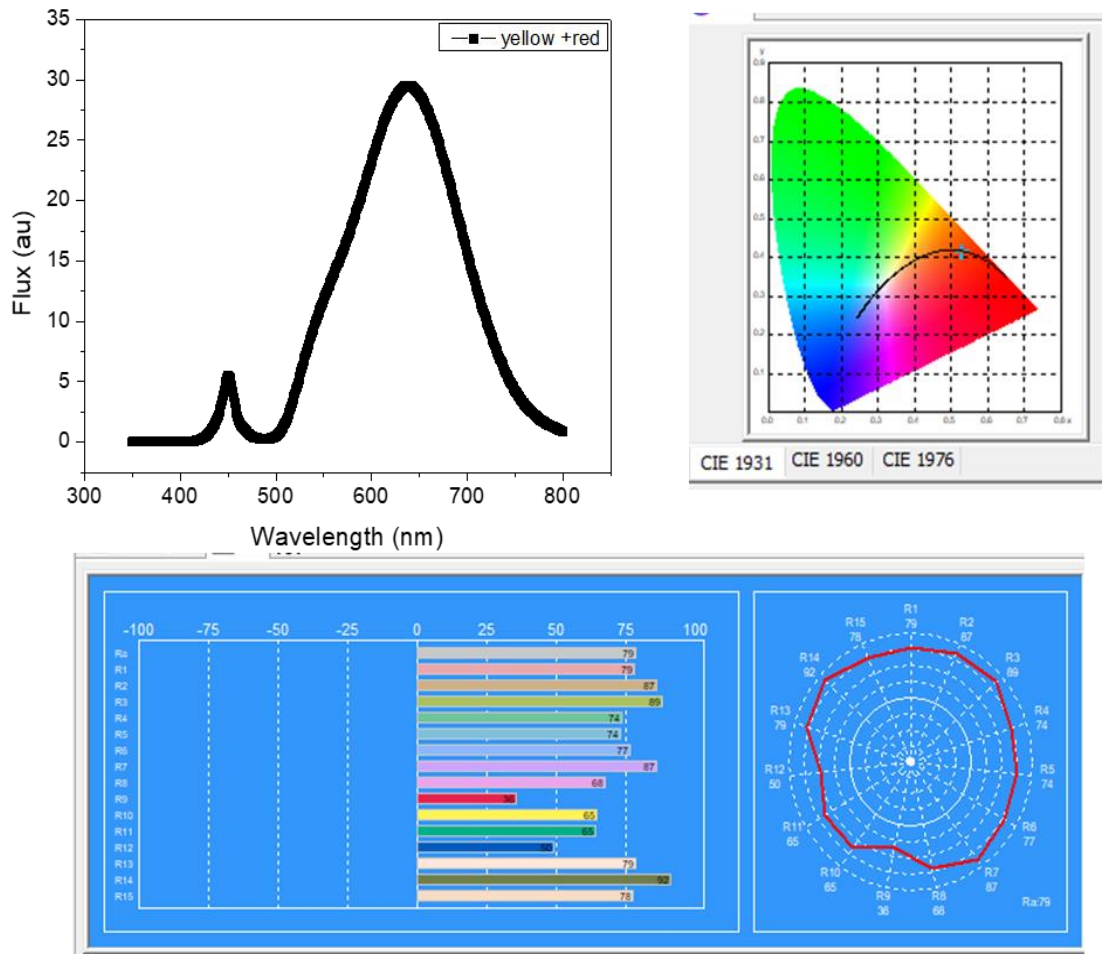


Figure 3.31: Properties of configuration “Yellow+Red” obtained from experiment

The comparison between the two configurations of "Yellow+Red" and "Yellow" is displayed in Fig. 3.32 and Table 3.6 to help with comprehension. The "Yellow+Red" arrangement exhibits a stronger emission spectrum than the "Yellow" configuration at comparable CCT values.

Table 3.6 demonstrated that the CRI value for the "Yellow+Red" configuration is greater than the CRI value for the "Yellow" configuration.

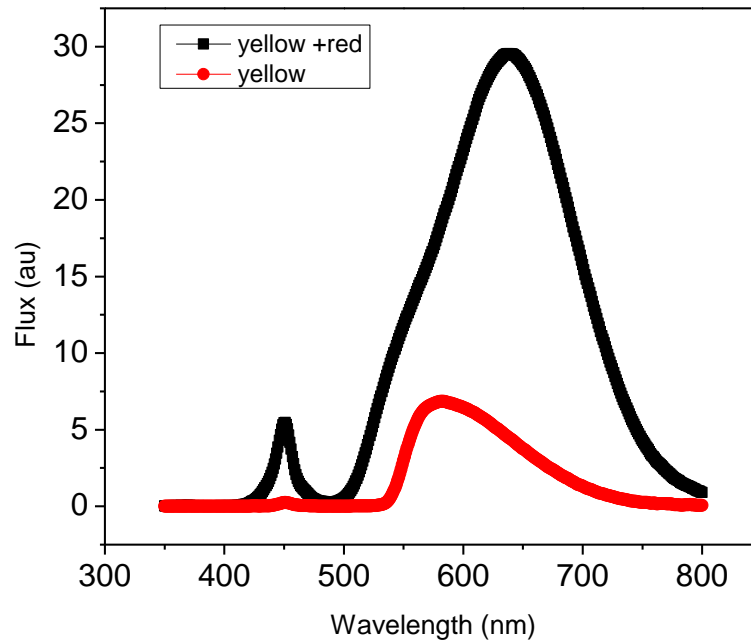


Figure 3.32: Comparison of spectra between YL and YRL structure

Table 3.6: Comparison between configuration of “Yellow” and “Yellow+Red”

Configuration	CCT (K)	Illuminant (lx)	CRI
Yellow	1986	261	40.3
Yellow +Red	1992	1015	79.4

3.3.5 Experiment results with using integrating sphere

The experiment findings using an integrating sphere are shown in this section. An experiment with an integrating sphere was feasible at the time this experiment was carried out since the lab had already imported one. Figure 3.33 depicts the setup for the experiment.

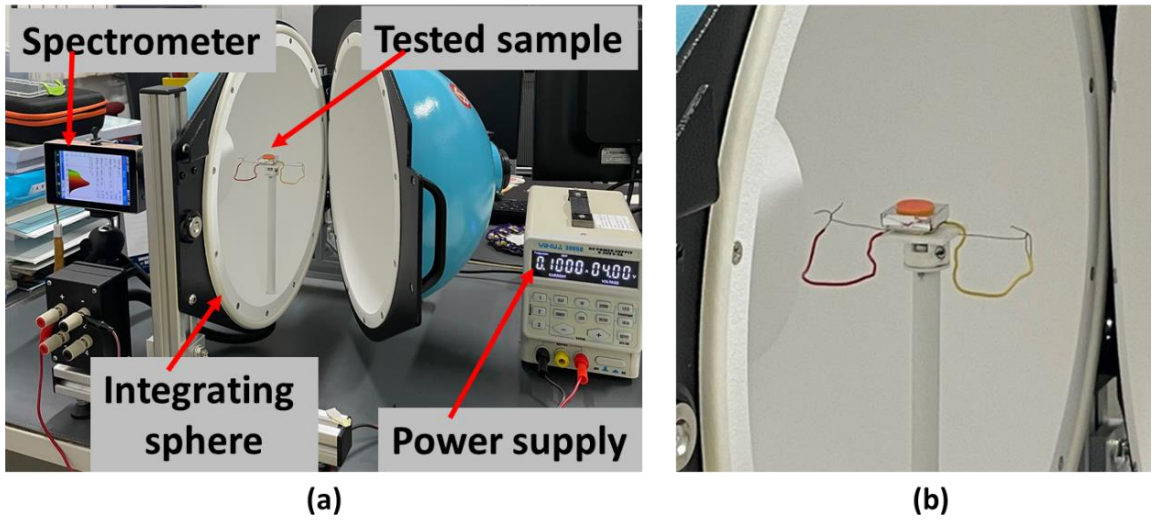


Figure 3.33: Experiment setup with using integrating sphere

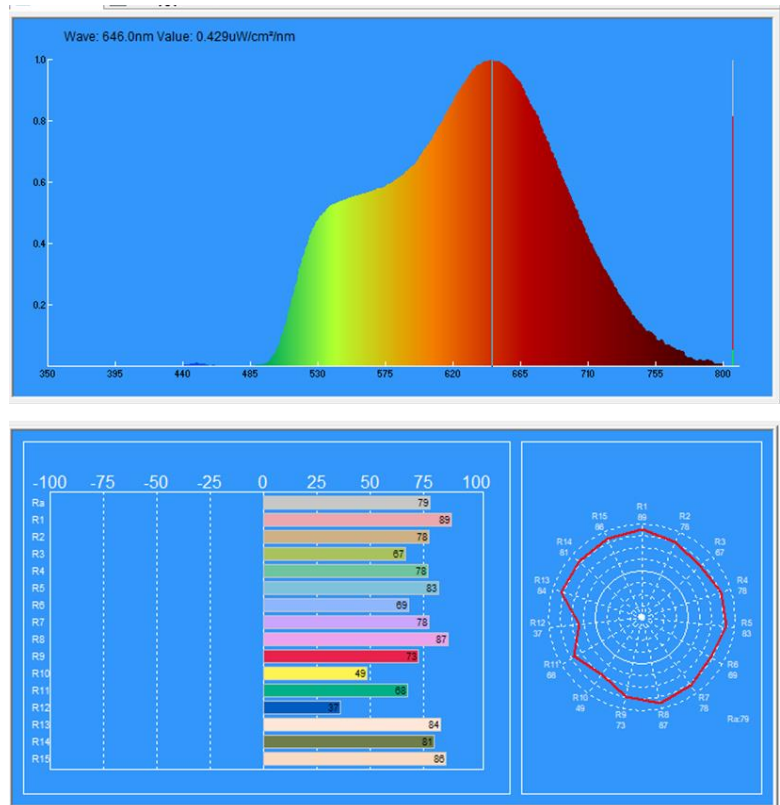


Figure 3.34: Properties of configuration “Yellow+Red” obtained from experiment

An experiment was done to compare two configurations of "Yellow+Green+Red" and "Yellow+Red" at a same CCT value. The experiment was based on the setup with an integrating sphere as illustrated in Figure 3.33. The Figures 3.34 and 3.35 display the results.

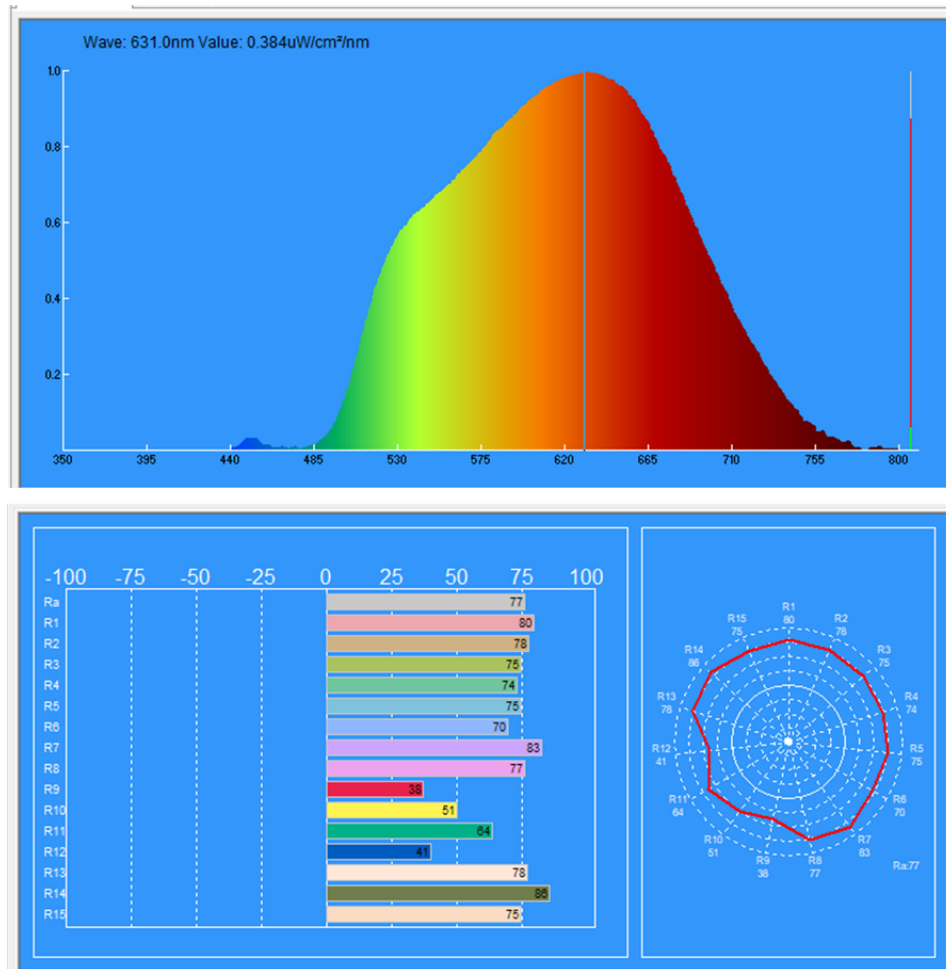


Figure 3.35: Properties of configuration "Yellow+Green+Red" obtained from experiment

In order to facilitate comprehension of the differences between the two configurations of "Yellow+Green+Red" and "Yellow+Red," Fig. 3.36 and Table 3.7 have comparisons between them. For a better understanding between two configurations

of “Yellow+Green+Red” and configuration “Yellow+Red”, the comparison is shown in Fig. 3.36 and Table 3.7.

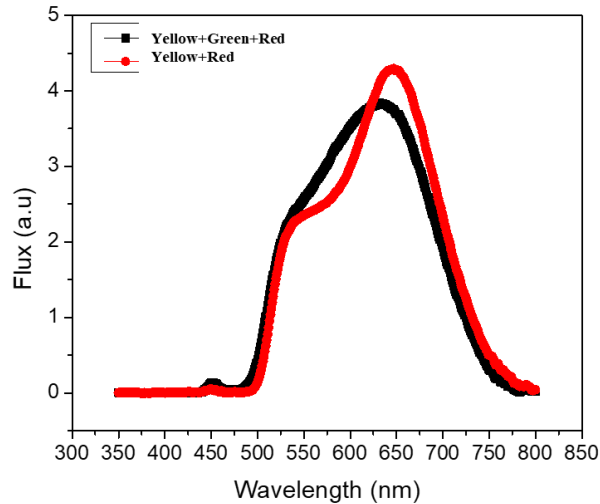


Figure 3.36: Comparison of emission spectrum between configuration of “Yellow+Red” and “Yellow+Green+Red”

The "Yellow+Green+Red" configuration exhibits a stronger emission spectrum than the "Yellow+Red" configuration at a comparable value of CCT of 2500 K. Nevertheless, the CRI value of the "Yellow+Green+Red" arrangement is lower than that of the "Yellow+Red" configuration.

Table 3.7: Comparison between configuration of “Yellow+Red” and “Yellow+Green+Red”

Configuration	CCT(K)	CRI	E (lux)
Yellow+Green+Red	2552	76.6	187.2
Yellow+Red	2392	78.5	167

3.3.6 Comments on obtained of experiment results and some results of the simulation for different configuration

According to the experiment findings obtained for CCT value 2000 K, configuration "Yellow+Red" had a lower flux and greater CRI than configuration "Yellow." In comparison to configuration "Yellow + Red," configuration "Green + Yellow + Red" displayed a lower CRI and a larger flux in the experiment results obtained for the CCT value of 2500 K.

Behavior in CRI and Flux in experiments generally resembles simulation behavior. The same behavior of CRI and Flux in the experiment has confirmed the simulation results, even though all of the conditions in the experiment were different from those in the simulation.

3.4 Summary

This chapter covers using LightTools 9.0 software to perform simulation results and validate them against data from international publications. Furthermore, the outcomes demonstrate that compared to a single-layer or two-layer distant structure, a three-layer remote structure generates more light. Additionally, the simulations clearly demonstrate the results of using different phosphor materials with different targets. It is especially recommended to utilize green phosphor material in conjunction with a yellow phosphor layer that is the right size and concentration for the distant structure in order to maximize the luminous flux. When red phosphor material is required to increase color rendering index and color consistency, that is the best course of action. Specifically, the experimental findings in this chapter show how accurate the trend simulated in the earlier studies was.

CHAPTER 4. RESEARCH ON SCATTERING ENHANCEMENT MATERIALS TO INCREASE THE OPTICAL CHARACTERISTICS OF LED LAMPS

4.1 MIE scattering theory for the approach using scattering enhancement particles

The Mie scattering equation used employs Maxwell's equations exclusively for the scattering of spherical particles. In this context, the theory is utilized to elucidate the particles contained in phosphor materials, with the aim of increasing the output lumen. Given small particle size and low concentration, the use of this theory appears to be the most optimal approach.

Furthermore, this theory distinctly illustrates the backscatter of light, a crucial factor in determining a reasonable particle size and aperture to prevent backscattered energy from causing optical loss. There is no text provided. Note that the Mie scattering theory does not have a maximum size restriction, and for larger particles, convergence occurs to the geometric optical limit (Hanh et al., 2009).

4.1.1 Influences of different particle sizes on the light scattering properties

According to the Mie hypothesis, bigger particles produce more rays that are forward-scattered and concentrate on a single angle. Smaller particle sizes, on the other hand, uniformly spread scattered rays from all directions. This implies that smaller particles lessen the likelihood of the yellow ring phenomena and improve color quality more effectively. It becomes essential to improve the distribution of blue light in these periphery areas because this phenomenon is mainly confined to the borders and involves little blue light (Craig & Huffman, 1998).

Thus, minute particles contribute in the balanced mixing of blue and yellow light by facilitating the equal dispersion of blue light amplitude in all directions. Larger particles, on the other hand, have a tendency to scatter blue rays primarily in the middle, leading to an uneven light mixing (see Figure 4.1).

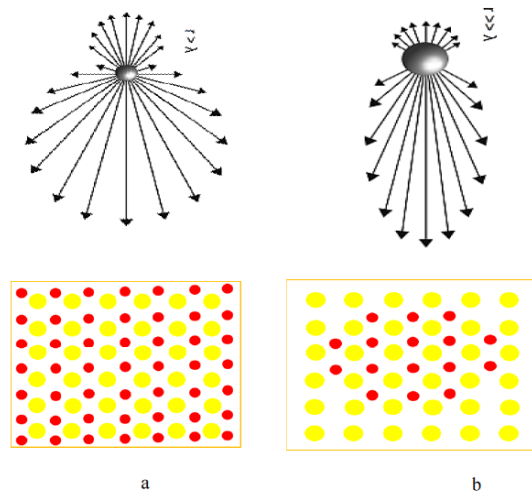


Figure 4.1: Effect of particle size on scattered rays (shows that scattered rays transmit more evenly in the phosphor layer in figure a than in figure b)

Using small particles improves scattering, leading to more equal angular scattering and smaller backscatter rays, in accordance with the established Mie-scattering hypothesis (see Figure 4.1).

As a result, this method makes it easier to achieve improvements in color consistency and lessen the yellow ring problem. Important scattering characteristics that directly affect the particle's capacity to scatter will be covered in detail in the paragraphs that follow.

4.1.2 Scattering coefficients

The scattering coefficient is the first important distribution-related metric to grasp after understanding the particle scattering concept. This parameter shows how many dispersed rays are created inside the particle as a result of the interaction between the electrons within the particle and the incident ray, and it might be more or less.

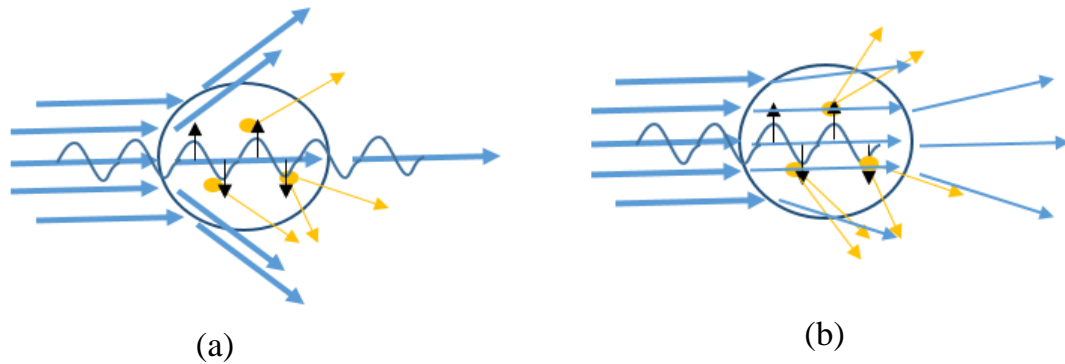


Figure 4.2: (a)The particle with high scattering coefficient.(b)The particle with low scattering coefficient

The blue rays indicate the energy from the blue chip, while the gold rays indicate the energy from the phosphor. When there is a large attenuation factor, the energy required to collide with the yellow phosphor particles is considerably reduced at the LED's output. Once this bright flux is used up, only a tiny amount of blue rays remains. A larger scattering coefficient indicates more incident rays scattered beyond the particle or the particle's propensity to reject or quickly expel the incident rays (see Figure 4.2a).

In contrast are particles with a low scattering coefficient. Most of the incident light in this case strikes the particle, travels through it, and starts to break the electrons, releasing light energy. A significant amount of light is scattered outward due to interference with the incident wavelength. But because of the strong interaction, when they disperse, so does their scattered energy (refer to Figure 4.2b). Particles with a low dispersing index exhibit an increase in the number of scattered rays while experiencing a decrease in the quantity of scattering energy. Bigger particles, due to their reduced ability to absorb or disperse light, increase the amount of light that passes through, a phenomenon known as light flux.

$$\mu_{\text{sca}}(\lambda) = \int N(r)C_{\text{sca}}(\lambda, r)dr \quad (4.1)$$

The dispersion coefficient, $\mu_{sca}(\lambda)$, can be calculated using Equation 4.1 (Sheng & Liu, 2011). It says that $N(r)$ is the number density distribution of particles (mm^{-3}), $C_{sca}(\lambda, r)$ is the scattering cross-sections (mm^2), λ is the wavelength of the incoming light's emission (nm), and r is the radius of the protons. A higher scattering coefficient results in a bigger region of scattering due to the proportional relationship between μ_{sca} and C_{sca} . Software commonly uses this equation to calculate and display the scattering coefficient. Now, let us examine and draw conclusions from the simulations presented below, which demonstrate the impact of the scattering coefficient on particle size.

Table 4.1: Analysis the influence of SiO₂ particle size on the scattering coefficient

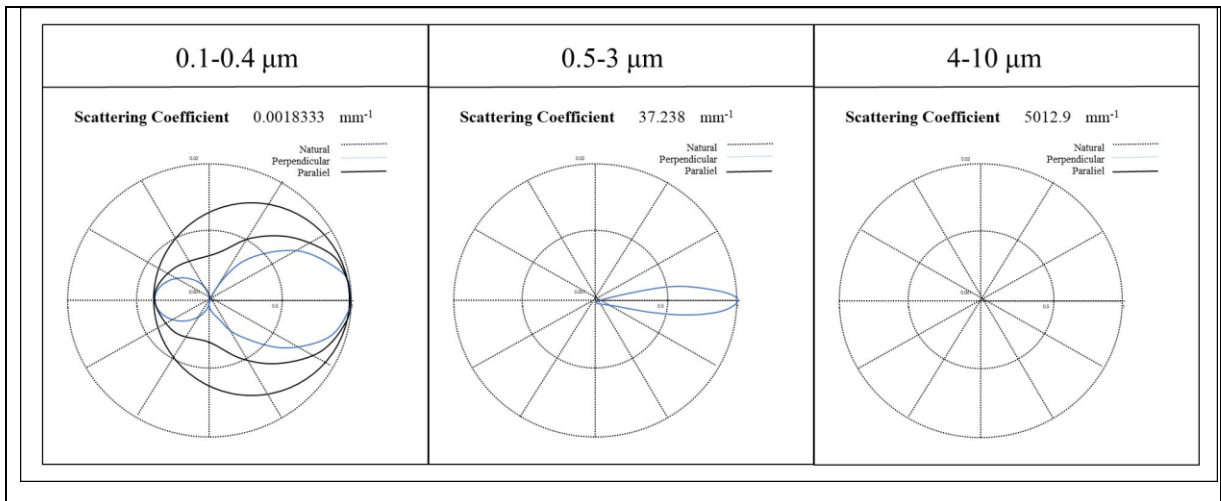


Table 4.1, which summarizes the scattering particle test results, highlights the importance of small particle size in accordance with the MIE scattering theory to boost luminous flux. Employing particles with small dimensions becomes crucial for enhancing the performance of WLEDs. A small scattering coefficient contributes to the generation of more scattered rays compared to larger particles, ultimately improving luminous efficiency. The abundance of scattering leads to a significant enhancement in light energy, minimizing energy loss during transfer to material particles mixed with phosphors. This inclination to increase particle scattering for enhanced luminous flux output aligns seamlessly with the physical properties governing the process.

4.1.3 Reduced scattering coefficient

The particle size has a direct relationship with the scattering attenuation coefficient. Greater attenuation due to larger particle sizes results in less light energy being produced. Stated differently, the energy of the scattering rays produced by larger particles is reduced, rendering them nearly incapable of propagating to additional particles. They don't have enough energy, even if they are able to transmit, to keep interacting and producing scattered rays. Larger particle sizes hence result in a higher scattering attenuation coefficient and a lower amount of scattered energy (see Figure 4.3a). It is important to understand that scattering energy here refers to the number of rays generated inside the particle rather than the power of the number of rays outside the particle.

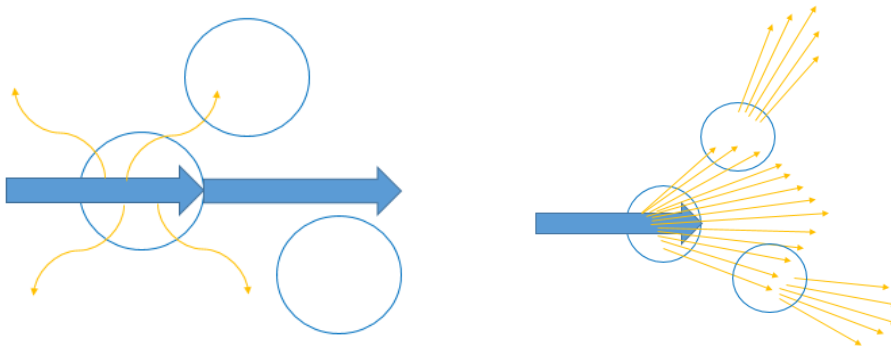


Figure 4.3: (a).Simulation the scattering attenuation of large particle size.(b)Simulation the scattering attenuation of small particle size

Conversely, because they generate more dispersed rays, small-sized particles show a low scattering attenuation coefficient. Compared to larger particles, there are more rays that are passed straight through the particle, even though some may still be carried in other directions.

Furthermore, the light that collides with small-sized particles exhibits a different linear trend than that of large-sized particles, leading to reduced attenuation, because the

majority of the incident light's energy is transformed into a scattered energy beam (see Figure 4.3b). Moreover, a clearer understanding of why straightly propagated scattered rays consume less energy compared to scattered rays transmitted at different angles can be obtained by referring to Figure 4.4, which is another outcome of my research. Put simply, when you recharge two identical vehicles, the one that takes a direct route from point A to point B consumes less fuel compared to the one that takes a detour from point A to point C and then returns to point B.

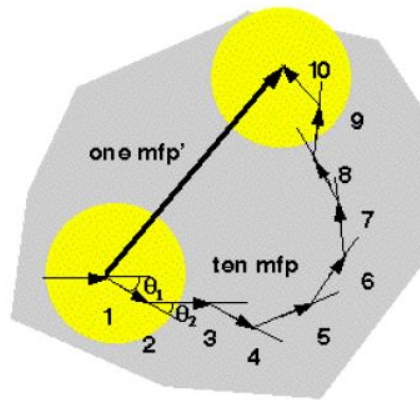


Figure 4. 4: Illustrate the attenuation of scattered energy between particles
The scattering reduction factor is calculated according to the following formula

$$\delta_{sca} = \mu_{sca}(1 - g) \quad (4.2)$$

The reduction scattering coefficient, δ_{sca} , μ_{sca} the scattering coefficient, and the anisotropy factor, g , are all found in Equation 4.2. This formula shows that attenuation increases with a higher scattering coefficient since the reduction scattering coefficient is directly proportional to the scattering coefficient. Software for determining the reduction scattering coefficient also uses this equation.

Table 4.2: Relationship between scattering coefficient and scattering attenuation coefficient

Particle size (μm)	Scattering coefficient (μm^{-1})	Reduction scattering coefficient (μm^{-1})																								
0.1	<table border="1"> <caption>Scattering coefficient (μs) vs Wavelength (nm) for 0.1 μm particles</caption> <thead> <tr> <th>Wavelength (nm)</th> <th>μs (mm^{-1})</th> </tr> </thead> <tbody> <tr><td>380</td><td>0.20</td></tr> <tr><td>480</td><td>0.12</td></tr> <tr><td>580</td><td>0.08</td></tr> <tr><td>680</td><td>0.05</td></tr> <tr><td>780</td><td>0.04</td></tr> </tbody> </table>	Wavelength (nm)	μs (mm^{-1})	380	0.20	480	0.12	580	0.08	680	0.05	780	0.04	<table border="1"> <caption>Reduction scattering coefficient ($\mu\text{s}'$) vs Wavelength (nm) for 0.1 μm particles</caption> <thead> <tr> <th>Wavelength (nm)</th> <th>$\mu\text{s}'$ (mm^{-1})</th> </tr> </thead> <tbody> <tr><td>400</td><td>0.020</td></tr> <tr><td>480</td><td>0.017</td></tr> <tr><td>580</td><td>0.014</td></tr> <tr><td>680</td><td>0.012</td></tr> <tr><td>800</td><td>0.011</td></tr> </tbody> </table>	Wavelength (nm)	$\mu\text{s}'$ (mm^{-1})	400	0.020	480	0.017	580	0.014	680	0.012	800	0.011
Wavelength (nm)	μs (mm^{-1})																									
380	0.20																									
480	0.12																									
580	0.08																									
680	0.05																									
780	0.04																									
Wavelength (nm)	$\mu\text{s}'$ (mm^{-1})																									
400	0.020																									
480	0.017																									
580	0.014																									
680	0.012																									
800	0.011																									
1	<table border="1"> <caption>Scattering coefficient (μs) vs Wavelength (nm) for 1 μm particles</caption> <thead> <tr> <th>Wavelength (nm)</th> <th>μs (mm^{-1})</th> </tr> </thead> <tbody> <tr><td>420</td><td>585</td></tr> <tr><td>480</td><td>590</td></tr> <tr><td>580</td><td>530</td></tr> <tr><td>680</td><td>455</td></tr> <tr><td>780</td><td>390</td></tr> </tbody> </table>	Wavelength (nm)	μs (mm^{-1})	420	585	480	590	580	530	680	455	780	390	<table border="1"> <caption>Reduction scattering coefficient ($\mu\text{s}'$) vs Wavelength (nm) for 1 μm particles</caption> <thead> <tr> <th>Wavelength (nm)</th> <th>$\mu\text{s}'$ (mm^{-1})</th> </tr> </thead> <tbody> <tr><td>380</td><td>4.38</td></tr> <tr><td>480</td><td>4.18</td></tr> <tr><td>580</td><td>4.02</td></tr> <tr><td>680</td><td>3.88</td></tr> <tr><td>780</td><td>3.75</td></tr> </tbody> </table>	Wavelength (nm)	$\mu\text{s}'$ (mm^{-1})	380	4.38	480	4.18	580	4.02	680	3.88	780	3.75
Wavelength (nm)	μs (mm^{-1})																									
420	585																									
480	590																									
580	530																									
680	455																									
780	390																									
Wavelength (nm)	$\mu\text{s}'$ (mm^{-1})																									
380	4.38																									
480	4.18																									
580	4.02																									
680	3.88																									
780	3.75																									
10	<table border="1"> <caption>Scattering coefficient (μs) vs Wavelength (nm) for 10 μm particles</caption> <thead> <tr> <th>Wavelength (nm)</th> <th>μs (mm^{-1})</th> </tr> </thead> <tbody> <tr><td>420</td><td>50240</td></tr> <tr><td>480</td><td>50330</td></tr> <tr><td>580</td><td>50160</td></tr> <tr><td>680</td><td>50180</td></tr> <tr><td>780</td><td>50430</td></tr> </tbody> </table>	Wavelength (nm)	μs (mm^{-1})	420	50240	480	50330	580	50160	680	50180	780	50430	<table border="1"> <caption>Reduction scattering coefficient ($\mu\text{s}'$) vs Wavelength (nm) for 10 μm particles</caption> <thead> <tr> <th>Wavelength (nm)</th> <th>$\mu\text{s}'$ (mm^{-1})</th> </tr> </thead> <tbody> <tr><td>420</td><td>805</td></tr> <tr><td>480</td><td>795</td></tr> <tr><td>580</td><td>725</td></tr> <tr><td>680</td><td>635</td></tr> <tr><td>780</td><td>590</td></tr> </tbody> </table>	Wavelength (nm)	$\mu\text{s}'$ (mm^{-1})	420	805	480	795	580	725	680	635	780	590
Wavelength (nm)	μs (mm^{-1})																									
420	50240																									
480	50330																									
580	50160																									
680	50180																									
780	50430																									
Wavelength (nm)	$\mu\text{s}'$ (mm^{-1})																									
420	805																									
480	795																									
580	725																									
680	635																									
780	590																									

Table 4.2 indicates the use of the Mie simulator program to simulate the scattering and dispersion absorption coefficients for three specific particle sizes. The graphic demonstrates that there is a direct correlation between larger particles and higher dispersion coefficients. Similarly, the resultant absorption coefficient also increases.

Additionally, there is a decrease in the amount of energy scattered as particle sizes become smaller, especially within the wavelength range of 380–780 nm. The average cosine phase function, also known as the scattering angle, is a measure of the extent of the particle's angular spread in space after emitting a dispersed ray (refer to Figure 4.5). It speaks specifically of the forward-scattered ray's scattering angle. Smaller particles produce a more consistent scattering angle, as seen in Figures 4.3 and 4.4, suggesting that the scanning range of the scattered ray's changes less. Conversely, the scanning area is significantly altered by increasing particle sizes. The energy of the scattered beams is increased with smaller particles. Large particles, on the other hand, tend to travel at different angles before they reach other particles because their scattered rays contain less energy, as shown in Figure 4.5.

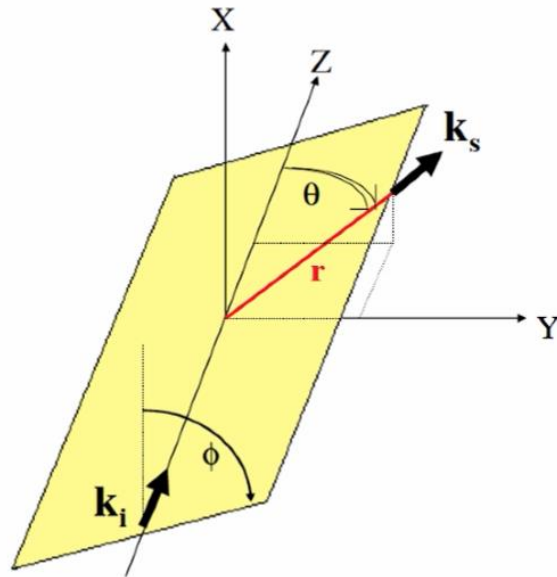


Figure 4.5: Represent the scattering angle in a plane

$$p(\theta, \lambda, r) = \frac{4\pi\beta(\theta, \lambda, r)}{k^2 C_{sca}(\lambda, r)} \quad (4.3)$$

A phase relationship between particles, denoted as $p(\theta, \lambda, r)$, in Equation 4.3 can be calculated using the method described by Sheng and Liu in their 2011 publication. Here, k represents the wave vector, $C_{sca}(\lambda, r)$ denotes the scattered section sizes in square millimeters (mm^2), λ represents the wavelength of incoming light in nanometers (nm), r represents the radius of the phosphor particle, and θ represents the scattering angle. The dimensionless dispersion function is represented by $\beta(\theta, \lambda, r)$. According to this equation, the scattering cross-section increases as the particle's diameter lowers or the scattering coefficient rises. A higher scattering coefficient leads to a decreased scattering angle because of the inverse relationship between this value and the scattering angle. Furthermore, Figures 4.6 and 4.7 below show the link between scattering angle and scattering coefficient.

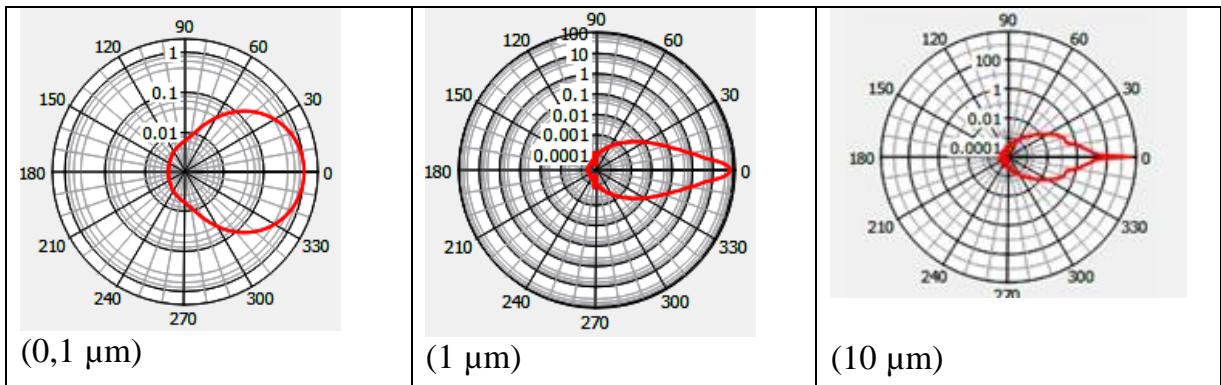


Figure 4.6: The scattering angle of different particles sizes

Mie scattering software was used to simulate the results, which are shown in Figure 4.6. The results show that bigger scattering angles are caused by smaller particle sizes, and this increases the output flux. Interestingly, a $0.1 \mu\text{m}$ particle size produces an exceptionally broad scattering angle, confirming that LED brightness tends to rise.

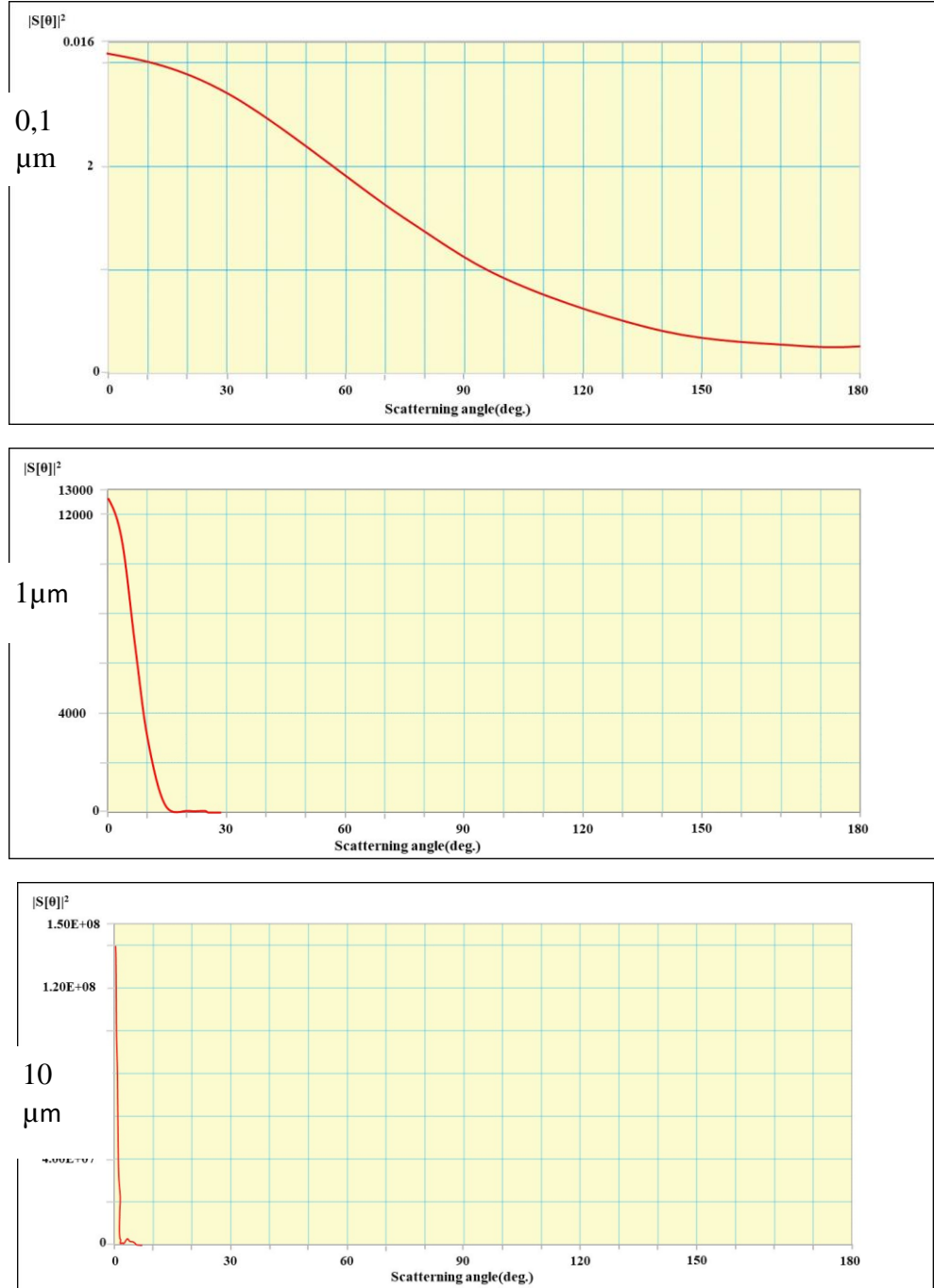


Figure 4.7: The relationship between scattering coefficient and scattering angle

Furthermore, a wider scattering angle makes it easier to eliminate and results in less eye refraction by facilitating sharper backward scattering. By assisting in the removal of the gold ring effect, this phenomenon encourages more energy to be sent forward. The results of modeling the correlation between scattering angle and scattering coefficient in the Mie scattering formula are presented in Figure 4.7.

The results indicate that a higher scattering coefficient corresponds to a smaller scattering angle, leading to a sharp reduction in output luminous flux. This decrease in luminous flux is accompanied by an increase in the yellow ring phenomenon due to the excessively small scanning angle, resulting in poor light quality. Conversely, a smaller scattering coefficient results in a larger scattering angle, allowing more energy to move forward. Consequently, the luminous flux increases, and the undesirable gold ring phenomenon can be easily eliminated. Furthermore, figure 4.7 vividly illustrates that smaller particle sizes correspond to larger scattering angles, resulting in smaller scattering coefficients. This relationship contributes to an increase in luminous flux, as the entire energy portion transitions to the front of the LED.

Through simulation with the Mie simulator software and Mie plot, the relationship between the scattering angle and scattering coefficient is revealed. To be more precise, the scattering angle is smaller for larger particle sizes, which correspond to higher scattering coefficients (see figure 4.6). On the other hand, a bigger scattering angle corresponds to a larger luminous flux that is emitted, and smaller particle sizes are inversely proportional to the scattering angle. The findings of Mie scattering theory are consistent with this result.

Figure 4.7 presents the correlation between the scattering angle and scattering attenuation coefficient. A greater scattering angle corresponds to a smaller scattering attenuation coefficient, favoring the luminous flux surface. Notably, the table underscores that small particle sizes achieve a small scattering attenuation coefficient. The Mie Plot software consistently reveals that employing small-sized particles, in line

with the Mie scattering formula, results in higher luminous flux compared to large-sized particles. The next section will delve into advanced particle scattering using small particle sizes in simulation, with the anticipated outcome being a marked improvement in luminous flux.

4.2 Scattering enhancement particles

In order to conduct a comprehensive analysis of four distinct types of scattered particles, it is necessary to have a solid understanding of the fundamental scattering parameters, namely the diffusion angle, dispersion attenuated factor, and scattering coefficient. To achieve this, the utilization of Mie simulation programs is vital. The objective of this analytical approach is to ascertain the level of precision in the study's findings.

Table 4.3: The parameters of scattering enhancement particles

Particles Types	Refractive Index	Weight (g/m ³)
CaCO ₃	1.86	2.83
CaF ₂	1.44	3.18
SiO ₂	1.54	2.56
TiO ₂	2.6	4.23

The article "Utilizing CaCO₃, CaF₂, SiO₂, and TiO₂ particles to enhance color homogeneity and luminous flux of WLEDs" focuses on explaining the details of the four types of scattering enhancement particles. The two most important factors that determine the quality of phosphor-converted LEDs (pc-LEDs) are chromatic uniformity and luminous efficiency (Loan & Anh, 2020). These factors are thoroughly investigated. As a result, this work is useful in the selection of particles that improve the lighting characteristics of high-performance pc-LEDs. Lighting devices use a combination of

yellow phosphor YAG:Ce³⁺ and scattering enhancement particles (SEPs) like CaCO₃, CaF₂, SiO₂, and TiO₂ (Table 4.3). The LightTools program is used to aid with the first optical simulations, and Mie theory is then applied to compute and validate the results. The computations are centered on the scattering characteristics of SEPs in the 455 nm - 595 nm wavelength range. Interestingly, TiO₂ scattering studies show that it is the best option for improving the color quality of pc-LEDs when compared to other SEPs; however, this comes at the expense of a notable drop in luminous flux as concentration increases. SiO₂ particle integration also results in increased lumen production for all particle sizes. Concurrently, the strategic addition of 30 % CaCO₃ reduces the CCT variation by 620 K, establishing CaCO₃ as a possible particle for improving light output and chromatic quality in pc-LEDs.

4.2.1 Scattering analysis

The scattering characteristics change as the percentage of Scattering Enhancement Particles (SEPs) increases, as shown by the diagrams in Figures 4.8 and 4.9. It is interesting to note that there is a noticeable increase in blue light absorption with greater SEP concentrations. CaCO₃ particles have the best scattering coefficient among the SEPs. Furthermore, the difference in scattering coefficients between 455 nm and 595 nm wavelengths is lessened when CaCO₃ is present, suggesting that it is useful for controlling the transmission coefficient of yellow phosphor and blue chips. Figures 4.6 and 4.7 show the theoretical anisotropy factor $g(\lambda)$ for blue and yellow chromatic radiation, which is obtained from Equation 4.7. Anisotropy factor $g(\lambda)$, like the coefficient of scattering, is independent of SEP characteristics.

The impact of SEP thickness on $g(\lambda)$ expansion is frequently disregarded because of its negligible nature. The reduced scattering SEPs coefficients at 455 nm and 595 nm wavelengths are, for the most part, virtually equivalent. For example, the anisotropy

factor of CaCO_3 is 0.9 μm at 595 nm and 0.8 μm at 455 nm, which is not a significant difference.

As a result, it is not difficult to increase spatial shading consistency using CaCO_3 and TiO_2 particle scattering security. Lighttools 9.0 software is used to extract the data from the simulation, and Excel software is then used to process the figures.

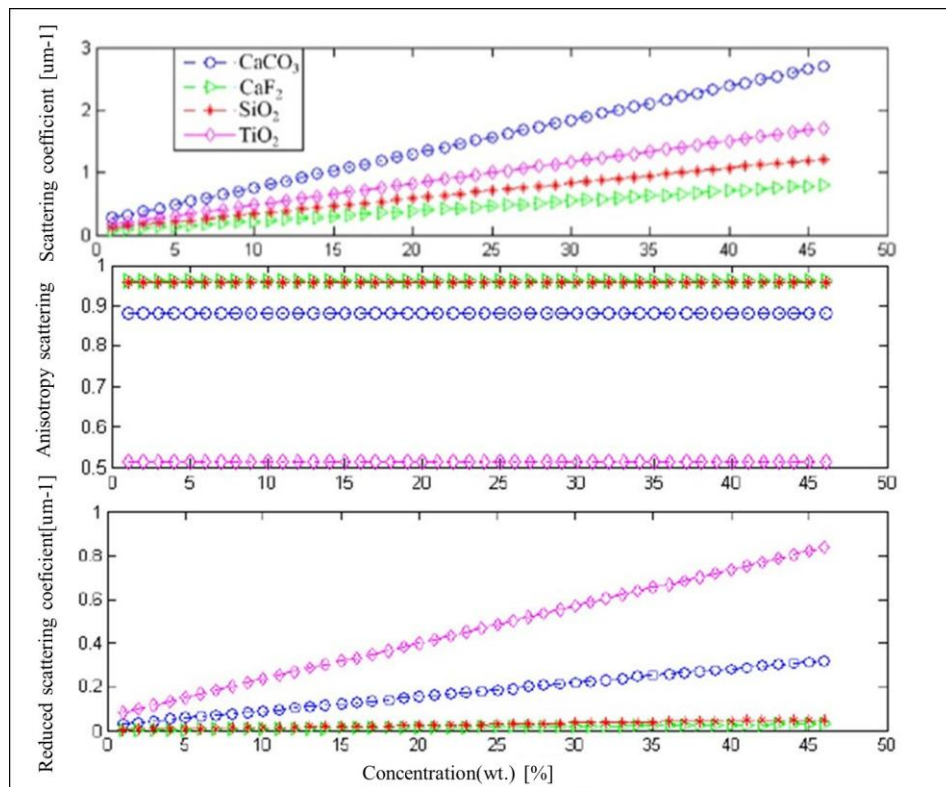


Figure 4.8: Computation of scattering coefficient, anisotropic scattering and reduced scattering coefficient of the SEPs at 455 nm

In Figure 4.8, there is a detailed explanation of the exact scattering amplitudes of SEPs, which are calculated using a MATLAB program. SEPs are particularly significant

for blue-light scattering due to the sufficient compensation for blue light, as well as their efficiency in enhancing color quality and light output.

The selected spectral energy distributions (SEPs) with specific scattering wavelengths of 455 nm in blue-light and 595 nm in yellow-light have a significant impact on determining the magnitude of the beneficial effect. In comparison to SiO_2 , CaCO_3 particles with irregular scattering wavelengths show less variation across the range of 455 nm–595 nm.

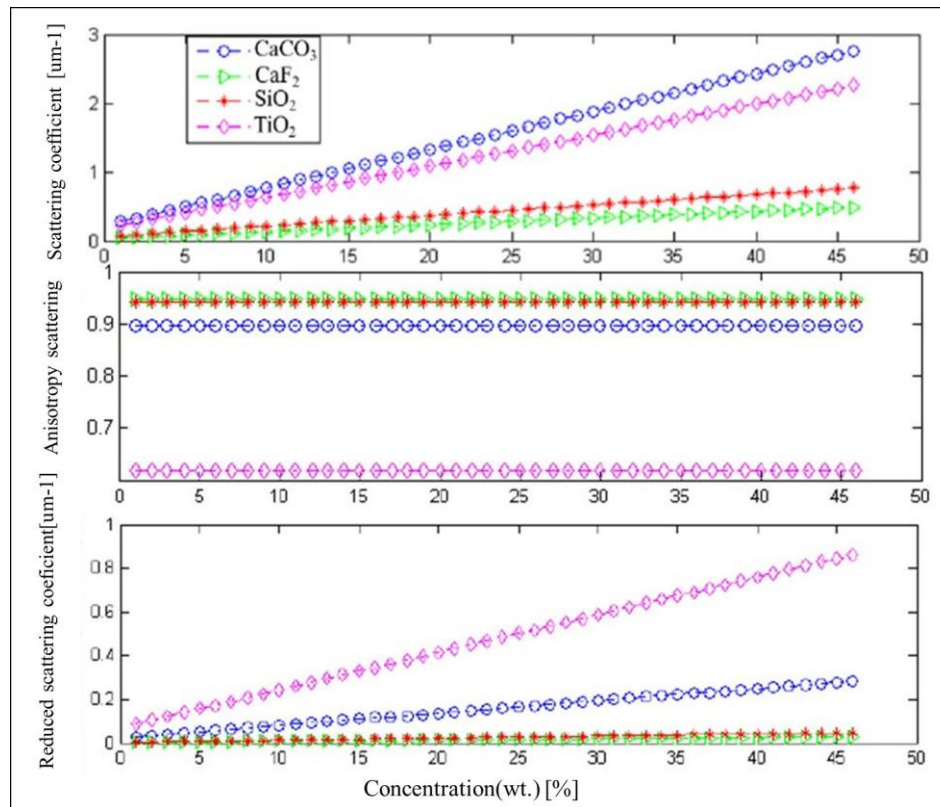


Figure 4.9: Computation of scattering coefficient, anisotropic scattering and reduced scattering coefficient of the SEPs at 595nm

Figure 4.9 illustrates the results of the dispersion reduction value, anisotropic scattering, and dispersing value for four types of particles— CaCO_3 , CaF_2 , SiO_2 , and TiO_2 —that intensify scattering.

The simulation findings indicate that CaCO_3 is the most favorable material for emitted luminous flux due to its low scattering coefficient and attenuation coefficient. The enhanced flow of CaCO_3 particles, in comparison to the other three types, can be explained by Mie scattering theory. This theory suggests that particles with low scattering coefficients and attenuations result in higher energy output in white light LEDs.

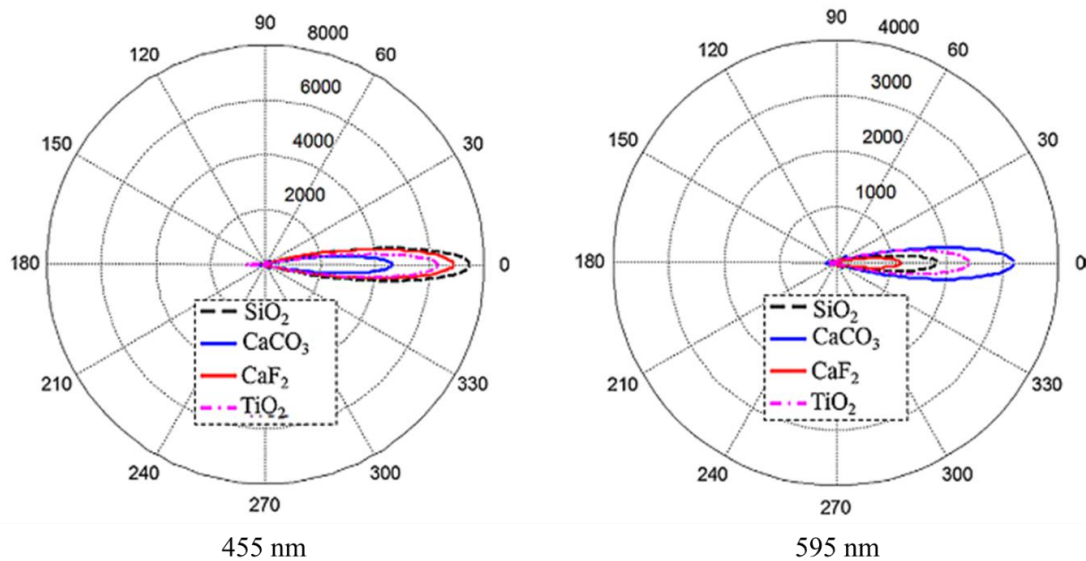


Figure 4.10: Angular scattering amplitudes of different SEPs at (a) 455 nm and (b) 595 nm

4.2.2 Computation and discussion

This part assesses the light performance of Scattering Enhancement Particles (SEPs) in the configuration of phosphor-converted LEDs (pc-LEDs), utilizing Light Tools 9.10 software to carry out the analysis. Figure 4.11 illustrates the schematic diagram of pc-LEDs. The LED absorber has dimensions of approximately 2.1 mm in depth, 8 mm in inner dimensions, and 10 mm in outside diameter. Each of the nine chips is covered with a phosphor coating that has a fixed density of 0.08 mm. The refractive

indices of CaCO_3 , CaF_2 , SiO_2 , and TiO_2 are 1.66, 1.44, 1.47, and 2.87, respectively. All SEPs are presumed to be spherical, with a radius of $0.5 \mu\text{m}$. Each phosphor particle has an average radius of $7.25 \mu\text{m}$ and a refractive index of 1.83 for all wavelengths in the visible spectrum. Furthermore, the silicone adhesive possesses a refractive index of 1.5. The diffusional particle density is adjusted to enhance the uniformity of Correlated Color Temperature (CCT) and improve the efficiency of light production.

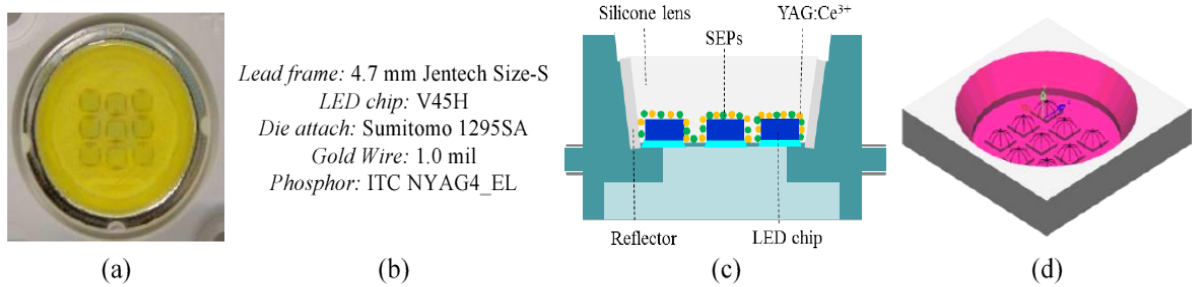


Figure 4.11: (a) Photograph of WLEDs sample, (b) parameter of WLEDs, (c) illustration of 2D WLEDs model, and (d) the simulated WLEDs model.

$$W_{phosphor} + W_{silicone} + W_{SEP} = 100\% \quad (4.4)$$

Equation 4.4 describes the composition percentage of pc LEDs, $W_{silicone}$, $W_{phosphor}$, and W_{SEP} , specifying the weight proportions of silicone, phosphor, and SEPs in the phosphor composition of the structure. To ensure stability of the correlated color temperature (CCT) at 8500 K, it is important to maintain a balanced ratio between phosphor and secondary electron producers (SEPs). Color divergence is a crucial measure of the quality of a lighting device. When using Light-Emitting Diodes (LEDs) in applications, a significant difference in Correlated Color Temperature (CCT) at various angles can cause issues like the yellow ring effect and uneven white light. These problems can reduce the lighting performance of LEDs used in personal computers (PCs). The calculation of CCT deviation can be represented by the following equation:

$$D-CCT = CCT_{(Max)} - CCT_{(Min)} \quad (4.5)$$

Equation 4.5 defines CCT(Max) as the maximum Correlated Color Temperature observed at a 0-degree viewpoint, and CCT(Min) as the lowest Correlated Color Temperature observed at a 90-degree viewpoint. The differences in lighting characteristics of phosphor-converted LEDs (pc-LEDs) result from the variances in the emitted light of individual molecules within the pc-LEDs. Nevertheless, the key aspect to consider is that the reduction of CCT deviation can be accomplished by successfully intensifying the scattered blue light.

The Figures 4.8 and 4.9 clearly demonstrate that CaCO_3 grains have the least variation in angular dispersing abundance among various Scattering Enhancement Particles (SEPs) at both 455 nm and 595 nm wavelengths. Using CaCO_3 minimizes color variation during the scattering of LED chips' light and yellow-emitting phosphor. In addition, unlike all other scattering enhancement phenomena (SEPs), the angular scattering amplitude for CaCO_3 particles at a wavelength of 595 nm exceeds the value obtained at 455 nm. When blue and yellow light are combined, they produce white light.

However, if there is a significant discrepancy between these two colors, it may result in the appearance of a "yellow ring". Thus, an ample amount of blue light enables better control over CCT deviation and eliminates the occurrence of the yellow ring effect. On the other hand, the variation in CCT increases when there is either a shortage or a surplus of scattered blue light in pc-LEDs.

Figure 4.10 also shows that the ratio of angular scattering amplitudes between 455 nm and 595 nm for other SEPs, such as SiO_2 , CaF_2 , and TiO_2 , is many times greater. This feature is advantageous for maintaining consistent shading and smooth transitions of light.

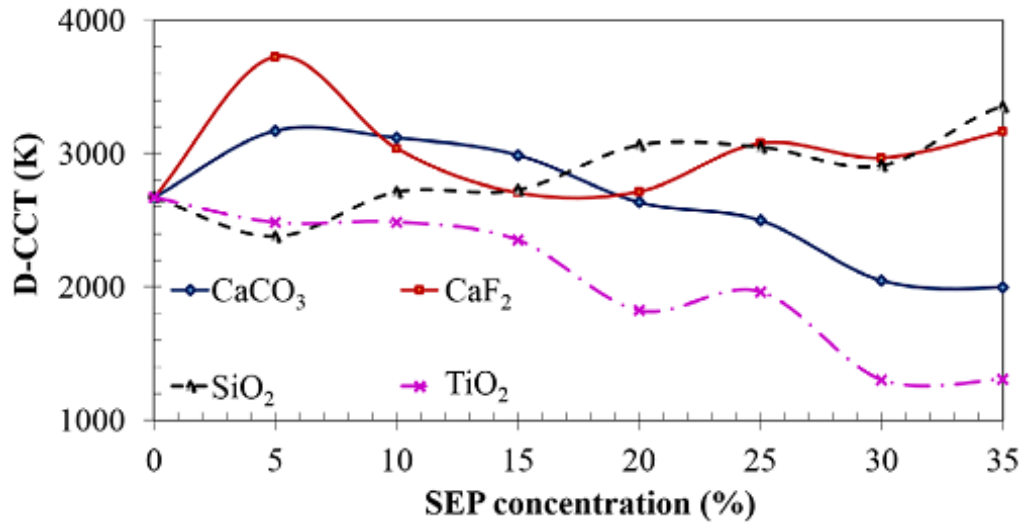


Figure 4.12: Comparison of CCT deviation of pc-LEDs using different SEPs

Figure 4.12 presents a graphical representation of the patterns in CCT deviation, which are influenced by varying concentrations of SEPs. This figure provides a full overview of all the data that have been addressed. The inclusion of CaCO₃ and TiO₂ in the setup results in a decrease in deviations of the relevant color temperature (CCT). Phosphor-converted LEDs (PC-LEDs) exhibit a color variation of 2670 K in the absence of scattering enhancement particles (SEPs). However, the addition of 30 % CaCO₃ results in a substantial decrease in CCT deviation, reaching a minimum value of 2050 K. Hence, it can be inferred that a CaCO₃ concentration of 30 % has a substantial impact on reducing the divergence of CCT by 620 K. Similarly, the divergence in CCT is reduced by half when a 30 % concentration of TiO₂ is present compared to when TiO₂ is not present. On the other hand, the increase in CaF₂ and SiO₂ concentrations clearly leads to the expansion of CCT deviations. These observations provide a strong basis for using these SEPs to develop high-quality white light-emitting diodes (WLEDs).

Like CaF₂, WLEDs with TiO₂ show an initial increase in luminous flux between 0% and 10 %, followed by a significant decrease as the concentration increases for all particle sizes. Lambert-Beer's law and Mie theory can explain the decrease in luminous

flux as the percentage of solid-state energy particles (SEPs) grows. This research looked into how different dispersion enhancement particles (SEPs) affect two important optical properties of phosphor-converted LEDs (PC-LEDs): how uniform the color is and how well they light up. The study used Mie-scattering and Monte Carlo methods to look at how well and how differently different types of SEP improved light scattering in PC-LEDs. This discovery introduces a novel, successful approach to regulating the optical properties of PC LEDs by selecting appropriate SEPs that align with the desired concentration.

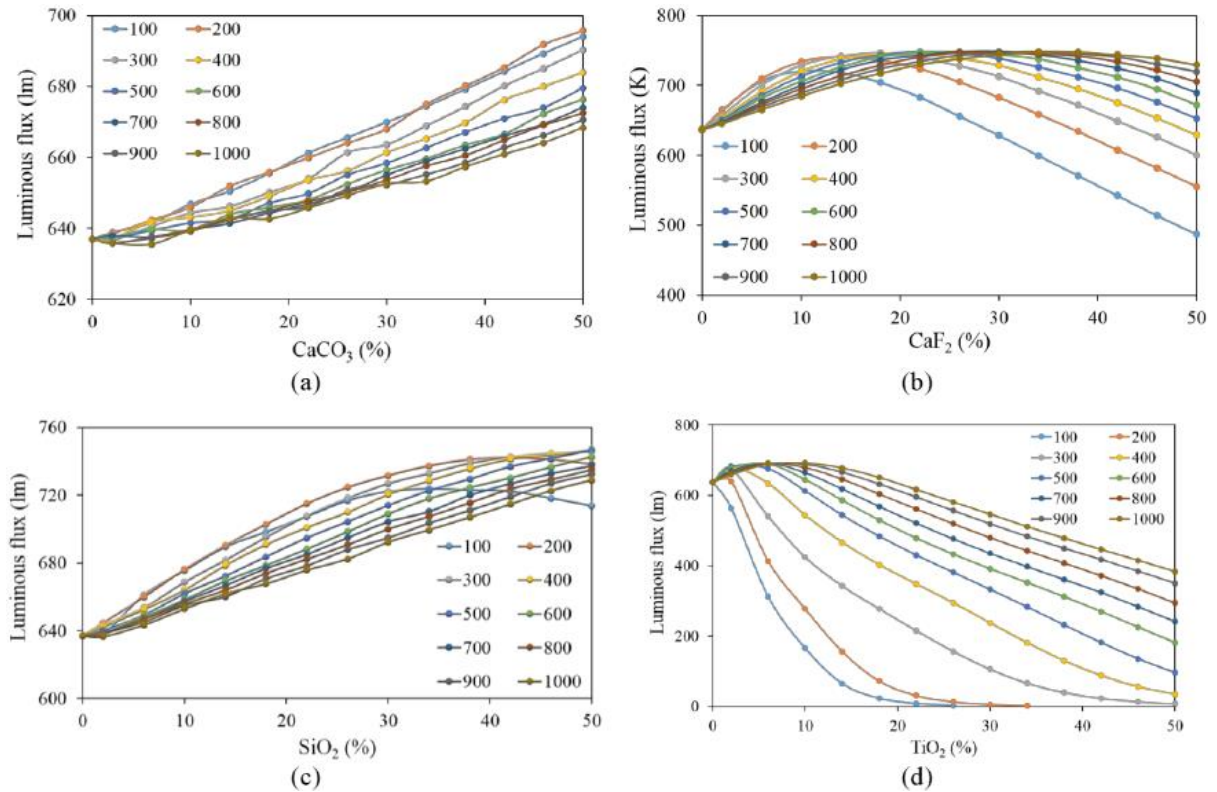


Figure 4.13: Comparison of LF using different SEPs: (a) CaCO₃, (b) CaF₂, (c) SiO₂, and (d) TiO₂

The results show that an increase in CaCO₃ and TiO₂ concentrations reduces the variation in correlated color temperature (CCT). Specifically, TiO₂ particles exhibit the capacity to attain the lowest color deviation value

4.2.3 Simulation of results

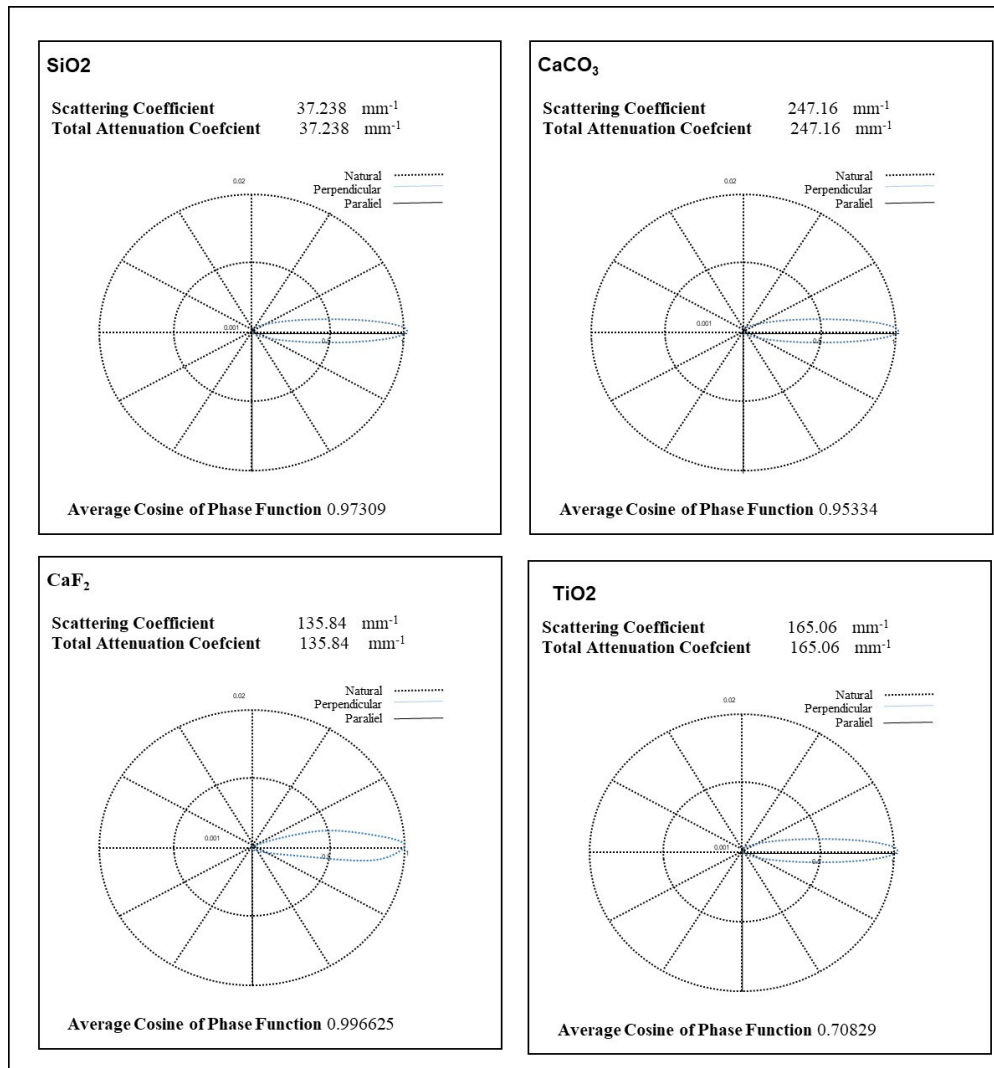


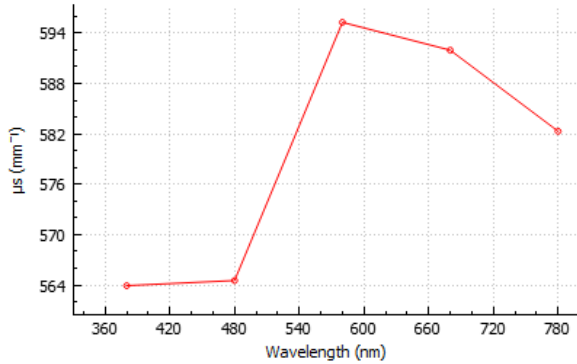
Figure 4.14: Simulation 4 SEPs on Mie Scattering Calculator software

. Nevertheless, an excessive concentration of TiO₂ leads to a significant decrease in emitted luminous flux. Adding CaCO₃, CaF₂, and SiO₂ to the phosphor layer simultaneously increases the lumen output. SiO₂ is favorable because it has a larger lumen value compared to the others, as seen in Figure 4.13. Furthermore, when the concentration of CaCO₃ is 30 %, it can decrease the divergence in CCT by around 620 K. Therefore, utilizing CaCO₃ particles is the most advantageous option for improving

the optical performance of PC-LEDs in the majority of situations. This research provides valuable insights that allow manufacturers to thoroughly evaluate the advantages and disadvantages of several types of SEPs. As a result, they can make well-informed judgments regarding the most appropriate phosphor particle for their specific LED needs. The utilization of ZnO particles as scattering enhancers in white LEDs has been explored in the article "Enhancing light scattering effect of white LEDs with ZnO nanostructures" by Hanh, Loan, and Ngoc (2021). The study indicates that while ZnO particles prove effective in enhancing color quality, their scattering characteristics are not particularly favorable. This results in a significant reduction in the amount of scattered light produced. Despite this limitation, ZnO-doped phosphor-converted LEDs (pc-LEDs) demonstrate practical applicability, presenting advantages such as being cost-effective and easy to install. Comparatively, the study highlights the superior lumen output achieved when incorporating SiO₂ particles. Specifically, the yielded light with SiO₂ particles is reported to be 2.25 % higher when subjected to the same energy source of 120 mA. This observation suggests that SiO₂ particles may offer a more efficient enhancement in terms of luminous output compared to ZnO in the context of pc-LEDs (Figure 4.14). The comparison of SiO₂ and ZnO materials in terms of luminous output has been explored in two studies: "Utilizing CaCO₃, CaF₂, SiO₂, and TiO₂ particles to enhance color homogeneity and luminous flux of WLEDs" and "The effects of ZnO particles on the color homogeneity of phosphor-converted high-power white LED light sources" (Loan & Anh, 2020). The research findings indicate that SiO₂ outperforms ZnO in terms of achieved output luminous flux. Specifically, in the study, the luminous flux achieved with SiO₂ is reported to be 760 Lm, while that of ZnO is 720 Lm. This suggests that SiO₂ particles contribute to a higher luminous output compared to ZnO in the context of phosphor-converted white LEDs. Furthermore, the research on SiO₂ materials reveals that the collision between particles and phosphor increases, resulting in a 5 % increase

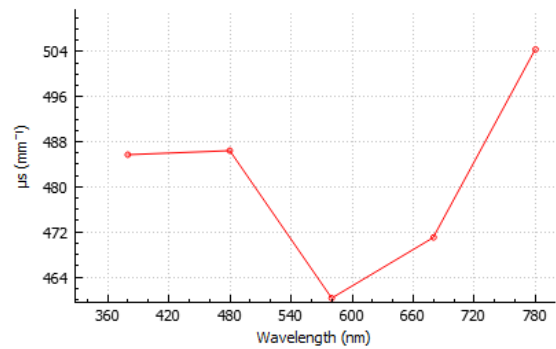
in the output luminous flux. This emphasizes the positive impact of SiO₂ on enhancing the scattering properties and overall performance of white LEDs.

CaCO₃



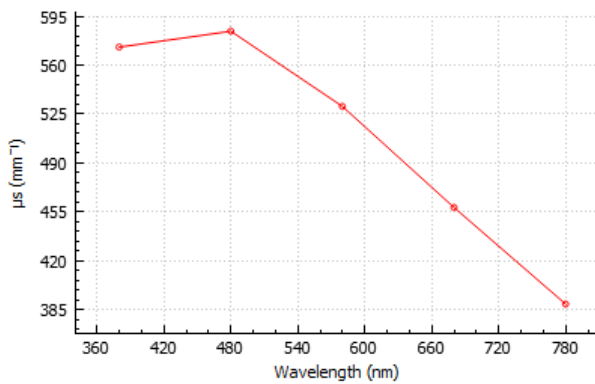
Ave. scattering coefficient 579.5mm⁻¹

CaF₂



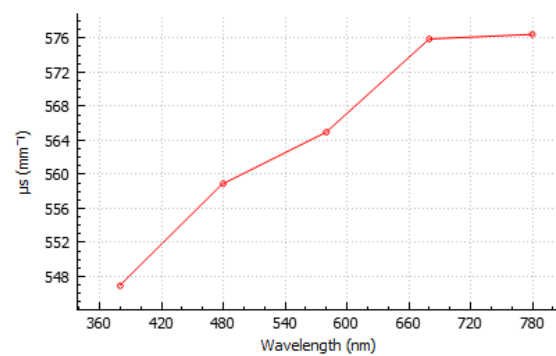
Ave. scattering coefficient 482 mm⁻¹

SiO₂



Ave. scattering coefficient 504.8mm⁻¹

TiO₂



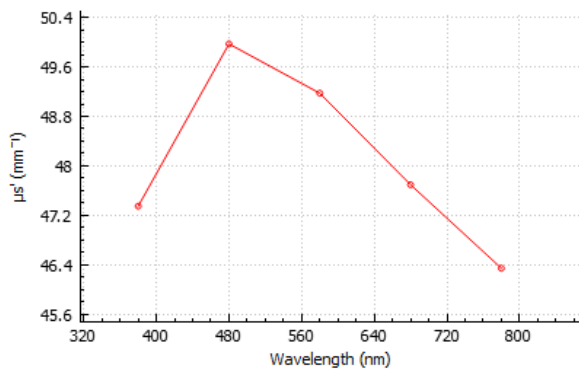
Ave. scattering coefficient 564.8mm⁻¹

Figure 4.15: Simulation scattering coefficient of 4 SEPs on Mie Simulator software

Moreover, the analysis of SiO₂ scattering properties with haze intensity provides insights into determining the optimal amount of SiO₂ for the development of white LEDs. The conclusion that 10 mg/cm² is the best setting for achieving optimal color quality further contributes to understanding the practical applications and considerations for using SiO₂ particles in the enhancement of phosphor-converted LEDs. The

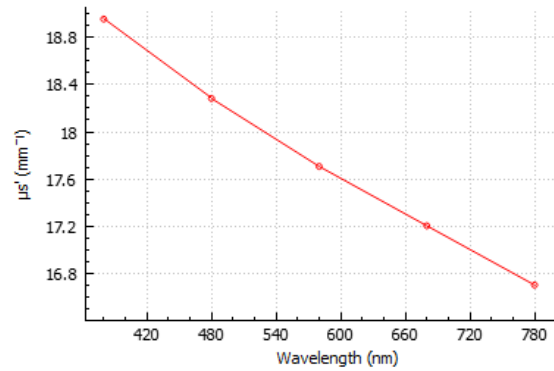
simulation results obtained using the Mie Scattering Calculator program, as shown in Figure 4.16, demonstrate that SiO_2 particles have the most favorable scattering performance compared to the other four particles. They have the lowest scattering and scattering attenuation coefficients.

CaCO_3



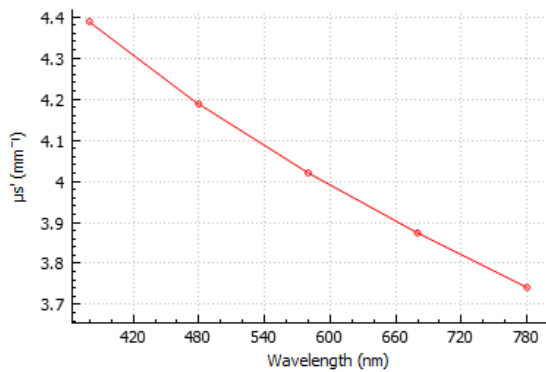
Ave. reduce scattering 47.93 mm^{-1}

CaF_2



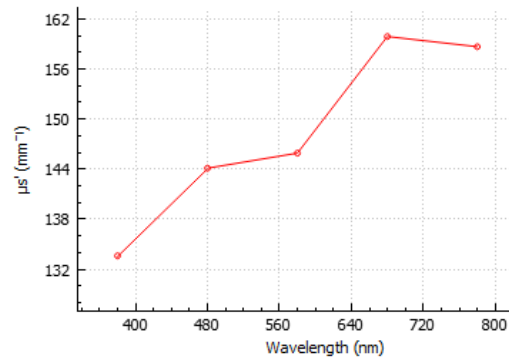
Ave. reduce scattering 17.76 mm^{-1}

SiO_2



Ave. reduce scattering 4.04 mm^{-1}

TiO_2



Ave. reduce scattering 148.4 mm^{-1}

Figure 4.16: Simulation reduce scattering coefficient of 4 SEPs on Mie Simulator software

These essential scattering factors play a key role in comprehending the performance of SiO_2 particles in terms of light scattering. In order to verify and improve the accuracy of these findings, the study utilizes the Mie Simulator program,

as explained in Figure 4.16. This software enhances the simulation by incorporating further input variables, such as discrete sphere size (the maximum calculation limit) and standard deviation, enabling a more comprehensive analysis

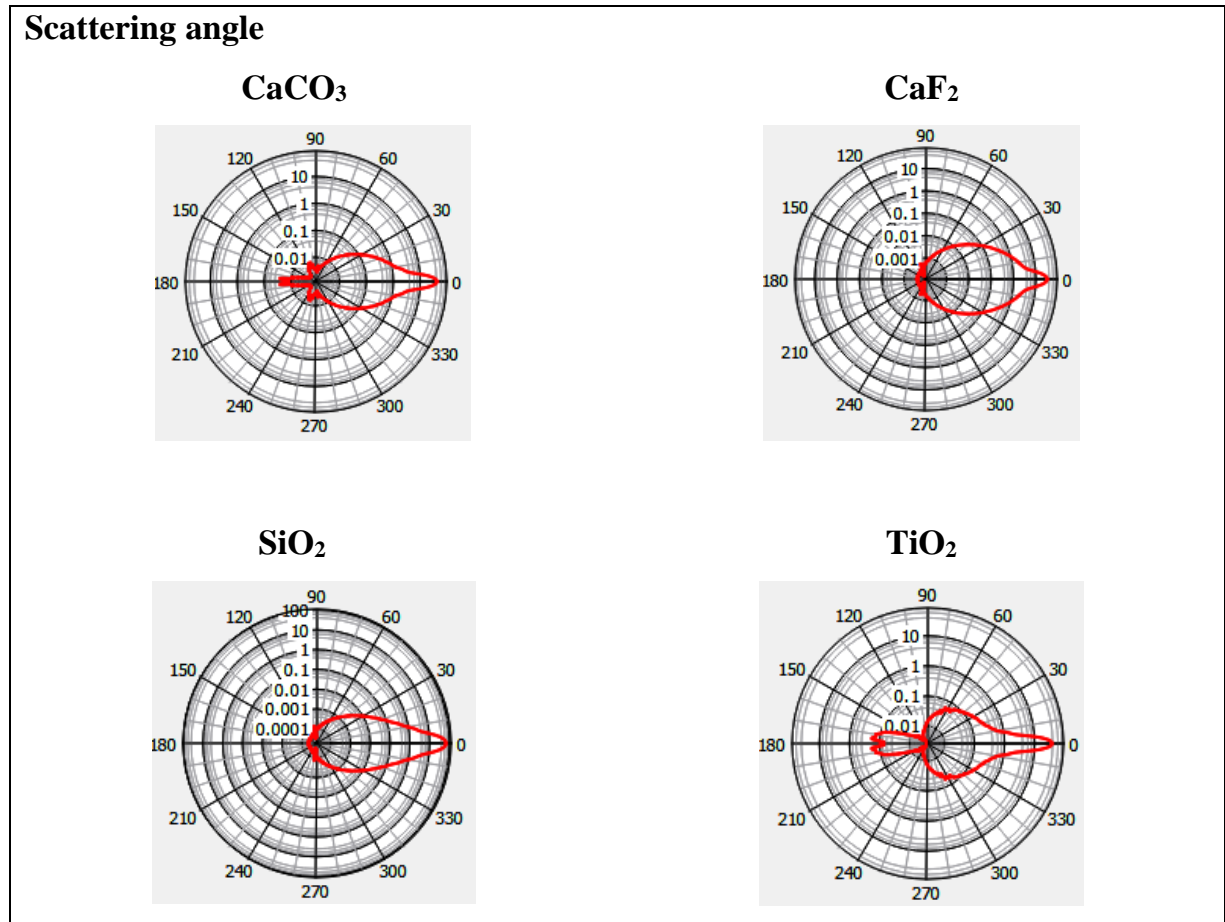


Figure 4.17: Simulation scattering angle of 4 SEPs on Mie Simulator software

. In addition, the Mie Simulator program provides the option to choose a wider range of wavelengths, spanning from 380 nm to 780 nm, which encompasses all of the visible light spectrum. By extending the range of wavelengths, a more thorough assessment of SiO_2 particle behavior can be achieved, overcoming the constraints of the Mie Scattering Calculator software, which is exclusively optimized for blue light wavelengths.

Utilizing both software tools improves the reliability of the study's results, enabling a comprehensive investigation of SiO_2 scattering properties and their significance in the context of phosphor-converted LEDs. The combination of these simulation outcomes contributes to a thorough understanding of how SiO_2 particles interact with light under a variety of parameters and situations. In terms of results, both software programs produce nearly identical outcomes.

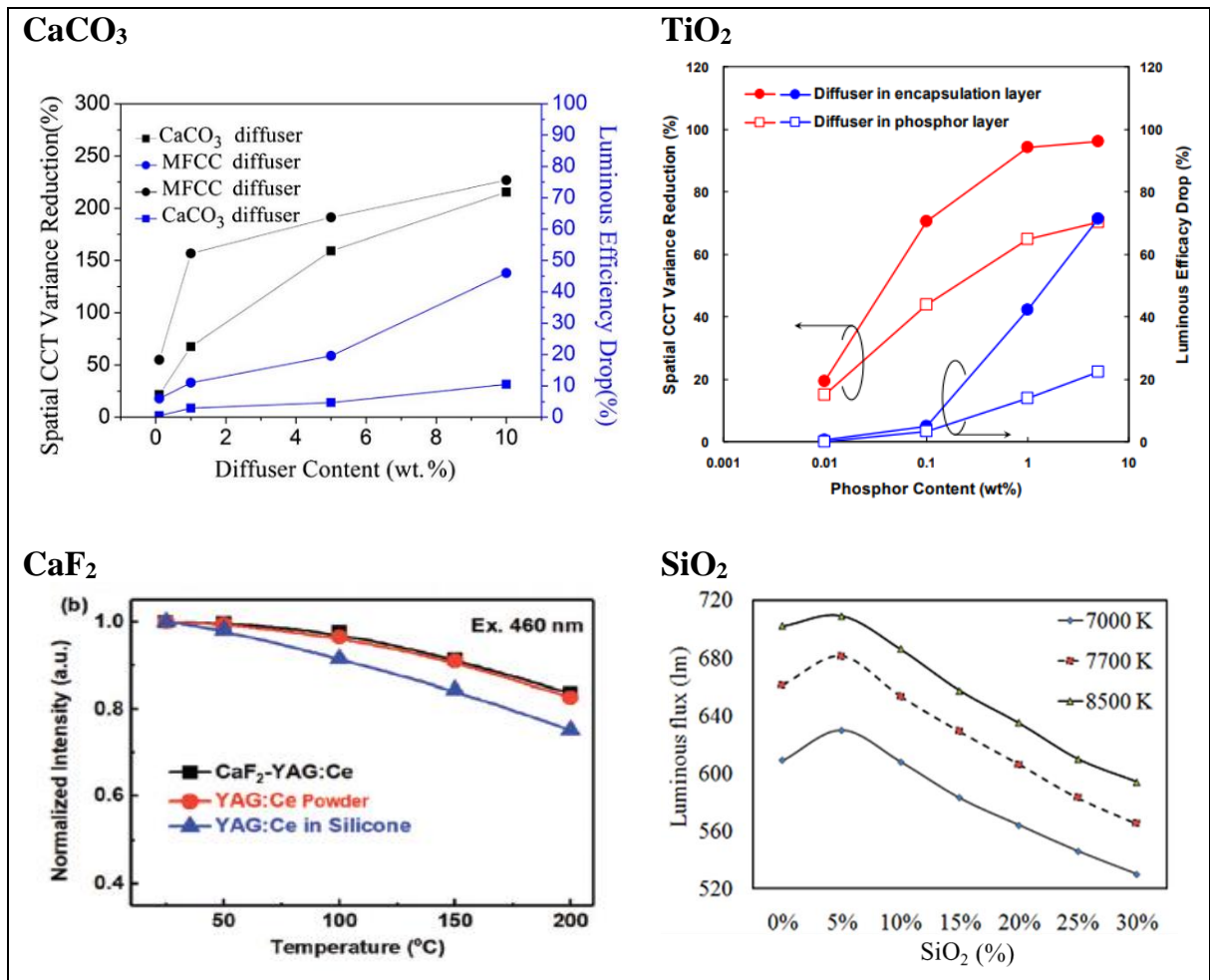


Figure 4.18: The affected of 4 SEPs to output parameters DCCT and Luminous efficiency

However, in the Mie Simulator, the CaF_2 particle exhibits the highest scattering coefficient, followed by SiO_2 , TiO_2 , and finally, CaCO_3 . However, SiO_2 still has the

lowest level of attenuation among the four particles, specifically in terms of scattering attenuation coefficient (Figure 4.17).

The data comparison between the Mie Scattering Calculator and Mie Simulator software programs provides significant insights into the scattering characteristics of various particles. Although the two software programs produce comparable outcomes, there are variations in the scattering coefficients. According to the Mie Simulator software, CaF_2 has the highest scattering coefficient, followed by SiO_2 , TiO_2 , and CaCO_3 . However, SiO_2 continues to hold the lowest scattering attenuation coefficient, signifying its minimal impact from scattering. This discovery suggests that SiO_2 undergoes lower energy dissipation in comparison to the other particles, demonstrating a significant benefit. The claim that SiO_2 particles perform better than others by 4.04 mm1 emphasizes how big of an advantage this is. Compared to CaF_2 , SiO_2 particles lose 77 % less energy, 91 % less than CaCO_3 , and 97 % less than TiO_2 . This data highlights the effectiveness of SiO_2 in conserving energy throughout the scattering process. Furthermore, it is essential to note that CaCO_3 and TiO_2 particles exhibit a backscattering phenomenon, while SiO_2 and CaF_2 particles scatter rays in the forward direction. This discovery is depicted in Figure 4.18. Forward scattering enhances both luminous flux and color quality. This observation gives us useful information for understanding how different particles affect the optical properties of phosphor-converted LEDs. It shows how important it is to know both the scattering coefficient and how the scattering behavior is directional. Concisely, this study has examined and evaluated the impact of CaCO_3 and TiO_2 particles on two optical characteristics of pc-LEDs: color consistency and brightness. By applying the Mie-scattering theory, a significant finding has been confirmed, demonstrating that each category of SEPs used in PC-LEDs may greatly improve the scattered light produced. This discovery serves as a fundamental foundation for effectively managing the optical characteristics of PC-LEDs by utilizing the optimal amount of incorporated SEPs. These findings provide manufacturers with essential and

significant data for the efficient production of W-LEDs, ensuring the achievement of predetermined standards for illumination quality.

At first, the variation in CCT will decrease due to the higher concentrations of CaCO_3 and TiO_2 . People widely recognize titanium dioxide (TiO_2) for its crucial role in reducing color variation to the lowest possible level. However, increasing the concentration of CaCO_3 will significantly decrease the luminous flux when the TiO_2 concentration significantly increases (Tran et al., 2020). Furthermore, the dissertation collects data from supplementary papers to validate the statement's accuracy, as well as the simulation conducted using Mie scattering software. Figure 4.19, as presented below, succinctly outlines the findings of relevant articles.

Based on Figure 4.16's analysis, it is evident that the addition of both CaCO_3 and TiO_2 particles improves color uniformity. Simply put, they help to minimize color variation. More precisely, Yang et al.'s 2013 study observed that the inclusion of CaCO_3 causes the CCT to decrease from 9000 K to 6000 K. Furthermore, the addition of TiO_2 causes a notable change in the color distribution, with the peak shifting from 5000 K to 4600 K. According to Chou et al. (2019), there is a significant decrease in color deviation from 500 K to approximately 50 K, which corresponds to a reduction of over tenfold.

Simultaneously, as the concentration of these two particles increases, the brightness noticeably decreases by a minimum of 10 %–20 %. CaF_2 particles also demonstrate the same phenomenon (Chi Gu et al., 2019). Thus, these three particles are not the most advantageous choices. When it comes to SiO_2 particles, choosing the appropriate concentration can lead to a decrease in color temperature variation and an increase in luminous flux.

The simulation results from LightTools software, in particular, demonstrate that adding 5 % to 30 % SiO_2 to the phosphor layer increases the uniformity of white-light color. In addition, the LED package's luminescence efficiency shows a negligible drop when the amount of SiO_2 exceeds 10%. The provided table demonstrates that selecting

a SiO₂ concentration of approximately 5 % enhances both the luminous flux and luminescence efficiency of white light LEDs. LightTools software has confirmed this finding, as shown in Figure 4.19. Thus, SiO₂ particles measuring 1 μm in size and having a concentration of 5 % will be the most suitable for investigating the blend of novel substances.

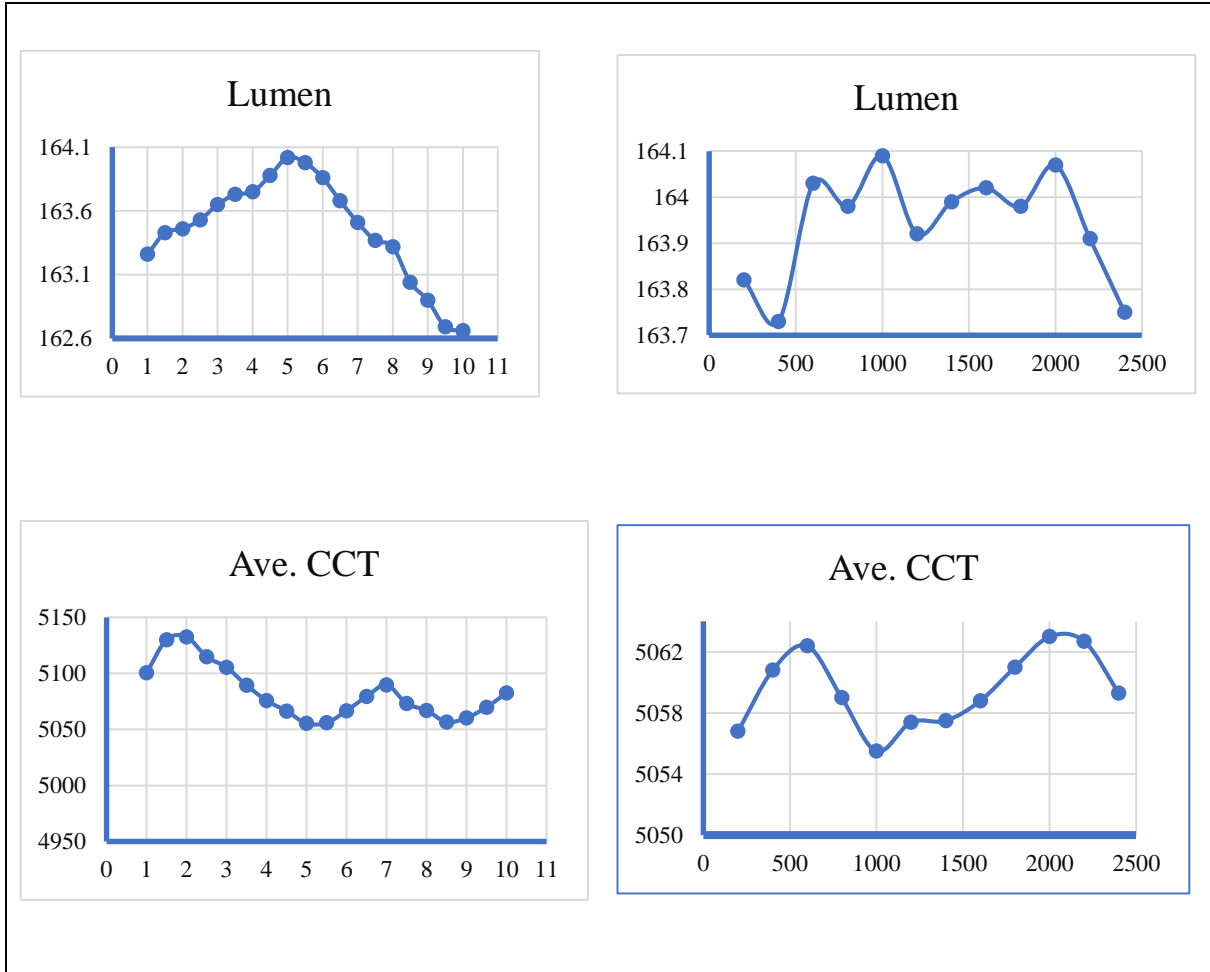


Figure 4.19: Simulation of Lumen and D-CCT from 5000 K- 8000 K of SiO₂ particle

In the following section, we will incorporate particles of SiO₂ with enhanced scattering properties, at this specific size and concentration, into the green phosphor layer through doping. The work at hand involves using Mie scattering theory and LightTools

software to accurately measure the size and concentration of green and yellow phosphor particles.

4.3 Using of green phosphor materials and scattering enhancement particles

4.3.1 The role of green phosphor in the mixture

In this section, researchers demonstrate the function and influence of green phosphor by modeling G-P particles using a detailed Mie scattering simulation with LightTools software. We accurately carry out the simulation using the supplied parameters described in Table 4.4. The size and concentration of SiO₂ particles stay constant at 1 μm and 5 %, respectively, which is worth mentioning. Within this particular framework, my research sets SiO₂ particles as the standard for comparison, specifically identifying a minimum size of 1 μm for thorough examination.

Table 4.4: Optical parameters of each particles in the mixture

Parameter	SiO ₂	Y-P	G-P
Refractive index	1.54	1.83	1.85
Density	2.65 g/cm ³	4.83 g/cm ³	4.2 g/cm ³
Dimension	1 μm	1 μm	1÷20 μm
Concentration	5 %	Change follow G-P concentration	1 % ÷ 20 %

Because of the innovative nature of our study, we have chosen to investigate G-P particles. Specifically, we have selected yellow phosphor particles with a size of 1 μm as the smallest size, and their concentration will fluctuate proportionally to the concentration of G-P particles. Concerning G-P, the simulations will cover a range of diameters from 1 μm to 20 μm, as specified in Table 4.5. Additionally, the concentrations will be systematically modified from 1 % to 30 %. This extensive investigation seeks to

evaluate the impact of G-P on improving the efficiency and chromatic accuracy of white-light LEDs. In order to thoroughly investigate the matter, we will begin by analyzing how the size of G-P particles affects the quality of color at a temperature of 5000 K while maintaining a G-P concentration of 5 %. This analysis is performed by utilizing both the Mie Simulator and LightTools software. This enables us to determine the relationship between scattering phenomena and important parameters for evaluating color quality, such as luminance (Lumen), color rendering index (CRI), color quality scale (CQS), and delta-correlated color temperature (D-CCT). This technique offers a detailed comprehension of how G-P parameters impact the overall performance and color accuracy of white-light LEDs in these specific settings.

Table 4.5: Correlation between G-P particle size and color quality

Particles size	Color rendering index (CRI)	Color quality scales (CQS)	Lumen
1 μm	45,32	41,25	200,3
5 μm	54,91	60,03	162,5
10 μm	61,83	63,19	149,9
20 μm	65,65	63,65	143,4

According to Table 4.5, there is a significant correlation: as the G-P particle size increases, both the scattering coefficient and scattering attenuation increase. Therefore, the higher G-P particle sizes result in a greater decrease in luminous flux.

Luminous flux and color rendering quality have an inverse relationship, as quantified by the Color Rendering Index (CRI) and Color Quality Scale (CQS). Therefore, when the backscatter effect of larger G-P particles reduces the amount of light emitted, it simultaneously enhances the LED's ability to accurately reproduce colors.

This delicate interplay highlights the complex relationship between particle size, scattering characteristics, and their effects on luminous flux and color quality in LED lighting.

4.3.2 Simulation Results

My study uses this new material for monitoring purposes across a range of CCTs from 5000 K to 8000 K to make comparisons and draw conclusions once we have established the appropriate combination of green phosphor material and enhanced scattering particle SiO₂.

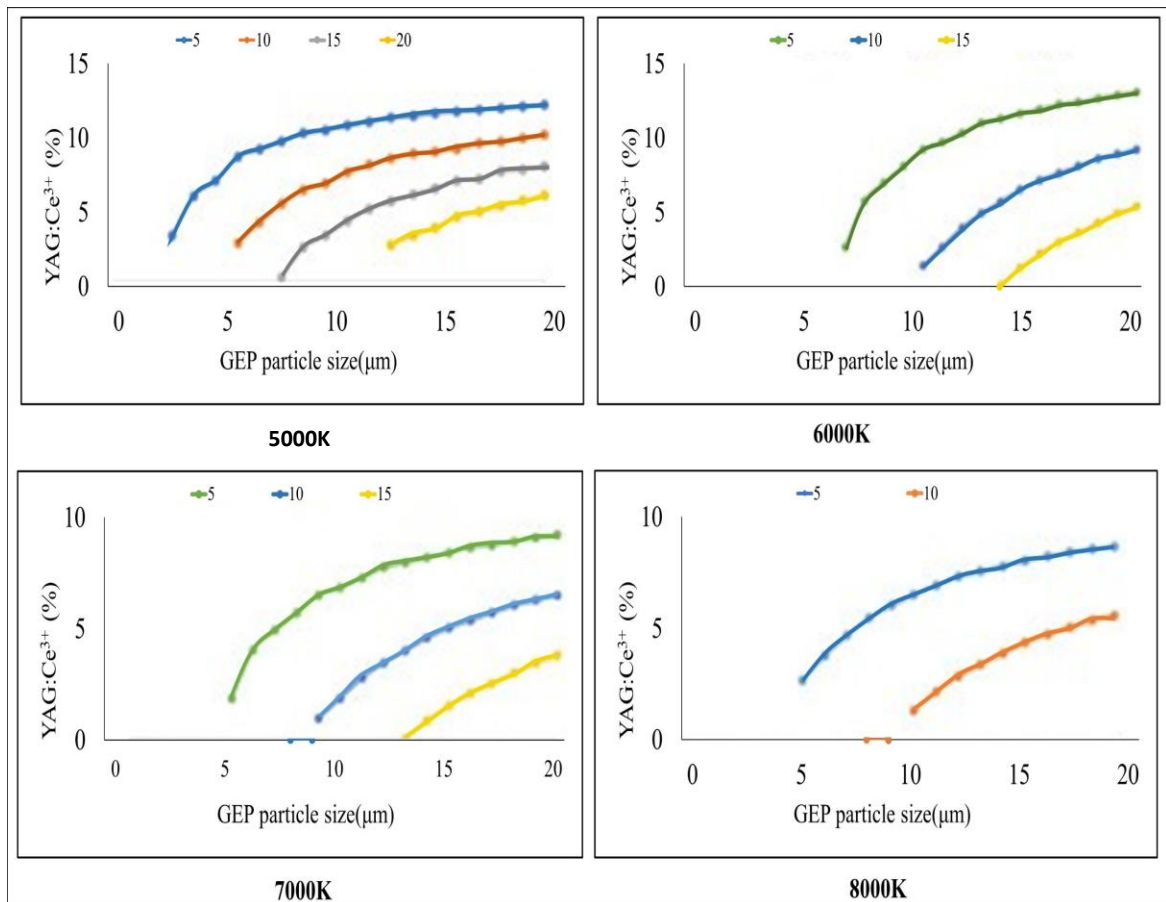


Figure 4.20: Simulation results of % Ratio

Figure 4.20 presents the simulation findings, which lead to the following observations for the four different color temperatures: When the size of G-P particles grows from 0 to 20 μm across all four concentrations of G-P, there is a corresponding increase in the concentration of Y-P particles. Nevertheless, as the concentration of G-P increases from 5 % to 20 %, it will be necessary to decrease the percentage concentration of yellow phosphor in order to maintain the color temperature at an acceptable level. For a concentration of 20 %, the line performance is at its lowest, while for a concentration of 5 %, it is at its maximum.

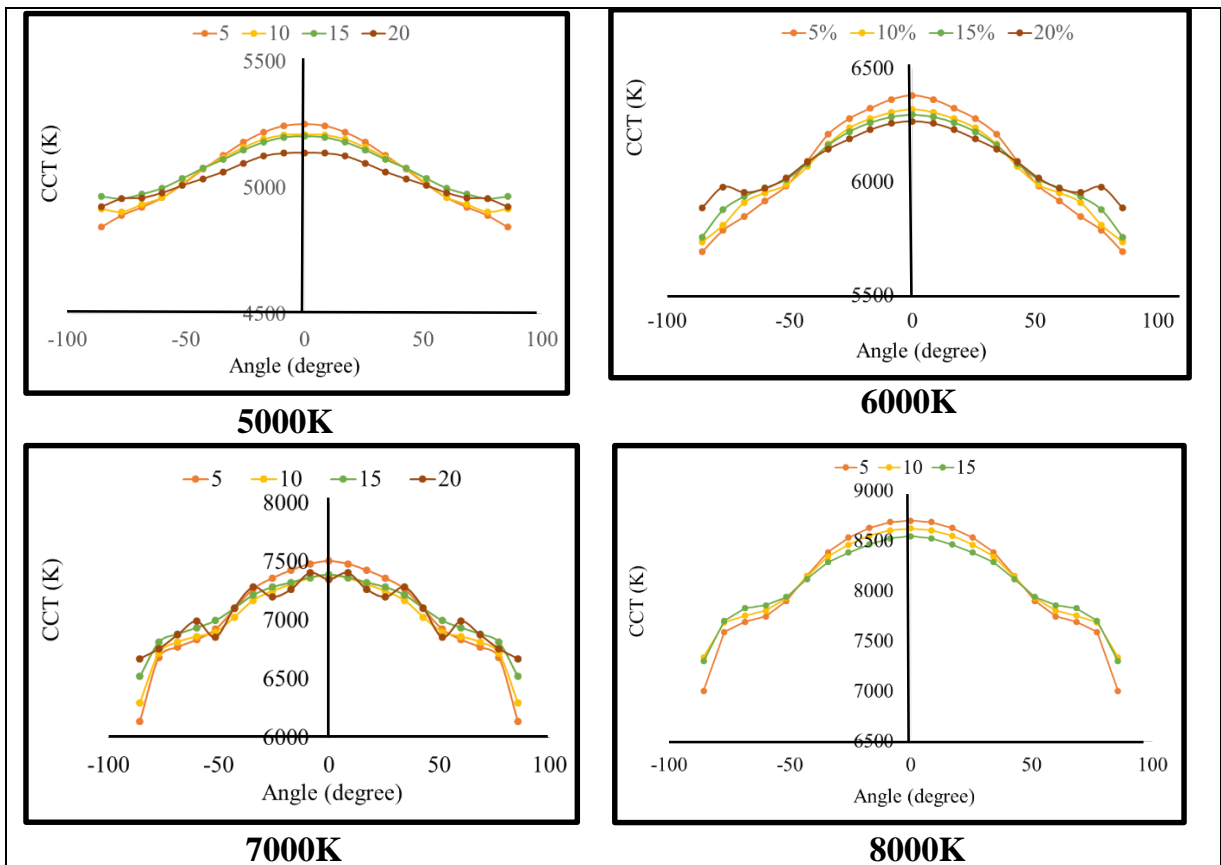


Figure 4.21: Simulation results of CCTs

Figures 4.20 to 4.25 display the results of simulations performed using LightTools 9.0 software. The results provide a clear breakdown of the percentage concentration of

highly scattered particles (SEPs) that are present in the YAG:Ce³⁺ yellow phosphorus material combination. The results identify the optimal concentration that yields the highest light output, corresponding color temperature, spectrum maximizing range, and percentile values for color rendering indices (CRI) and the Color Quality Scale (CQS).

The choice of the most suitable concentration depends on a variety of factors that align with the simulation's goals. When placing great importance on achieving a consistent color appearance, it is critical to consider both high brightness and minimal variation in color temperature. The accompanying tables methodically present the justification and details for each criterion, providing a thorough reference for selecting the most appropriate percentage concentration to enhance the desired performance and quality in the synthesized material.

When analyzing Figure 4.21, it is clear that increasing the particle size of G-P does not always result in a larger luminous flux, even when maintaining a consistent Correlated Color Temperature (CCT) value. Conversely, an increase in G-P concentration is directly related to luminous flux.

Furthermore, as previously mentioned, a reduced particle size promotes increased dispersion of light, resulting in higher luminous flux and improved color uniformity. Figure 4.21 demonstrates that a G-P concentration of 20% results in the lowest deviation of Correlated Color Temperature (CCT), while a concentration of 5% records the maximum deviation of CCT. This detailed analysis emphasizes the complex relationship between the properties and concentration of G-P particles, as well as how they affect luminous flux and color uniformity. It also provides guidance on selecting the best settings to get the desired lighting results. Figure 4.21 displays the simulation results from LightTools 9.0 software. The figure displays different color rendering temperatures (CCT) at four specific levels: 5000 K, 6000 K, 7000 K, and 8000 K. The results indicate that when the concentration of scattered particles increases, there is a decrease in the deviation of the related color temperature (DCCT). More specifically, at

a temperature of 7000 K, the DCCT reaches its lowest value when the concentration of scattered particles increases to 20 %. This discovery highlights the ideal circumstances for achieving better color consistency, as lower DCCT values indicate improved color temperature stability. Among the four temperatures considered, 7000 K stands out as the most advantageous, exhibiting the greatest stability in DCCT. At temperatures higher than this, DCCT becomes unstable, resulting in reduced color consistency. Therefore, the main conclusion is that a 20 % concentration of enhanced scattering particles (SEPs) is the most effective for obtaining excellent color uniformity, especially at a temperature of 7000 K.

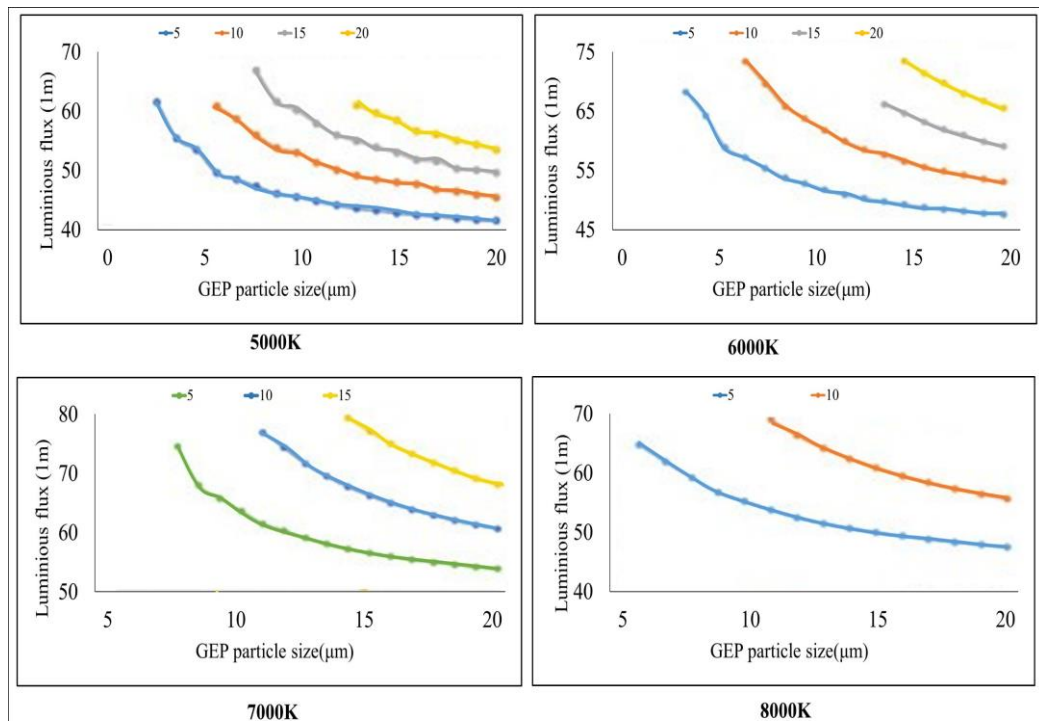


Figure 4.22: Simulation results of Luminous flux

At both CCT levels (5000 K and 6000 K), the luminous flux reaches its peak within the phosphor particle concentration range of 5 % to 10 % (Figure 4.22). However,

a prudent assessment extends beyond measuring luminous flux alone. When evaluating the ideal value, it is crucial to take into account elements other than just luminous flux. If a significant difference in correlated color temperature (CCT) coincides with an excessive concentration of light flux, it may negatively affect the homogeneity of the LED's color, making it less ideal.

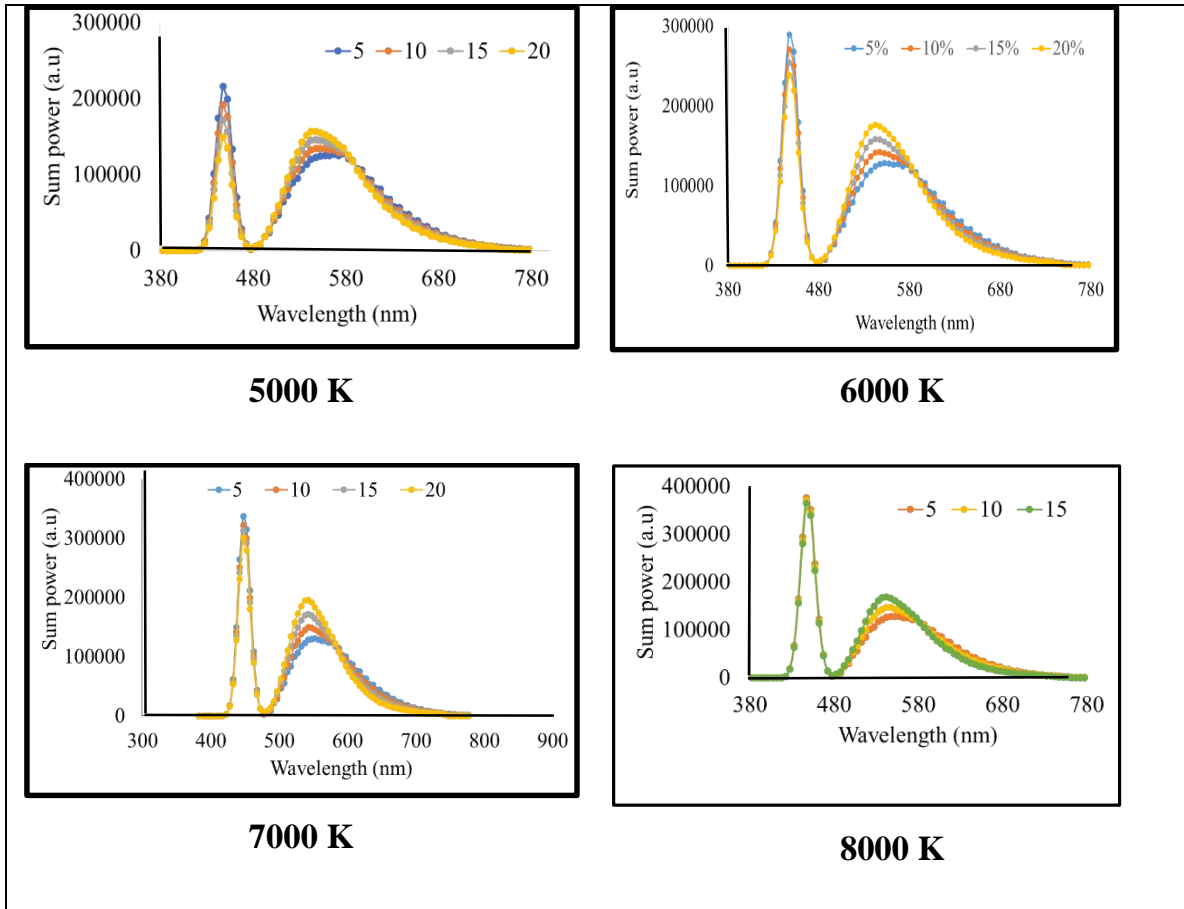


Figure 4.23: Simulation results of spectrum

Moreover, raising the temperature might result in significant degradation of optical properties, rendering it an unfavorable option. Hence, a thorough evaluation entails taking into account supplementary aspects such as spectrum and color quality indexes such as CRI and CQS.

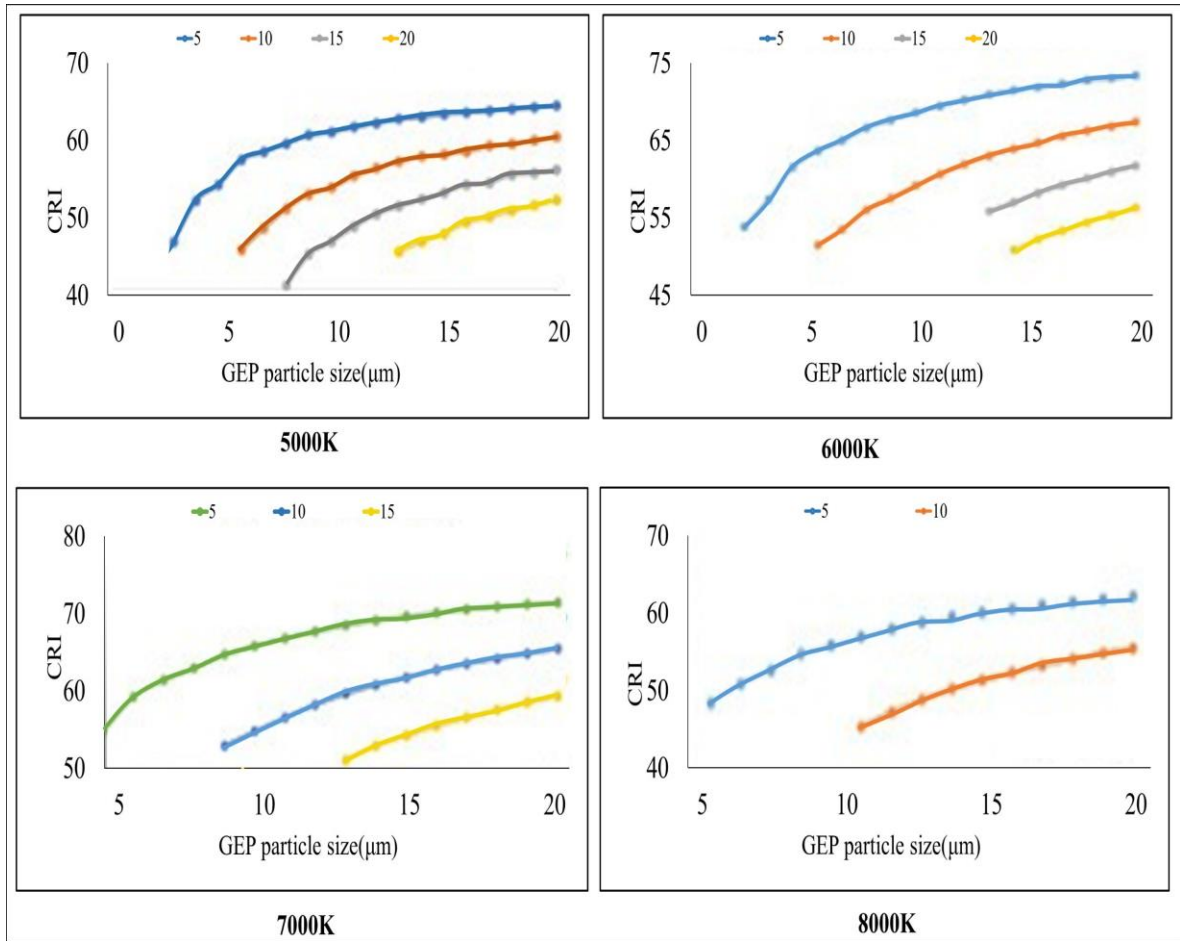


Figure 4.24: Simulation results of CRI

Figure 4.24 presents the specific outcomes of these variables, providing a comprehensive perspective to select the optimal phosphor particle concentration for LED applications, ensuring high luminous flux while maintaining color uniformity and overall quality.

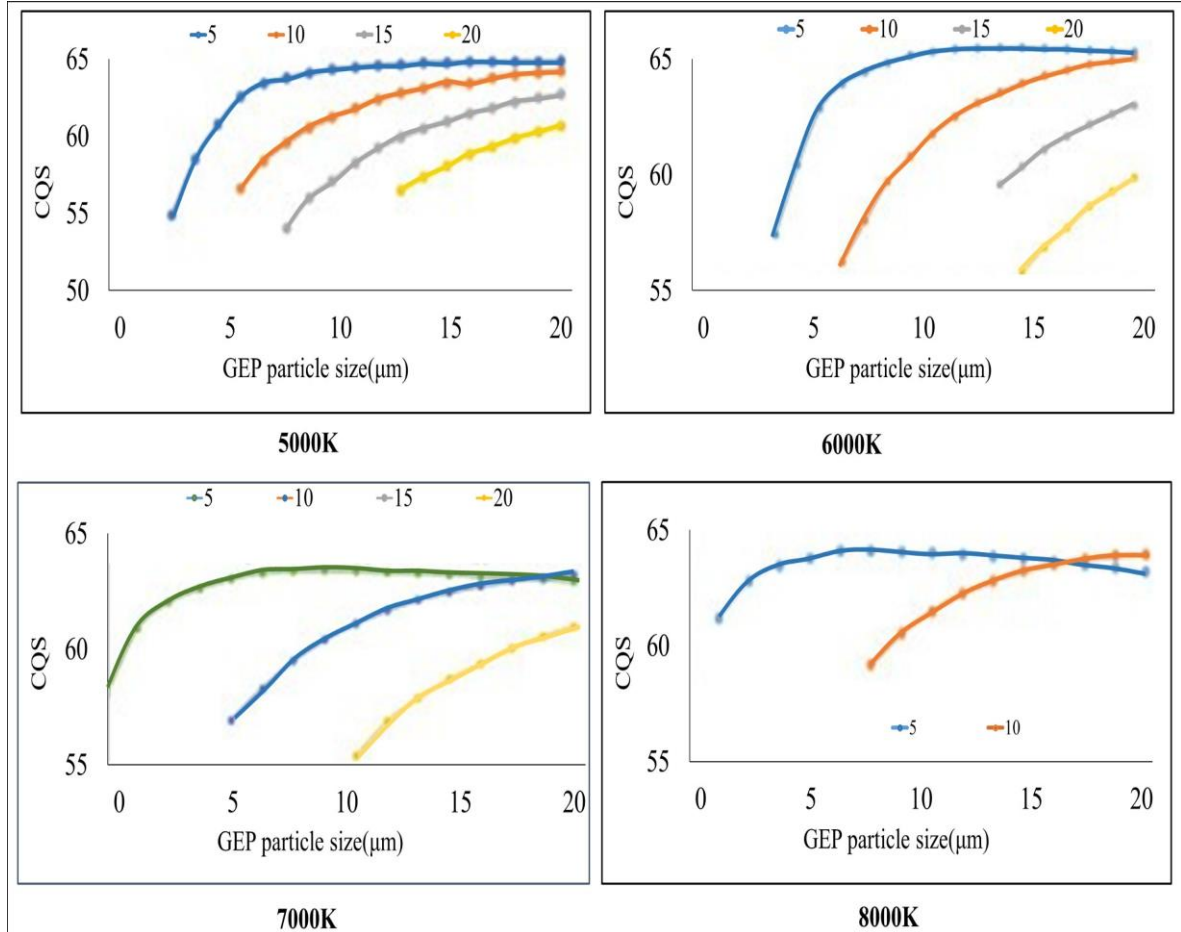


Figure 4.25: Simulation results of CQS

Upon analyzing the spectrum data depicted in Figure 4.23, it becomes apparent that as the related hue temperatures (CCT) increase, the hue shifts towards blue or cooler tones. At 5000 K, the radiant spectrum's total power or energy is slightly above 200,000 au. However, at 8000 K, this value almost doubles, reaching about 400,000 au. The increase in CCT is associated with a shift towards a colder color, specifically blue light. The addition of green phosphor (G-P) is critical for increasing blue light absorption in the phosphor layer. Consequently, the presence of additional phosphor colors alongside yellow phosphor (Y-P) decreases the amount of light reabsorbed by the LED chip. As a

result, the green and yellow regions can convert blue light into light with longer wavelengths. This phenomenon is critical for color reproduction because it enhances the overall range and intensity of colors. The use of G-P is essential for enhancing color rendering and improving the quality of LED applications. Upon further analysis of the color rendering index (CRI) and color quality scale (CQS) in Figures 4.24 and 4.25, a clear and identifiable pattern emerges. Contrary to luminous flux, both the Color Rendering Index (CRI) and Color Quality Scale (CQS) show a progressive rise when the particle size increases from 5 % to 20 %. This effect suggests that larger particles lead to less energy loss upon contact, thereby contributing to an improvement in color quality. This demonstrates the inverse correlation between the efficiency of luminescence and the ability to accurately represent colors. Within this particular context, it is of utmost importance to attain a state of equilibrium, and reducing the disparity between these parameters is essential for obtaining the best possible performance of LED technology. Interestingly, increasing the amount of green phosphor (G-P) to 20 % reduces the noticeable increase in CRI and CQS indices. In this study, the choice of G-P particle size and concentration is critical because it primarily aims to optimize color performance and uniformity. The best results are expected when the particle size is set to its maximum level, specifically 20 μm , and the concentration reaches 20 %, producing an ideal equilibrium between light flux and Delta Correlated Color Temperature (D-CCT).

4.4 Using $\text{Y}_2\text{O}_3:\text{Ho}^{3+}$ and $\text{ZnO}:\text{Bi}^{3+}$ for enhancing color quality and luminous flux of WLEDs

Green phosphor was used in earlier studies to increase the energy of green light scattering and hence increase luminous output. According to Kolahdouz et al. (2018), red phosphor improves color quality and uniformity by increasing red light scattering energy. These phosphor materials are prepared according to specified criteria by steps

like mixing, dilution, heating, drying, and grinding. In order to create a three-layer phosphor arrangement, this study uses green phosphor and red phosphor.

4.4.1 Preparation of phosphor materials

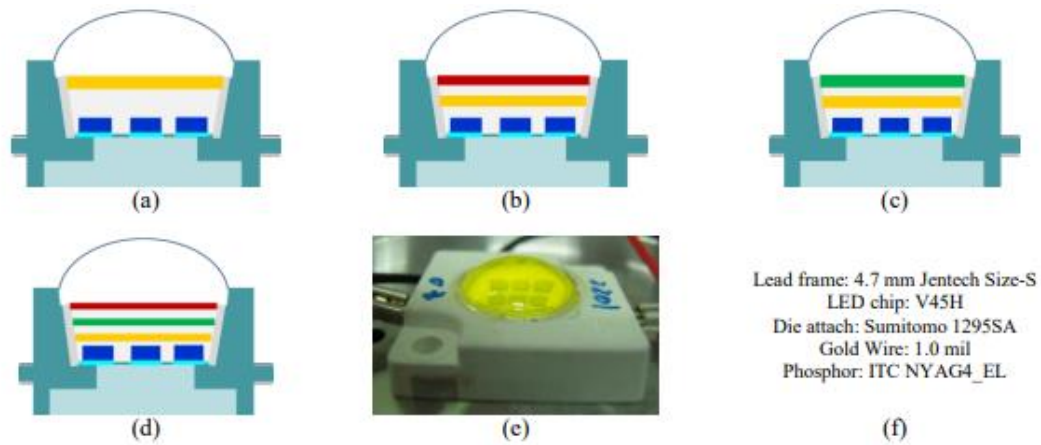


Figure 4. 26: Illustration of multi-layer remote structures and associated parameters

Exact experimentation is necessary to determine factors such as phosphorus content, particle size, excitation and absorption spectra, and emission spectrum. LightTools 9.0 simulation software will be used to test the concentration and size, which are currently unknown. An average particle size of $14.5 \mu\text{m}$ is predicted. The different model representations (4.26(a), 4.26(b), 4.26(c), and 4.26(d)) show that backscatter is lessened to improve luminosity flux, which is especially noticeable when yellow light is obscured. Normal parameters are shown in Figure 4.26(f), and the physical model with an aluminum nitride substrate (Zhao et al., 2018) is shown in Figure 4.12(e).

Throughout the simulation, temperatures ranging from 5600 K to 8500 K are compared. In examining optical properties, variations in color temperature prompt distinctive changes in phosphor concentrations, influencing particle scattering

differently. In Figure 4.27, augmenting yellow phosphor concentration in a single-layer structure markedly diminishes luminous flux due to yellow light backscattering.

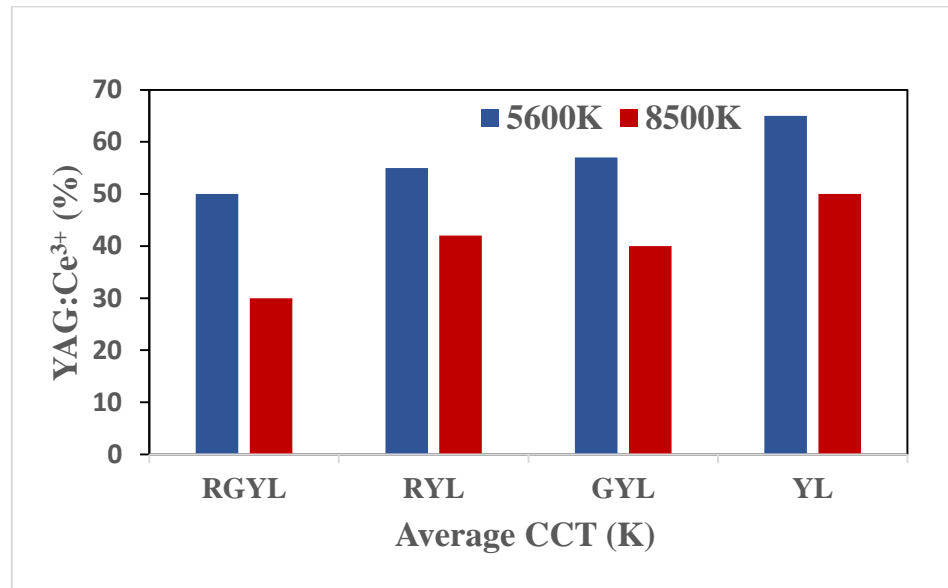


Figure 4. 27: Concentration YAG: Ce³⁺ phosphor at different correlated color temperatures

On the other hand, a two-layer green-yellow arrangement shows higher luminous flux by amplifying blue light via yellow-to-blue conversion. The three-layer structure consisting of yellow, green, and red highlights excellent color quality by exhibiting exceptional color consistency and excelling in luminous flux at carefully chosen color temperatures.

Overabundance of yellow phosphor can interfere with the production of white light, resulting in imbalance and unwanted backscatter, which can cause a dramatic decrease in luminous flux. An increase in red phosphor concentration raises the energy of red and blue light, which increases luminosity and the Color Rendering Index (CRI). Therefore, in order to maintain brightness, color consistency, and CRI in the three-layer

yellow, green, and red arrangement during temperature changes, it is imperative to maintain the ideal particle concentration. Different color temperatures lead to different phosphor concentration variations, which in turn cause different particle scattering behaviors when analyzing optical characteristics. Because yellow light scatters, adding more yellow phosphor to a single-layer arrangement in Figure 4.27 significantly reduces the output luminous flux.

On the other hand, compared to a single-layer yellow structure, a two-layer green-yellow structure experiences a greater rise in luminous flux due to the absorption of yellow energy and the emission of additional blue light. Superior color consistency and quality are highlighted by the luminous flux output that excels at considered color temperatures in the three-layer yellow, green, and red structure.

Overuse of yellow phosphor can interfere with the production of white light, leading to imbalance, unwanted backscatter, and a sudden reduction in the input luminous flux. Increasing the proportion of red phosphor increases the energy of red and blue light, which raises the luminous output and the Color Rendering Index (CRI).

For this reason, as temperatures rise, maintaining the proper particle concentration in the three-layer yellow, green, and red design is essential to preserving brightness, CRI, and color uniformity.

4.4.2 Scattering computation

The scattering coefficients $\mu_{sca}(\lambda)$, anisotropy factor $g(\lambda)$, and decreased scattering coefficient $\delta_{sca}(\lambda)$ can be determined using Mie's scattering theory. You can perform the calculations using formulas (4.6), (4.7), and (4.8), as illustrated below:

$$\mu_{sca}(\lambda) = \int N(r) C_{sca}(\lambda, r) dr \quad (4.6)$$

$$g(\lambda) = 2\pi \int \int_{-1}^1 p(\theta, \lambda, r) f(r) \cos \theta d \cos \theta dr \quad (4.7)$$

$$\delta_{sca} = \mu_{sca} (1 - g) \quad (4.8)$$

The function $N(r)$ represents the density distribution of scattered particles in cubic millimeters (mm^3). C_{sca} represents the scattering cross section in square millimeters (mm^2). The phase function is $p(\theta, \lambda, r)$, where θ is the scattering angle in degrees Celsius, λ is the wavelength of light in nanometers, and r is the radius of the scattering particle in micrometers. The distribution function $f(r)$ is dependent on the particle size in phosphor layers. You can determine these parameters using the formulas (Liem et al., 2022).

$$f(r) = f_{dif}(r) + f_{phos}(r) \quad (4.9)$$

$$N(r) = N_{dif}(r) + N_{phos}(r) = K_N \cdot [f_{dif}(r) + f_{phos}(r)] \quad (4.10)$$

The quantity $N(r)$ encompasses the combined mass of both diffusing particles, $N_{dif}(r)$, and phosphorus particles, $N_{phos}(r)$. The probability density functions $f_{dif}(r)$ and $f_{phos}(r)$ represent the size distribution of diffuse and phosphorus particles, respectively. Calculating the K_N dispersion unit index is necessary for determining the scattering concentration. You can obtain it using the following formula:

$$C = K_N \int M(r) dr \quad (4.11)$$

Where $M(r)$ is the mass distribution of the scattering unit and is determined by:

$$M(r) = \frac{4}{3} \pi r^3 [\rho_{dif} f_{dif}(r) + \rho_{phos} f_{phos}(r)] \quad (4.12)$$

$\rho_{dif}(r)$ and $\rho_{phos}(r)$ is the mass of the diffuse particle and the phosphor particle.

In Mie doctrine, C_{sca} can be determined with the following formula:

$$C_{sca} = \frac{2\pi}{k^2} \sum_0^{\infty} (2n - 1)(|a_n|^2 + |b_n|^2) \quad (4.13)$$

With $k = 2\pi/\lambda$ and a_n, b_n calculated according to the formula

$$a_n(x, m) = \frac{\Psi'_n(mx)\Psi_n(x) - m\Psi_n(mx)\Psi'_n(x)}{\Psi'_n(mx)\xi_n(x) - m\Psi_n(mx)\xi'_n(x)}$$

$$b_n(x, m) = \frac{m\Psi'_n(mx)\Psi_n(x) - \Psi_n(mx)\Psi'_n(x)}{m\Psi'_n(mx)\xi_n(x) - \Psi_n(mx)\xi'_n(x)} \quad (4.14)$$

With $x = k.r$, with m is the refractive coefficient and $\psi_n(x)$, $\xi_n(x)$ is the Riccati – Bessel function.

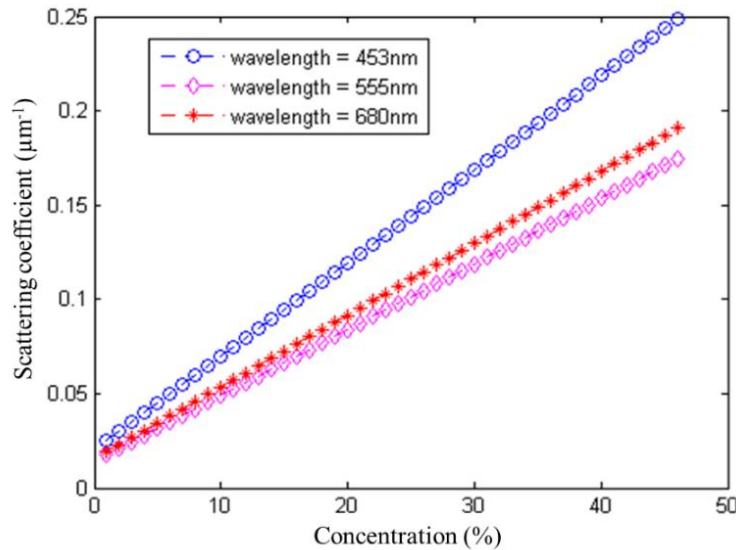


Figure 4.28: Scattering coefficient of ZnO:Bi³⁺ phosphor at wavelengths 453 nm, 555 nm, 680 nm

According to Figure 4.28's findings, the concentration of phosphorus affects how much the scattering coefficient increases. WLEDs are significantly impacted by the ZnO:Bi³⁺ scattering effect, more specifically ZnO:Bi³⁺ produces a greater quantity of red light than blue light from LEDs because ZnO:Bi³⁺ phosphors can absorb more blue light.

Lack of red light in WLED can be made up for with Bi^{3+} red phosphors. The anisotropy factor of $\text{ZnO}:\text{Bi}^{3+}$ phosphorus at wavelengths of 453 nm, 555 nm, and 680 nm is then displayed in the results. The anisotropy factor is greatest at 453 nm, as shown in Figure 4.29. It demonstrates why $\text{ZnO}:\text{Bi}^{3+}$ phosphor is good for WLED color consistency.

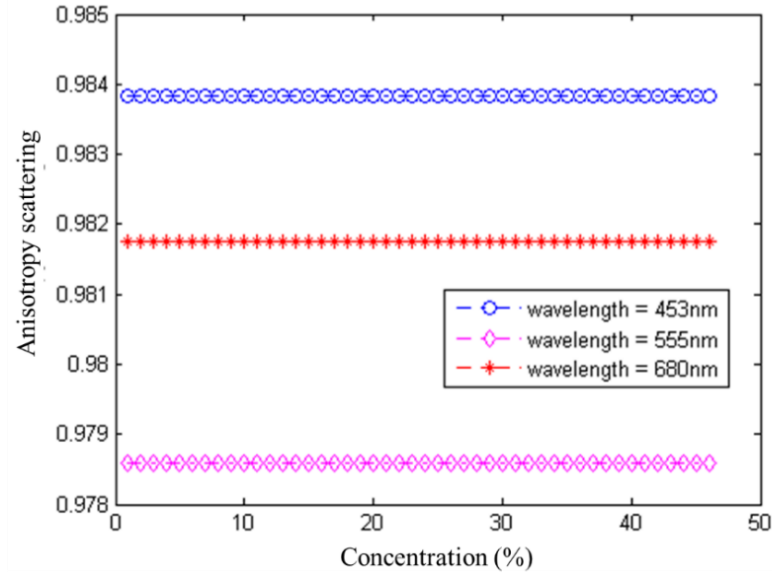


Figure 4.29: Anisotropic scattering of $\text{ZnO}:\text{Bi}^{3+}$ phosphor at wavelengths 453 nm, 555 nm and 680 nm

For the phosphor layers, silicon has a refractive index of 1.5. The refractive coefficient of phosphorus particles in silicon and the refractive coefficient of diffuse particles can then be found. According to the phase function, in this manner:

$$p(\theta, \lambda, r) = \frac{4\pi\beta(\theta, \lambda, r)}{k^2 C_{sca}(\lambda, r)} \quad (4.15)$$

In there, $\beta(\theta, \lambda, r)$, $S_1(\theta)$ and $S_2(\theta)$ represent angular scattering amplitude and are calculated according to the formulas:

$$\beta(\theta, \lambda, r) = \frac{1}{2} (|S_1(\theta)|^2 + |S_2(\theta)|^2) \quad (4.16)$$

$$S_1 = \sum_{n=1}^{\infty} \frac{2n+1}{n(n+1)} [a_n(x, m)\pi_n(\cos \theta) + b_n(x, m)\tau_n(\cos \theta)] \quad (4.17)$$

$$S_2 = \sum_{n=1}^{\infty} \frac{2n+1}{n(n+1)} [a_n(x, m)\tau_n(\cos \theta) + b_n(x, m)\pi_n(\cos \theta)] \quad (4.18)$$

All three wavelengths (453 nm, 555 nm, and 680 nm) exhibit nearly similar scattering coefficients for ZnO: Bi³⁺ phosphors, Figure 4.30 demonstrates. This stability for the scattering process is advantageous for the color quality of WLED.

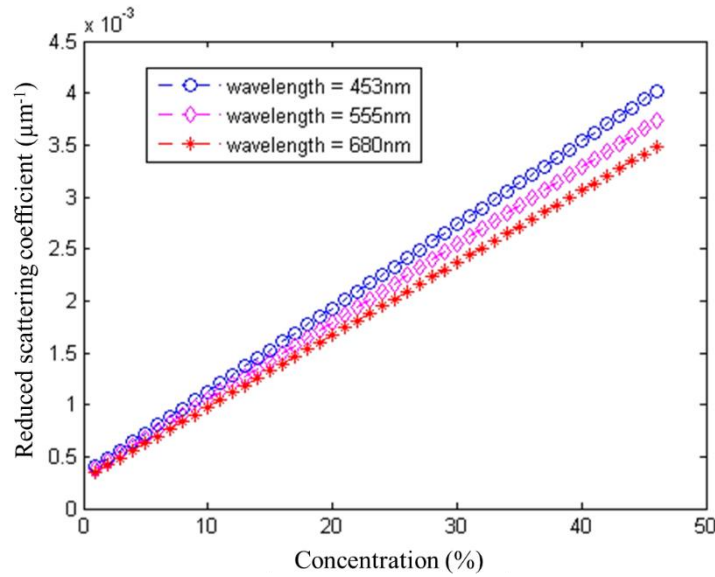


Figure 4.30: Reduced scattering coefficient of ZnO:Bi³⁺ phosphors at wavelengths of 453 nm, 555 nm and 680 nm

Further evidence that ZnO: Bi³⁺ enhances blue light scattering comes from the measured angular scattering amplitude data in Figure 4.31. The reduction of the yellow ring phenomenon that degrades WLED color quality is more likely to occur with higher blue light emission levels.

Applying ZnO: Bi³⁺ phosphors to WLEDs can enhance their color quality by producing higher proportions of red and blue light, as per the findings of Liem et al. (2022).

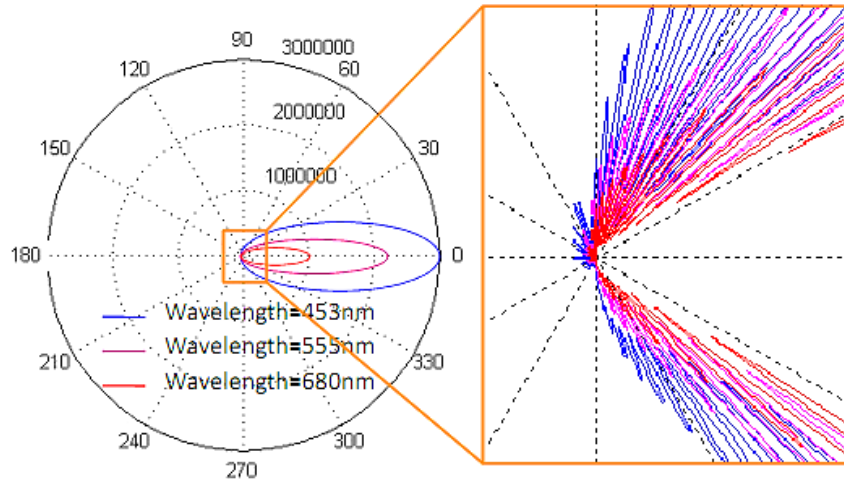


Figure 4.31: Angular scattering magnitude of ZnO:Bi³⁺ phosphors at wavelengths of 453 nm, 555 nm and 680 nm

4.4.3 Results and analysis

A comparison of the color rendering index and color quality index of phosphors in various structures is presented in Figure 4.31, whereas Figure 4.32 displays the emission spectrum of phosphors. The correlation among different types of remote structures is displayed at the same color temperature. The red-yellow structure's improved optical qualities improve the color quality, while the green-yellow structure's exceptional luminous flux is a result of the blue phosphor materials' improved scattering capabilities.

The most challenging aspect of this situation is that altering the high temperature will alter the phosphor particle concentration. The two-layer red-yellow distant structure and the three-layer yellow-green-red remote structure could be effectively simulated, demonstrating the optical characteristics of the red phosphor. This kind of phosphor can

alter the regularity and quality of the color of any structure in which it is present. The color quality index, or CQS for short, is the objective criteria used to assess the dependability of WLED but was left out of earlier research. CQS rises specifically in this three-layer arrangement.

Based on the research above, the manufacturer should select a structure with three layers of yellow, green, and red if the goal is to provide genuine color images. However, if the goal is to achieve high luminous flux for commercial production, only the green-yellow remote structure is required.

In this instance, despite the fact that the single-layer yellow remote structure does not, to a certain extent, increase color quality or luminous flux, it was selected to bring about high economic efficiency due to its low production cost and practical fabrication.

This study examines the impact of the phosphorus red on the quality assessment factor of WLEDs at a high temperature of 8500 K. Moreover, the results are verified by LightTools simulations and mathematical techniques. This is an encouraging outcome for producers seeking to modify the Color Rendering Index (CRI) for White Light Emitting Diodes (WLED).

In comparison to yellow, blue, and red phosphor materials, the findings of simulated emission spectroscopy are shown in Figure 4.32. According to the findings, the emission spectra is highest in the wavelength range of 550 nm to 580 nm at a high temperature of 8500 K. This is a significantly improved spectrum for blue light emission.

According to Figure 4.32, the YRG structure will result in the greatest amount of luminous flux. This structure also enhances the CRI.

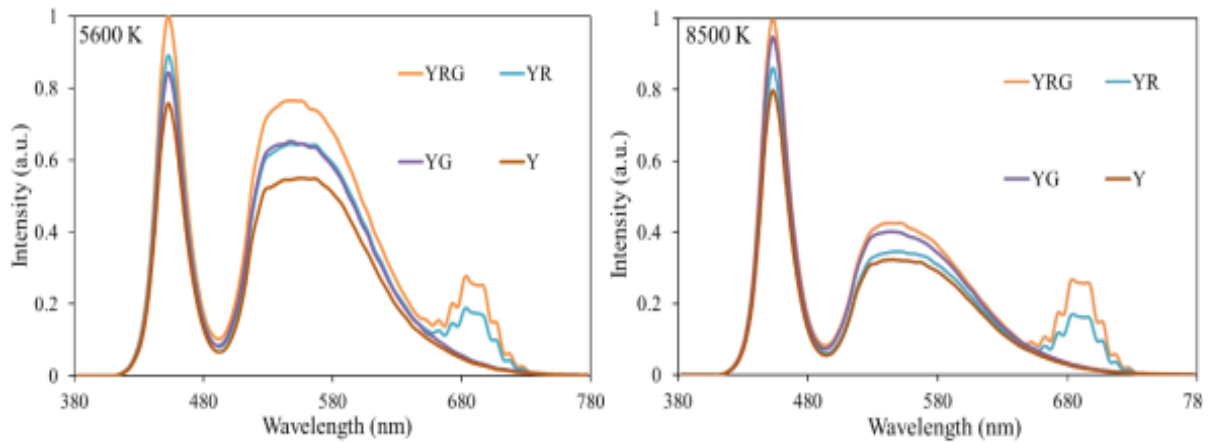


Figure 4.32: Emission spectrum image of phosphor remote structures

The emission spectrum of red light, ranging from 650 nm to 730 nm, exhibits its highest intensity at 680 nm. This particular wavelength significantly influences the energy of red light, resulting in the most pronounced enhancement of the Color Rendering Index (CRI). To summarize, the YRG structure is the most suitable option for enhancing luminous flux and color rendering index, thereby meeting the objective of this study. The emission spectrum of remote phosphor structures demonstrates a clear contrast. Upon comparing the emitter spectrum of the YL structure with that of three other remote phosphor structures at two ACCTs, we observe that the YL structure has the lowest intensity. This indicates that the luminous flux produced by the YL structure is the lowest. On the other hand, the YRG structure has the greatest spectral intensity within the wavelength range of 380 nm to 780 nm. The YG structure has a higher spectral intensity than the YR structure in the wavelength range of 400 nm to 500 nm, suggesting that the luminous flux of the YG structure may surpass that of the YR structure. Nevertheless, the YR structure exhibits a higher spectral intensity than the YG structure in the wavelength range of 650 nm to 750 nm. This feature allows the YR structure to have a higher color rendering index than the YG structure. Figure 4.33 presents the result that confirms the analysis mentioned before.

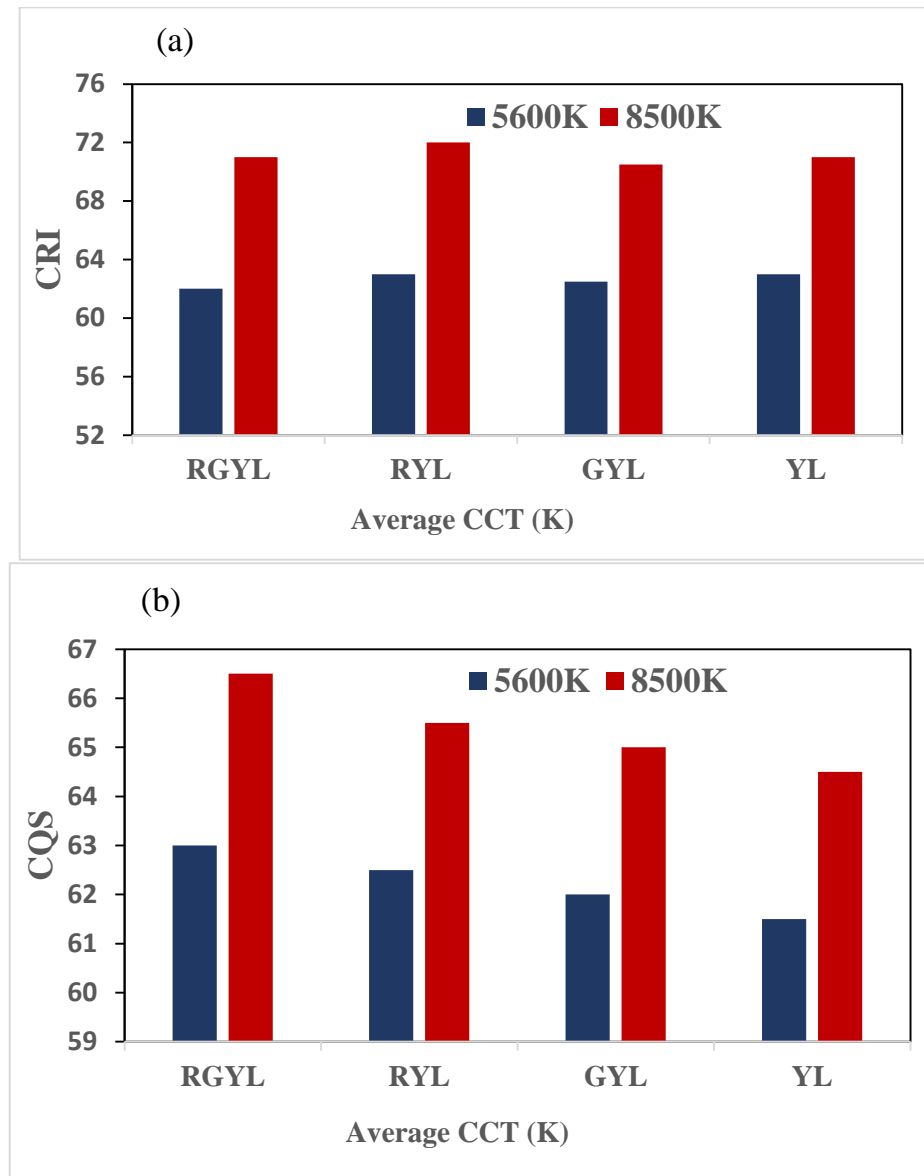


Figure 4.33: CRI and CQS indices of structures with different correlation temperatures

Figure 4.33a illustrates the comparative Color Rendering Index (CRI) of remote phosphor structures. It is clear that the RYL structure produces the highest CRI,

regardless of ACCT. The Color Rendering Index (CRI), for example, achieves its highest value at 8500 K and increases with the Absolute Color Temperature (ACCT). This discovery is highly important for improving the color rendering index (CRI) of remote phosphor structures. Controlling the color rendering index (CRI) at high-correlated color temperature (ACCT) levels above 7000 K is difficult. However, the RYL class is capable of doing this because of the inclusion of a red phosphor layer, which enhances the CRI of the RYL structure by introducing a red light component.

Based on the obtained CRI value, the RGYL structure ranks second. Meanwhile, the GYL structure has the lowest CRI. When considering CRI, choosing the RYL structure for mass production of WLEDs is a prudent decision. However, we only use CRI as one measure to assess color quality. Recently, CQS has gained more interest as a focal point for academic investigation. Three components make up CQS: the viewer's choice, color coordinates, and CRI. The three-factor coverage suggests that CQS is the most prominent indicator for assessing color quality, making it a primary priority.

The study presents a comparison of the color quality scale (CQS) for the distant phosphor structures in Figure 4.33b. At the point where the Color Rendering Index (CRI) of the Red-Yellow-Light (RYL) reaches its highest value, the Color Quality Scale (CQS) of the Red-Green-Yellow-Light (RGYL) similarly reaches its maximum level. The three primary hues are yellow, red, and green, and their equilibrium elucidates this concept. The color's quality positively correlates with the CQS value. The CQS is the lowest rank in the YL hierarchy. The YL structure often exhibits a high luminous flux; nevertheless, due to the absence of additional red and green light components, it poses difficulties in adjusting the color quality. Despite its color quality deficit, the YL structure nevertheless provides advantages in production.

Furthermore, this particular option not only boasts a more streamlined production procedure compared to the others, but it also incurs lower production costs. By incorporating the supplementary red material, the dual-layer structure will increase the

intensity of red light emitted, thereby enhancing the color rendering index. The three-layer structure's CRI performance is superior to that of the green-yellow and yellow-distant structures, regardless of the tested CCT.

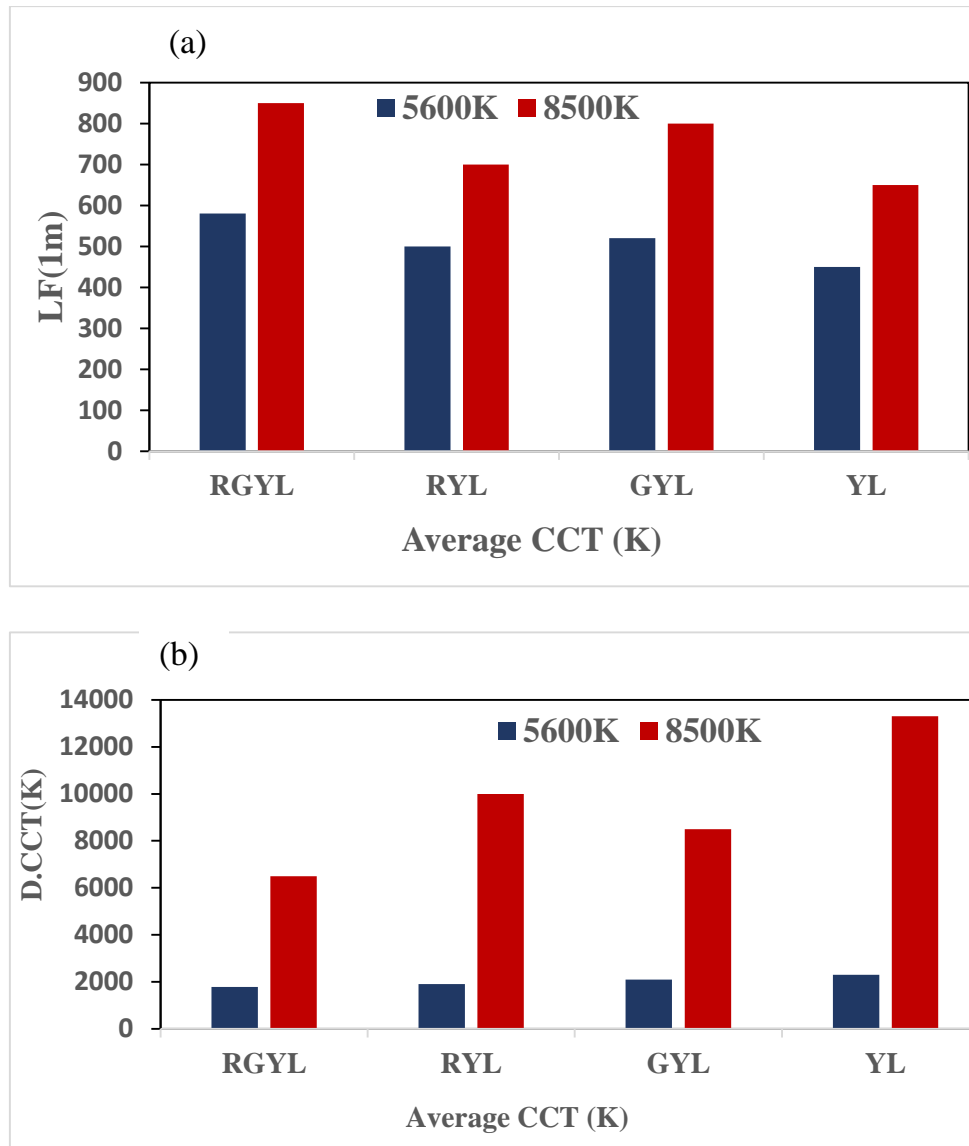


Figure 4.34: Luminous flux and color temperature deviation of different structures

This is due to the phosphor layer's inclusion. However, the release of red, yellow, green, and blue light creates white light, which is why the three-layer structure has the highest CQS value.

The color rendering index is displayed in medium white because, as Chapter 2 demonstrates, CQS uses a mixture of 15 hues to evaluate; the greater the temperature, the more beneficial the cold light. A more thorough metric for color rendition performance is the CQS. Therefore, it can be concluded that the greatest improved color rendering efficiency is provided by the three-layer distant phosphor structure.

Figure 4.34 displays the output luminous flux results of distant objects with DCCT contrast color temperature attenuation. The three-layer YGRL structure exhibits the maximum luminous flux, as demonstrated by the data (Figure 4.34a). When the Lambert formula is introduced, this result is further demonstrated. The 3-liner remote structure exhibits low temperature attenuation, especially at higher temperatures.

The findings from Figure 4.34a support the assumption that structure YL consistently has the lowest luminous flux among the four structures in all ACCTs. Conversely, the RGYL structure attains the greatest amount of luminous flux. The optical gain of RGYL is unquestionable, especially when the RGYL structure also provides the highest color quality. The GYL structure ranks second in terms of optical gain, thanks to the green phosphor it contains. The presence of the green phosphor leads to an augmentation in the proportion of green light and an expansion in the range of spectra between 500 and 600 nm.

It is clear that GYL has a greater intensity in this specific band of wavelengths compared to both YL and YL. The RGYL structure preserves ACCT due to the lowest concentration of YAG:Ce³⁺ phosphor. Decreasing the concentration of YAG:Ce³⁺ results in a reduction of scattered light due to the decrease in the RGYL structure. LED chips can easily transmit blue light rays through other layers because of the YAG:Ce³⁺ layer's high penetration susceptibility. In other words, the RGYL structure helps to effectively

convert the blue light energy emitted by the LED chip. As a result, RGYL's spectral intensity is highest in the wavelength area of white light compared to other distant phosphor architectures. Consequently, the RGYL structure exhibits the highest luminous flux. The superior optical properties of WLEDs, such as CQS and LE, allow for the adoption of the RGYL structure. The findings from Figure 4.34a support the assertion that structure YL consistently exhibits the lowest luminous flux among the four structures in all ACCTs. Conversely, the RGYL structure attains the greatest luminous flux. The optical gain of RGYL is unquestionable, especially when the RGYL structure also provides the highest color quality. The GYL structure ranks second in terms of optical gain, thanks to the green phosphor it contains.

The presence of the green phosphor leads to an augmentation in the proportion of green light and an expansion of the spectra in the wavelength range of 500–600 nm. Clearly, GYL exhibits a greater intensity in this specific band of wavelengths compared to both YL and YL. The low concentration of YAG:Ce³⁺ phosphor in the RGYL structure ensures the maintenance of ACCT. Decreasing the concentration of YAG:Ce³⁺ results in a reduction of scattered light due to the decrease in the RGYL structure. Even when passing through other layers, the YAG:Ce³⁺ layer is highly susceptible to the transmission of blue light rays emitted by LED chips. In other words, the RGYL structure helps to efficiently convert blue light energy from the LED chip.

Consequently, throughout the wavelength range of white light, the RGYL spectral intensity is highest in comparison to alternative remote phosphor designs. Consequently, the RGYL structure exhibits the highest luminous flux. The superior optical properties of WLEDs, such as CQS and LE, allow for the adoption of the RGYL structure.

On the other hand, color consistency also plays a significant role in the color quality element. Enhancing color uniformity can be achieved in a number of ways, for as by utilizing conformal phosphor setup or sophisticated scattering particles. If the two approaches are applied, light flux can be much decreased even though color homogeneity

was enhanced. Both the red and the green phosphors can increase scattering events and add the green or red light component to WLEDs to increase the amount of white light they produce. The light flux output is enhanced by the distant phosphor structure, which reduces the back reflection of the LED chip. To get the maximum transfer energy, you must regulate the concentration of the phosphor layer.

The comparison of color deviation between the structures is displayed in Figure 4.34b. The color homogeneity increases with decreasing color deviation. It is evident that RGYL has the smallest color deviation. This is explained by dispersion inside the LED package prior to the formation of white light. Scattering events increase with the number of phosphor layers. WLEDs exhibit improved color consistency as a result. Numerous scattering events can lower the luminous flux; therefore, they are not necessarily a good thing. Still, this decrease pales in comparison to the gain from a decreased backscattering. As a result, the RGYL structure with the greatest luminous flux and finest color consistency has the most phosphor layers. On the other hand, the YL structure exhibits the largest color deviation across all ACTTs.

Once more, increased color uniformity is more affected by high temperatures than by low ones. While improving luminous flux in the three-layer YGRL structure at high temperatures is the main objective of this study, color uniformity, CRI, and CQS have little bearing. This dissertation has added to the body of knowledge and information regarding developments in the production of white LEDs, as opposed to Liem et al.'s 2022 research. This dissertation specifically tackles the problem that the earlier study had: the LED optical determination did not take the color temperature component into account.

4.5 Summary

The main focus of this chapter is to explore particles of materials that can enhance scattering. $Y_2O_3:Ho^{3+}$ phosphor particles are introduced into the phosphor mixture to

increase light emission, thereby enhancing luminous flux. Alternatively, red phosphor material is added to increase the energy of red light with a wavelength of 680nm in the spectrum. Scatter-enhancing particles such as CaCO_3 , CaF_2 , TiO_2 , and SiO_2 are simulated using LightTools 9.0 software. The results are compared with different particle types, and SiO_2 particles are selected to be added to the phosphor mixture due to their optimal scattering properties, significantly increasing luminous flux.

Additionally, color quality is improved. LightTools simulation results indicate that the SiO_2 concentration and the smallest particle size are optimal. Why particles with a small size should be used? All of the questions is addressed by applying MIE theory for simulation. Simulation results define the research objective using scattering particles to enhance luminous flux, improve color uniformity, and color quality indices. Although CRI has a slight decrease, it is not significant. These results have demonstrated the potential of the second approach to accomplish the main goal of the dissertation. The proposed method suggests a remote structure combined with scatter-enhancing materials for the improvement of luminous flux and color uniformity of WLEDs.

CHAPTER 5 CONCLUSION AND FUTURE RESEARCH DIRECTIONS

5.1 Conclusion

A novel technique for comparing objects with various optical characteristics at various correlated color temperatures is presented in this dissertation. It also suggests that you consider the size and concentration of the chosen particles when utilizing distant buildings for various producing objectives. The traditional method of producing white light involves combining several yellow phosphors to change light to yellow-green.

However, because of the backscattering of yellow light, this approach produces a low output luminous flux. Second, the green-yellow structure's luminous flux is obviously enhanced when more green phosphor is used; yet, the structure's color rendering index and color quality are constrained. Third, because the energy qualities of the red phosphor material are significantly enhanced when it is used in the red-yellow structure, the color quality index is improved. Fourth, employing a mix of green, red, and yellow structures is the best possible option in the end. This structure improves the WLED's color quality as well as the luminous flux and color rendering index for real images. This leads to increased WLED quality reliability when a three-layer yellow-green-red remote structure is used. These are significant references because they discuss the necessity for creative approaches to LED lighting solutions and give producers the appropriate framework in certain situations to meet their WLED manufacturing needs (Loan et al., 2020).

In particular, this dissertation accurately models the operation of white LEDs using a range of luminescent material parameters. The outcomes of the experiments and simulations show the effectiveness and promise of the strategies suggested in the dissertation. while it comes to the method of using multi-layer remote phosphor structures, the dissertation unequivocally demonstrates that, in contrast to the data

gathered while using the single-layer remote one, employing two- and three-layer remote phosphor structures can enhance the optical performance of the white LED.

In particular, the two-layer structure with layers of yellow and green phosphors is good for increasing luminosity, while the structure with layers of red and yellow phosphors is good for color rendering. On the other hand, the three-layer distant phosphor structure can enhance the LED's luminance and color rendition. More specifically, the three-layer structure produced a more luminous flux than the two-layer and single-layer arrangements. Furthermore, it performs better at color rendition than both the single-layer and the yellow-green structures, but being slightly worse than the yellow-red structure. To put it briefly, every phosphor material in multi-layer remote phosphor structures has unique optical properties; yet, improper arrangement of the structure will lead to unwanted outcomes. Therefore, a yellow-green structure should be chosen in order to improve the output luminous flux. The red-yellow remote phosphor arrangement should be used if the requirements call for a high color rendering index. If the CQS color quality is required, the structure must be constructed in three layers of yellow, green, and red.

Several luminous particles are investigated utilizing the method of employing scattering enhancement materials. When the CaCO_3 , TiO_2 , CaF_2 , and SiO_2 are first compared, it is found that SiO_2 is the best particle to dope into the phosphor compound in order to induce the scattering performance. The recommended SiO_2 concentration and particle size for phosphor compound mixing are 5 weight percent and 1 μm , respectively. Next, a mixture of green phosphor and SiO_2 is added, adjusting the green phosphor concentration and particle size while maintaining the same SiO_2 parameters. For achieving sufficiently increased light flux and color homogeneity, 20 weight percent and 15-20 μm of green phosphor are the most ideal concentration and particle size, respectively. In the meantime, the applied green phosphor's specifications change to 5

weight percent and 20 micrometers for an increase in CRI and CQS. In particular, for CQS at high temperatures (7000–8000 K), 10 weight percent and 20 μm are the most suitable green-phosphor characteristics. Next, Mie scattering is used to model the scattering factors of the extra red phosphor material for the three-layer remote phosphor structure. The outcomes demonstrate that the prepared package's scattering is improved by the extra phosphor layer. Using the studied $\text{ZnO}:\text{Bi}^{3+}$ red phosphor, a comparison is made between the three-layer phosphor structure and the other remote phosphor structures (two- and single-layer structures). The results obtained are in good agreement with the conclusions from the preceding chapter, indicating that the three-layer distant phosphor structure is the best structure to achieve WLED enhancement. Additionally, the scattering results help to clarify the effectiveness and potential of the suggested multi-layer remote structures. As a result, the main objectives mentioned at the start of the dissertation have been met.

5.2 Future research directions

In the future, with the growing research trend along with the problematic conditions at universities today, the need to coordinate research between students and teachers to create a solid foundation for lighting materials instead of optical lamps and extensive financial resources are required. While our country's funding is minimal, it is difficult for some universities to build experimental labs. Therefore, it is necessary to convert from complex to simple, which means that simulation software in other countries is costly, so currently, the only popular and widely used software in universities is MATLAB. Therefore, this is the direction of future research to convert this application software into experimental LED thermal simulation to determine the change in output luminous flux, as well as the color quality of LED. At the same time, bringing mathematical models from 3D to 2D for easy application in research work helps to create close links between teachers and students in academic exchange. This is also a strong

point in research as the MATLAB software has never been utilized in heat treatment simulation.

LIST OF PUBLICATIONS

1. Ming, J. C., Lee, H., Nguyen, D. Q. A., **Nguyen, T. P. L.**, Le, V. T. (2020). Selection of Remote Phosphor Led Packages for Improving Luminous Flux. *Journal of Advanced Engineering and Computation (JAEC)*, **4**(2), P118-124. DOI: 10.25073/jaec.202042.259.
2. Tran, T. C., Guo, L., **Nguyen, T. P. L.**, Le, V. T., Nguyen, D. Q. A. (2020). The Application of $\text{Mg}_2\text{TiO}_4:\text{Mn}^{4+}$ and $\text{NaYF}_4:\text{Er}^{3+}$, Yb^{3+} and Double Convex Structure in Improving Optical Performance of Phosphor-in-Glass Based White Light-Emitting Diodes. *Journal of Advanced Engineering and Computation (JAEC)*, **4**(4), P218-225, DOI: 10.25073/jaec.202042.259.
3. **Nguyen, T. P. L.**, Le, A. T. (2020). Enhance the chromatic uniformity and luminous efficiency of WLEDs with triple-layer remote phosphor structures. *International Journal of Electrical and Computer Engineering IJECE*, **10**(6), PP: 6244-6150.
4. Phung, T. T., Thuc, M. B., **Nguyen, T. P. L.**, Phan, X. L., Nguyen, D. Q. A., Le, V. T. (2020). Dual-layer remote phosphor structure: a novel technique to enhance the color quality scale and luminous flux of WLEDs. *International Journal of Electrical and Computer Engineering IJECE*, **10**(4), PP: 4015-4022.
5. Nguyen, T. M. H., **Nguyen, T. P. L.**, Bui, T. M., Vu, T. V. (2020). Using SiO_2 nano-particles for better color uniformity and lumen output in 8500 K conformal and in-cup white LEDs. *International Journal of Electrical and Computer Engineering IJECE*, **11**(5), pp. 3897~3902. DOI: 10.11591/ijece.v11i5.pp3897-3902.

6. Nguyen, T. M. H., **Nguyen, T. P. L.**, Bui, T. M., Le, T. A. (2020). The effect green $\text{YF}_3:\text{Er}^{3+}$, YB^{3+} phosphor on luminous flux and color quality of multi-chip white light-emitting diodes. *International Journal of Electrical and Computer Engineering (IJECE)*, **11**(6), pp. 4810~4816. DOI: 10.11591/ijece.v11i6.pp4810-4816.
7. Nguyen, T. M. H., **Nguyen, T. P. L.**, Bui, T. M., Hoang, V. N. (2020). Using CaCO_3 -doped package to improve correlated color temperature uniformity of white light-emitting diodes. *International Journal of Electrical and Computer Engineering (IJECE)*, **11**(6), pp. 4817~4824. DOI: 10.11591/ijece.v11i6.pp4817-4824.
8. **Nguyen, T. P. L.**, Nguyen, D. Q. A. (2020). $\text{Y}_2\text{O}_3:\text{Ho}^{3+}$ and $\text{ZnO}:\text{Bi}^{3+}$: a selection for enhancing color quality and luminous flux of WLEDs. *International Journal of Electrical and Computer Engineering (IJECE)*, **10**(5), PP: 5162-5167.
9. **Nguyen, T. P. L.**, Nguyen, D. Q. A. (2020). The options in remote phosphor structure for better white LEDs color quality. *Telkomnika*, **18**(5), pp. 2606~2611.
10. Thuc, M. B., Phan, X. L., **Nguyen, T. P. L.**, Nguyen, D. Q. A., Le, A. T., Le, V. T. (2020). The application of $(\text{Y,Gd})\text{BO}_3:\text{Tb}^{3+}$ and $\text{CaGa}_2\text{S}_4:\text{Mn}^{2+}$ phosphors to remote white light-emitting diodes. *Telkomnika*, **18**(1), PP. 351-357.
11. **Nguyen, T. P. L.**, Nguyen, D. Q. A. (2020). The application of double-layer remote phosphor structures in increasing WLEDs color rendering index and lumen output. *International Journal of Electrical and Computer Engineering (IJECE)*, **10**(5), PP: 5183-5190.
12. **Nguyen, T. P. L.**, Nguyen, D. Q. A. (2020). $\text{Na}_3\text{Ce}(\text{PO}_4)_2:\text{Tb}^{3+}$ and $\text{Na}(\text{Mg}_{2-x}\text{Mn}_x)\text{LiSi}_4\text{O}_{10}\text{F}_2:\text{Mn}$ phosphors: a suitable selection for enhancing color quality and luminous flux of remote white light-emitting diodes. *Telkomnika*, **18**(4), PP. 2095-2010.

13. Phung, T. T., **Nguyen, T. P. L.**, Nguyen, D. Q. A., Le, A. T. (2020). Enhanced Luminous Efficacy of White LED with Flat Dual-Layer Remote Phosphor Structure. *Applied Physics*, **18**(2), PP. 107-114.
14. **Nguyen, T. P. L.**, Nguyen, D, Q. A. (2020). The effects of ZnO particles on the color homogeneity of phosphor-converted high-power white led light sources. *International Journal of Electrical and Computer Engineering (IJECE)*, **10**(5), PP: 5155-5161
15. **Nguyen, T. P. L.**, Nguyen, D. Q. A. (2020). Utilizing CaCO₃, CaF₂, SiO₂, and TiO₂ particles to enhance color homogeneity and luminous flux of WLEDs. *International Journal of Electrical and Computer Engineering (IJECE)*, **10**(5), pp. 5175~5182. DOI: 10.11591/ijece.v10i5.pp5175-5182.
16. **Nguyen, T. P. L.**, Tran, C. T. (2020). Green-emitting Gd₂O₂S:Tb³⁺ and red-emitting Y₃Al₅O₁₂:Cr³⁺ phosphors: a suitable selection for enhancing color quality of remote phosphor structure. *Telkomnika*, **18**(3), pp. 1561~1566 ISSN: 1693-6930, DOI: 10.12928/TELKOMNIKA.v18i3.13626.
17. **Nguyen, T. P. L.**, Tran, C. T. (2020). Design of freeform lens for WLEDs on the fishing boat. *Telkomnika*, **18**(3), pp. 1553~1560, ISSN: 1693-6930, DOI:10.12928/TELKOMNIKA.v18i3.12085.
18. **Nguyen, T. P. L.**, Nguyen, D. Q. A. (2020). Improving color quality and luminous flux of white LED utilizing triple-layer remote phosphor structure. *International Journal of Electrical and Computer Engineering (IJECE)*, **10**(5), PP: 5168-5174.
19. **Nguyen, T. P. L.**, Nguyen, D. Q. A. (2020). SrBaSiO₄:Eu²⁺ phosphor: a novel application for improving the luminous flux and color quality of multi-chip white LED lamps. *International Journal of Electrical and Computer Engineering (IJECE)*, **10**(5), pp. 5147~5154. DOI: 10.11591/ijece.v10i5.pp5147-5154.

REFERENCES

- Anton, A., Jean, P. L., Grigory, O., Kumar, A. and Genevieve, M. (2020). Dynamic response-based LEDs health and temperature monitoring Measurement. *Elsevier*, 156, 107599. DOI: 10.1016/j.measurement.2020.107599.
- Banjong, L., Zili, W., Cheng, Q., Yi, R., Bo, S., Dechen, Y., Zhou, J. and Jaimie, F. (2019). Investigation of Step-Stress Accelerated Degradation Test Strategy for Ultraviolet Light Emitting Diodes. *Materials*, 12(19), 3119. DOI: 10.3390/ma12193119.
- Bui, M. T., Loan, N. T. P., Le, X. P., Anh, N. D. Q., Le, A. T. and Tho, L. V. (2020). The application of (Y,Gd)BO₃:Tb³⁺ and CaGa₂S₄:Mn²⁺ phosphors to remote white light-emitting diodes. *Telecommunication, Computing, Electronics and Control*, 18(1), pp. 351~357. DOI: 10.12928/TELKOMNIKA.v18i1.13713.
- Chen, M. J., Loan, N. T. P., Tho, L. V., Bui, M. T., Phan, X. L., Anh, N. D. Q., Hsing, Y. L., Chang, C. J. and Hsiao, Y. L. (2020). The impacts of Ba₂Li₂Si₂O₇:Sn²⁺, Mn²⁺ and CaMgSi₂O₆:Eu²⁺, Mn²⁺ particles on the optical properties of remote phosphor LED. *Materials Science Poland*, 38(1), pp.197-205. DOI:10.2478/msp-2020-0002.
- Cheng, C. S., Chen, C. Y., Chen, C. C., Chiu, C. Y., Peng, Y. N., Wang, Y. H. and Yang, T. H. (2012). High uniformity in angular correlated-color-temperature distribution of white LEDs from 2800K to 6500K. *Opt. Express*, 20(6), pp.6622-6630. DOI:10.1364/OE.20.006622.
- Craig, F. B. and Huffman, D. R. (1998). *Absorption and Scattering of Light by Small Particles*. USA: John Wiley & Sons. Inc
- Chen, K. J., Kuo, H. T., Chiang, Y. C., Chen, H. C., Wang, H. C., Shih, M. H., Lin, C.C., Pan, C. J. and Kuo, H. C. (2013). Efficiency and Droop Improvement in Hybrid Warm White LEDs Using InGaN and AlGaInP High-Voltage LEDs.

Journal of Display Technology, 9(4), P280-284, DOI: opg.optica.org/jdt/abstract.cfm?URI=jdt-9-4-280.

- Chahed, S. Y., Xi, Y., Li, L. Y., Gassmann, Th. And Schubert, E. F. (2005). Influence of junction temperature on chromaticity and color-rendering properties of trichromatic white-light sources based on light-emitting diodes. *Journal of Applied Physics*, 97(5), 054506. DOI: 10.1063/1.1852073.
- Chang, Y. Y., Ting, Y. Z., Chen, C. Y., Yang, T. H. and Sun, C. C. (2014). Design of optical module with high stability, high angular color uniformity, and adjustable light distribution for standard lamps. *Journal of Display Technology*, 10(3), 223-227. DOI: 10.1109/JDT.2013.2294962.
- Chou, Y. F., Chen, C. F., Ying, S. P. and Yeh, Y. Y. (2019). The Effects of TiO₂ Diffuser-Loaded Encapsulation on Corrected Color Temperature Uniformity of Remote Phosphor White LEDs. *Applied of Scientific*, 9(4), P675-685. DOI:10.3390/app9040675
- Davis, J. L., Mills, K. C., Bogachev, G., Rountree, J. K., Landvik, M., Yaga, R. and Johnson, C. (2018). Understanding chromaticity shifts in LED devices through analytical models. *Elsevier, Microelectronics Reliability*, 84, P149-156. DOI: 10.1016/j.microrel.2018.03.023.
- Dang, H. P., Loan, N. T. P., Chung, N. T. K. and Anh, N. D. Q. (2021). The study of convex-dual-layer remote phosphor geometry in upgrading WLEDs color rendering index. *International Journal of Electrical & Computer Engineering*, 11(5), pp.3890-3896. DOI:10.11591/ijece. v11i5.pp3890-3896.
- David W, H. (2009). Light Scattering Theory. *Department of Mechanical and Aerospace Engineering University of Florida*, P1-13.
- Dang, S. J., Huang, W., Guo, Z and Gao, Z. (2015). A Transmission-Type Testing

System for Measuring Optical Characteristics of Phosphors for Remote-Phosphor-Based White LED. *IEEE photonic Journal*, 8(1), P1. DOI: 10.1109/JPHOT.2015.2513202

- David, A., Paul, T. F., Kevin, W. H., Ohno, Y., Micheal, P. R., Minchen, W. and Lorne, W. (2015). Development of the IES method for evaluating the color rendition of light sources. *Optics Express*, 23(12), pp. 15888-15906. DOI:10.1364/OE.23.015888
- Dupuis, R. D. and Kramer, M. R. (2008). History, development, and applications of high brightness visible light emitting diodes. *Journal of Lightwave Technology, IEEE*, 26(9), PP.1154–1171. DOI: 10.1109/JLT.2008.923628.
- Gu, C., Wang, XJ., Xia, C., Li, SX., Liu, P., Li, DZ., Li, HL., Zhou, GH., Zhang, J. and Xie, RJ. (2019). A new CaF₂-YAG: Ce composite phosphor ceramic for high-power and high-color-rendering WLEDs. *Journal of Materials Chemistry C*, 7(28), P8569-8574, DOI: 10.1039/c9tc02407g.
- János, H., Gusztáv, H. and András P. (2020). Lifetime Modelling Issues of Power Light Emitting Diodes. *Energies* 2020, 13(13), 3370. DOI:10.3390/en13133370.
- Jost, S., Cauwerts, C. and Avouac, P. (2018). CIE 2017 color fidelity index R_f: a better index to predict perceived color difference? *Journal of the Optical Society of America A*, 35(4), pp. B202-B213. DOI: 10.1364/JOSAA.35.00B202.
- Hung, P. C. and Tsao, J. Y. (2013). Comments on “Maximum White Luminous Efficacy of Radiation Versus Color Rendering Index and Color Temperature: Exact Results and a Useful Analytic Expression. *Journal of Display Technology*, 9(10), pp. 859-860. DOI: 10.1109/JDT.2013.2279275.
- Hanh, N. T. M., Loan, N. T. P and Anh, N. D. Q. (2020). The application of green

- YPO₄:Ce³⁺, Tb³⁺ and red LiLaO₂:Eu³⁺ layers to remote phosphor LED. *TELKOMNIKA Telecommunication, Computing, Electronics and Control*, 18(5), pp. 3216~3221. DOI: 10.12928/telkomnika. v18i6.13647
- Hanh, N. T. M., Loan, N. T. P. and Anh, N. D. Q. (2020). Improving optical properties of remote phosphor LED using green Y₂O₃:Ho³⁺ and red Mg₄(F)(Ge, Sn)O₆:Mn²⁺ layers. *TELKOMNIKA Telecommunication, Computing, Electronics and Control*, 18(6), pp. 3228~3233. DOI: 10.12928/telkomnika. v18i6.13797.
- Hanh, N. T. M., Loan, N. T. P. and Anh, N. D. Q. (2020). Acquiring higher lumen efficacy and color rendering index with green NaYF₄:Er₃₊Yb₃₊ and red α-SrO₃B₂O₃:Sm²⁺ layers for designing remote phosphor LED. *TELKOMNIKA Telecommunication, Computing, Electronics and Control*, 18(6), pp. 3222~3227 ISSN: 1693-6930. DOI: 10.12928/telkomnika. v18i6.13796.
- Huffman, R. D. and Buhner, H. C. (1998). *Absorption and Scattering of Light by Small Particles*. USA: John Wiley & Sons
- Heffernan, M. B., Heinson, W. Y., Maughan, B. J., Chakrabarti, A. and Sorensen, M. C. (2016). Backscattering measurements of micron-sized spherical particles. *Applied of Optics*, 55(12), pp. 3214-3218. DOI: 10.1364/AO.55.003214.
- Hanh, N. T. M., Loan, N. T. P. and Ngoc, H. V. (2021). Enhancing light scattering effect of white LEDs with ZnO nanostructures. *International Journal of Electrical and Computer Engineering*, 11(5), P3838-3843. DOI: 10.11591/IJECE.V11I5.PP3838-3843.
- Hanh, N. T. M., Loan, N. T. P., Bui, M. T. and Vu, T. V. (2021). Using SiO₂ Nano-particles for better color uniformity and lumen output in 8500 K conformal and in-cup white LEDs. *International Journal of Electrical and Computer Engineering (IJECE)*, 11(5), PP. 3897-3802. DOI: 10.11591/ijecev11i5.pp3897-3902.
- Hanh, N. T. M., Loan, N. T. P. and Anh, N. D. Q. (2020). The application of green

- YO₄:Ce³⁺, Tb³⁺ and red LiLaO₂:Eu³⁺ layers to remote phosphor LED. *Telecommunication Computing Electronics and Control*, 18(6), pp. 3216~3221. DOI: 10.12928/telkomnika.v18i6.13647.
- Hanh, N. T. M., Loan, N. T. P. and Anh, N. D. Q. (2020). Study of red-Emitting LaAsO₄:Eu³⁺ phosphor for color rendering index improvement of WLEDs with dual-layer remote phosphor geometry. *TELKOMNIKA Telecommunication, Computing, Electronics and Control*, 18(6), pp.3210~3215. DOI: 10.12928/telkomnika.v18i6.13637.
- Hanh, N. T. M., Loan, N. T. P. and Anh, N. D. Q. (2020). Acquiring higher lumen efficacy and color rendering index with green NaYF₄:Er³⁺Yb³⁺ and red α-SrO₃B₂O₃:Sm²⁺ layers for designing remote phosphor LED. *TELKOMNIKA Telecommunication, Computing, Electronics and Control*, 18(6), p. 3222~3227. DOI: 10.12928/telkomnika.v18i6.13796.
- Holon yak, J. N. and Bevacqua, S. F. (1962), (2004). Coherent (visible) light emission from Ga (As_{1-x}P_x) junctions. *Applied Physics Letters*, 1(4), PP82–83. DOI:10.1063/1.1753706
- Huadong, Z., Lingyan, L., Jiaqi, W., Brian, S. and Swung, W. R. (2017). Thermal Characterization of Multi-Chip Light Emitting Diodes with Thermal Resistance Matrix. *IEEE Xplore*, DOI: 10.1109/IFWS.2017.8245969.
- Kim, J. K., Hong, L., Eric, F. S., Cho, J., Sone, C and Park, Y. (2005). Strongly Enhanced Phosphor Efficiency in GaInN White Light-Emitting Diodes Using Remote Phosphor Configuration and Diffuse Reflector Cup. *Japanese Journal of Applied Physics*, 44(21), L 649–L 651. DOI: 10.1143/JJAP.44. L649
- Kolkhoz, A., Ali, R., Mohammadreza, K., Teng, M., Henk, V. Z. and Kouchi, Z. (2016). Output blue light evaluation for phosphor based smart white LED wafer level packages. *Optics Express*, 24(4), pp. 3216-3229. DOI:10.1364/OE.24.003216.

- Li, B., Zhang, D., Huang, Y., Ni, Z. and Zhuang, S. (2010). A new structure of multi-layer phosphor package of white LED with high efficiency. *Chinese Optics Letters*, 8(2), P221-223. <https://opg.optica.org/col/abstract.cfm?URI=col-8-2-221>.
- Liu, X and Xiaoping, L. (2011). *LED packaging for lighting applications: Design, Manufacturing and Testing*. Singapore: John Wiley & Sons (Asia) Pte Ltd. DOI:10.1002/9780470827857.
- Lai, C. F., Lee, Y. C. and Kuo, C. T. (2014). Saving Phosphor by 150% and Producing High Color-Rendering Index Candlelight LEDs Containing Composite Photonic Crystals. *IEEE, Journal of Lightwave Technology*, 32(10), pp. 1930-1935. DOI: 10.1109/JLT.2014.2309955.
- Le, P. X., Duc, L. P., Hoang, N. N. and Anh, N. D. Q. (2019). The Impacts of Distance Between Phosphor Layers on Optical Properties of Triple-Layer Phosphor Structure. *Advances in Electrical and Electronic Engineering*, 17(1), pp. 81-86. DOI: 10.15598/aeer.v17i1.3055.
- Lai, M. F., Anh, N. D. Q., Hsin, Y. M. and Hsiao, Y. L. (2016). Scattering effect of SiO₂ particles on correlated color temperature uniformity of multi-chip white light LEDs. *Journal of the Chinese Institute of Engineers*, 39(4), P468-472. DOI: 10.1080/02533839.2015.1117950.
- Lin, H. Y., Chen, K. J., Wang, S. W., Lin, C. C., Wang, K. Y., Li, J. R., Lee, P. T., Shih, M. H., Li, X. L., Chen, M. H. and Kuo, C. (2015). Improvement of light quality by DBR structure in white LED. *Opt. Express* 23(3), A27-A33. DOI: 10.1364/OE.23.000A27
- Liu, Z, Y., Liu, S., Wang, K. and Luo, X, B. (2010). Measurement and numerical studies of optical properties of YAG: Ce phosphor for white light-emitting diode packaging. *Applied Optics*, 49(2), PP. 247-257. DOI: 10.1364/AO.49.000247.
- Lee, Y. J., Lu, T. C., Kou, H. C. and Wang, S. C. (2007). High brightness GaN-based

- light emitting diodes. *Journal of Display Technology, IEEE*, 3(2), P118– 125. DOI: 10.1109/JDT.2007.894380.
- Liem, V. B., Loan, N. T. P. and Tran, N. M. H. (2023). For improvements in chromatic scales and luminescent fluxes of white lights: developing a dual-layer remote phosphor structure. *TELKOMNIKA Telecommunication Computing Electronics and Control*, 21(1), pp.178~185. DOI: 10.12928/TELKOMNIKA.v21i1.24239.
- Liem, B. V., Loan, N. T. P. and Phan, X. L. (2022). Study of ZnS: Mn²⁺, Te²⁺ phosphor for improving the hue rendering indicator of WLEDs. *Bulletin of Electrical Engineering and Informatics*, 11(4), pp. 1938~1944. DOI: 10.11591/eei.v11i4.4061.
- Linhares, J. M. M., Paulo, D. A. P. and Nascimento, C. M. S. (2009). Color rendering of art paintings under CIE illuminants for normal and color deficient observers. *Journal of the Optical Society of America*, 26(7). pp. 1668-1677. DOI: 10.1364/JOSAA.26.001668
- Li, X., Chen, J., Liu, Z., Deng, Z., Huang, Q., Huang, J. and Guo, W. (2021). (Ce, Gd):YAG-Al₂O₃ composite ceramics for high-brightness yellow light-emitting diode applications. *Research Square*. DOI: 10.1016/j.jeurceramsoc.2021.11.027.
- Loan, N. T. P. and Le, A. T. (2020). Improving color rendering index of WLEDs with convex-dual-layer remote phosphor geometry using red-emitting CaGa₂S₄:Mn²⁺ phosphor. *TELKOMNIKA Telecommunication, Computing, Electronics and Control*, 18(5), pp. 2702~2707. DOI: 10.12928/telkomnika.v18i5.14250
- Loan, N. T. P., Anh, N. D. Q., Nguyen, C. T. and Hsiao, Y. L. (2022). Better color distribution uniformity and higher luminous intensity for LED by using a three-layered remote phosphor structure. *Materials Science-Poland*, 40(1), pp. 60-67. DOI: 10.2478/msp-2022-0010.
- Loan, N. T. P. and Anh, N. D. Q. (2020). Improving color quality and luminous

- flux of white LED utilizing triple-layer remote phosphor structure. *International Journal of Electrical and Computer Engineering (IJECE)*, 10(5), pp. 5168~5174. DOI: 10.11591/ijece.v10i5.pp5168-5174.
- Loan, N. T. P. and Tran, C. T. (2020). Green-emitting $\text{Gd}_2\text{O}_2\text{S}:\text{Tb}^{3+}$ and red-emitting $\text{Y}_3\text{Al}_5\text{O}_{12}:\text{Cr}^{3+}$ phosphors: a suitable selection for enhancing color quality of remote phosphor structure. *TELKOMNIKA Telecommunication, Computing, Electronics and Control*, 18(3), pp. 1561~1566. DOI: 10.12928/TELKOMNIKA.v18i3.13626.
- Loan, N. T. P. and Anh, N. D. Q. (2020). The options in remote phosphor structure for better white LEDs color quality. *TELKOMNIKA, Telecommunication, Computing, Electronics and Control*, 18(5), pp. 2606~2611. DOI: 10.12928/telkomnika.v18i5.13526.
- Loan, N. T. P. and Anh, N. D. Q. (2020). $\text{Y}_2\text{O}_3:\text{Ho}^{3+}$ and $\text{ZnO}:\text{Bi}^{3+}$, A selection for enhancing color quality and luminous flux of WLEDs. *International Journal of Electrical and Computer Engineering (IJECE)*, 10(5), pp. 5162~5167. DOI: 10.11591/ijece.v10i5.pp5162-5167.
- Loan, N. T. P. and Anh, N. D. Q. (2020). The application of double-layer remote phosphor structures in increasing WLEDs color rendering index and lumen output. *International Journal of Electrical and Computer Engineering (IJECE)*, 10(5), pp.5183~5190. DOI: 10.11591/ijece.v10i5.pp5183-5190.
- Loan, N. T. P and Anh, N. D. Q. (2021). Enhancing optical performance of dual-layer remote phosphor structures with the application of $\text{LaAsO}_4:\text{Eu}^{3+}$ and $\text{Y}_2\text{O}_3:\text{Ho}^{3+}$. *Optoelectronics and advanced materials – rapid communications* 15(1-2), p. 71 – 78. DOI: 10.11591/ijece.v10i5.pp5183-5190
- Lu, L. and Price, A. (2012). Entropy, color, and color rendering. *Journal of the Optical Society of America*, 29(12), pp. 2557-2565. DOI: 10.1364/JOSAA.29.002557.
- Michael, I. and Mish, G. (2009). Gustav Mie and the fundamental concept of

- electromagnetic scattering by particles: A perspective. *Journal of Quantitative Spectroscopy & Radiation Transfer, Elsevier, 110(14-16)*, P1210–1222. DOI: 10.1016/j.jqsrt.2009.02.002.
- Michael, R. K., Julie, J. B. and Paul, L. H. (2002). Introduction to the issue on high-efficiency light-emitting diodes. *J. Sel. Topics Quantum Electron, IEEE, 8(2)*, PP. 185–188. DOI: 10.1109/2944.999171.
- Mehr, Y. M., Bahrami, A., Van, W. D., Driel, X., Fan, X. J., Davis, L. J. and Zhang, Q. G. (2020). Degradation of optical materials in solid-state lighting systems. *International Material Review 65(2)*, P102-128. DOI: 10.1080/09506608.2019.1565716.
- Muthu, S., Schuurmans, F. J. P. and Pashley, M. D. (2002). Red, green, and blue LEDs for white light illumination. *IEEE, 8(2)*, P333-338. DOI: 10.1109/2944.999188.
- Narendran, N and Gu, Y. (2005). Life of LED-based white light sources. *J. Disp. Technol, IEEE, 1(1)*. P167-171. DOI: 10.1109/JDT.2005.852510.
- Nakamura, S., Mukai, T. and Senoh, M. (2001). High-power GaN PN junction blue-light emitting diodes. *Japanese Journal of Applied Physics, 30(12A)*, L1998–L2001. DOI: 10.1143/JJAP.30. L1998.
- Narendran, N., Gu, Y., Fiessinger, J. P., Yu, H. and Deng, L. (2004). Solid-state lighting: Failure analysis of white LEDs. *Elsevier, Journal of Crystal Growth, 268(3-4)*, P449-456. DOI: 10.1016/j.jcrysgro.2004.04.071.
- Narendran, N., Gu, M. Y., Jayasinghe, L., Fiessinger, J. P. and Zhu, Y. (2007). Long-term performance of white LEDs and systems. *Proc of First international conference on White LEDs and Solid-State lighting, Tokyo, Japan*, P174-179.
- Oh, J. H., Yang, S. J., Sung, Y. G. and Do, Y. R. (2012). Excellent color rendering indexes of multi-package white LEDs. *Optics Express, 20(18)*, pp. 20276-20285. DOI: 10.1364/OE.20.020276.
- Peifen, Z., Hongyang, Z., Gopi, C. A. and Saroj, Th. (2019). Design of circadian white

- light-emitting diodes with tunable color temperature and nearly perfect color rendition. *OSA Continuum*, 2(8), P2413-2427. DOI: 10.1364/OSAC.2.002413
- Quintero, J. M., Antoni, S., Charles, E. H. and Carreras, J. (2012). Color rendering map: a graphical metric for assessment of illumination. *Optics Express*, 20(5), pp. 4939-4956. DOI: 10.1364/OE.20.004939.
- Ryu, G. H., Byungjin, M. and Han, Y. R. (2019). Temperature dependence of the color rendering index of a phosphor-conversion white light-emitting diode. *AIP Adv.* 9(1), 015009. DOI: 10.1063/1.5066351.
- Ryu, G. H. and Ryu, H. Y. (2015). Analysis of the temperature dependence of phosphor conversion efficiency in white light-emitting diodes. *Journal of the Optical Society of Korea*, 19(3), P311-316. DOI: 10.3807/JOSK.2015.19.3.311
- Singh, P. and Tan, M. C. (2016). Degradation physics of high-power LEDs in outdoor environment and the role of phosphor in the degradation process. *Scientific Report*. 6(1), 24052. DOI: 10.1038/srep24052.
- Senoh, M., Mukai, T. and Nakamura, N. (1993). High-power InGaN/GaN double-heterostructure violet light emitting diodes. *Applied Physics Letter*, 62(19), P2390– 2392. DOI: 10.1063/1.109374.
- Sheng, L. and Xiaoping, L. (2011). LED packaging for lighting applications: Design, Manufacturing and Testing. *Singapore: John Wiley & Sons (Asia) Pte Ltd.* DOI:10.1002/9780470827857
- Simin, W., Xing, C., Mingling, C. and Huai, Z. (2014). Improvement in angular color uniformity of white light-emitting diodes using screen-printed multilayer phosphor-in-glass. *Applied Optics*, 53(36), pp. 8492-8498. DOI: 10.1364/AO.53.008492.
- Sun, C. C., Lee, T. X., Ma, S. H., Lee, Y. L. and Huang, S. M. (2006). Precise optical modeling for LED lighting verified by cross correlation in the midfield region. *Optics Letters*, 31(14), P2193–2195. DOI: 10.1364/OL.31.002193.

- Su, F. S., Yang, S. Y., Hung, T. H., Lee, C. C. and Chiang, K. N. (2012). Light degradation test and design of thermal performance for high-power light-emitting diodes. *Elsevier, Microelectronics Reliability*, 52(5), P794-803. DOI: 10.1016/j.microrel.2011.07.059.
- Smet, K. A. G. and Hansel Aer, P. (2015). Impact of cross-regional differences on color rendition evaluation of white light sources. *Optics Express*, 23(23), pp. 30216-30226. DOI: 10.1364/OE.23.030216.
- Schubert, E. F. and Kim, J. K. (2005). Solid-state light sources getting smart. *Science* 308(5726). P1274-1278. DOI: 10.1126/science.1108712.
- Schubert, E. F. (2006). *Light-emitting diodes*. Cambridge University Press. Rensselaer Polytechnic Institute, New York. DOI: 10.1017/CBO9780511790546.
- Simi, W., Xing, C., Mingling, C. and Hua, Z. (2014). Improvement in angular color uniformity of white light-emitting diodes using screen-printed multilayer phosphor-in-glass. *Applied Optics*, 53 (36), pp. 8492-8498. DOI: 10.1364/AO.53.008492.
- Trang, T. T., Le, P. X. and Anh, N. D. Q. (2019). Improving luminous flux and color homogeneity of dual-layer phosphor structure. *TELKOMNIKA Telecommunication Computing Electronics and Control*, 17(5), pp. 2643-2649. DOI: 10.12928/telkomnika.v17i5.11038.
- Thuc, M. B., Loan, N. T. P., Phan, X. L., Anh, N. D. Q. and Le, V. T. (2020). The application of (Y,Gd)BO₃:Tb³⁺ and CaGa₂S₄:Mn²⁺ phosphors to remote white light-emitting diodes. *TELKOMNIKA Telecommunication, Computing, Electronics and Control*, 18(1), pp. 351~357. DOI: 10.12928/TELKOMNIKA.v18i1.13713.
- Ton, T. P., Loan, N. T. P., Anh, N. D. Q. (2020). Enhanced Luminous Efficacy of White LED with Flat Dual-Layer Remote Phosphor Structure. *Applied physics*, 18(2), P107-114. DOI: 10.15598/aeer.v18i2.3441.

- Tran, T. T., Pham, X. L. and Anh, N. D. Q. (2019). Improving luminous flux and color homogeneity of dual-layer phosphor structure. *Telecommunication Computing Electronics and Control*, 17(5). P2643-2649. DOI: 10.12928/TELKOMNIKA.v17i5.11038.
- Tung, H. T. and Phuc, H. D. (2023). The impacts from SrS:Cu²⁺,Na and LaO_F:Eu³⁺ phosphors on color and luminous performances at 5600 K–8000 K WLEDs. *Indonesian Journal of Electrical Engineering and Computer Science*, 30(2), P714-720. DOI: 10.11591/injects.v30.i2.pp714-720
- Verselets, G., Sadgati, D., Meneghini, H., Bottazzi, F., Guano, M., Meneghesso, G. and Zanoni, E. (2013). Efficiency droop in InGaN/GaN blue light-emitting diodes: physical mechanisms and remedies. *Journal of Applied Physics*, 114(7), 071101. DOI: 10.1063/1.4816434.
- Wang, K., Luo, X. B., Liu, Z. Y., Zhou, B., Gan, Z. Y. and Liu, S. (2008). Optical analysis of an 80W light-emitting diode street lamp. *Optical Engineering*, 47(1), P 0130021-01300213. DOI: 10.1117/1.2835010.
- Wang, X., Rao, B., Zhang, W., Lei, Q., Da, Z., Hang, Q., Li, A. and Zhou, C. (2016). An Improved Electrophoretic Deposition Method for Wafer Level White PC-LED Array Packaging. *Journal of Display Technology*, 12(12), pp. 1609-1612. DOI: 10.1109/JDT.2016.2614260.
- Wang, L., Zhang, X., Hao, Z. and Luo, Y. (2010). Enriching red emission of Y₃Al₅O₁₂:Ce³⁺ by cooping Pr³⁺ and Cr³⁺ for improving color rendering of white LEDs. *Optics Express*, 18(24), pp.177-25182. DOI: 10.1364/OE.18.025177.
- Yannick, D., Raphael, B., Simon, J., Yves, O. and Laurent, B. (2015). Overview on Sustainability, Robustness, and Reliability of GaN Single-Chip LED Devices. *Transactions on Device and Materials Reliability, IEEE*, 15(4), P621-625. DOI: 10.1109/TDMR.2015.2488978
- Yang, G., Jian, J., Yu jiao, R., Yulin, G., Lihong, Z., Ziquan, G., Yue, L., Zhong,

- C. and Yijun, L. (2019). Two-dimensional temperature distribution measurement of light-emitting diodes by micro-hyperspectral imaging–based reflected light method. *Optics Express*, 27(6), pp. 7945-7954. DOI: 10.1364/OE.27.007945.
- Yang, L., ZhiCheng, L., Liu, S. and JiaoJiao, Y. (2013). Effects of melamine formaldehyde resin and CaCO₃ diffuser-loaded encapsulation on correlated color temperature uniformity of phosphor-converted LEDs. *Applied Optics*, 52(22), P5539-5544. DOI:10.1364/AO.52.005539.
- Yang, C. C., Changa, L. C., Huangb, C. K. and Liaob, T. S. (2011). The Yellow Ring Measurement for the Phosphor-converted White LED. *Elsevier, Physics Procedia 19*, P182-187. DOI: 10.1016/j.phpro.2011.06.146
- Ying, S. P and Chien, H. Y. (2015). Effects of Phosphor Concentration and Lead frame Reflectivity for Phosphor-converted LEDs. *Journal of Display Technology*, 11(12), P993-996, DOI: 10.1109/JDT.2015.2448715
- Ying, S. P., Fu, H. K., Hsin, H. H. and Yang, K. H. (2017). Color design model of high color rendering index white-light LED module. *Applied Optics*, 56(14), pp. 4045-4051. DOI: 10.1364/AO.56.004045.
- Yu, Y., Cao, C., Wu, Z., Zhijun, W., Qihui, W., Wenyan, L., Xue Kang, P., Jin, J., Zhang X., Yang, H. and Tong, Q. (2019). Improving the color-rendering index of a tandem warm white organic light-emitting device by employing a simple fabrication process. *Optics Letters*, 44(4), pp. 931-934. DOI: 10.1364/OL.44.000931.
- Zong, Y. L, Cheng, L., Bin, H. Y., Yao, H. W., Sheng, L. and Han, B. N. (2011). Effects of YAG: Ce phosphor particle size on optical performance of white LEDs. *IEEE, Conference Location: Shanghai, China*. DOI: 10.1109/ICEPT.2011.6067012
- Zang T, L., Wang, H. B., Yu, H. B., Ding, X. R. and Tang, Y. (2017). High-efficiency

LED COB device combined diced V-shaped pattern and remote phosphor. *Chinese Optics Letters*, 15(4), pp. 42301-42304. DOI: <https://opg.optica.org/col/abstract.cfm?URI=col-15-4-042301>.

- Zhang, W. L., Yang, W., Zhong, P., Mei, S. L., Zhang, G. L., Chen, G. L., He, G. X. and Guo, R. Q. (2017). Spectral optimization of color temperature tunable white LEDs based on perovskite quantum dots for ultrahigh color rendition. *Optical Materials Express*, 7(9), P3065-3076. DOI: 10.1364/OME.7.003065.
- Zhao, Z., Zhang, H., Liu, S. and Wangen, X. (2018). Effective freeform TIR lens designed for LEDs with high angular color uniformity. *Applied Optics*, 57(15), pp. 4216-4221. DOI: 10.1364/AO.57.004216.
- Zhong, P., He, G. and Zhang, M. (2012). Spectral optimization of the color temperature tunable white light-emitting diode (LED) cluster consisting of direct-emission blue and red LEDs and a phosphor conversion LED. *Optics Express*, 20(55), A684-A693. DOI: 10.1364/OE.20.00A684

APPENDIX. SIMULATION PROGRESS

This section will give an overview of the process of simulation, data collection and data processing. The software used to determine the optimal size and concentration is the latest version of LightTools (version 9.0) and specialized software for simulating lens systems and LED chips.

Step 1: Single chip LED configuration built on LightTools 9.0 software. (Figure A1)

Step 2: Enter the input parameters. Note that, there are main tags: Ray trace, illumination manager, and user materials (Figure A2).

Step 3: Enter the number of light rays to calculate, and the illumination manager card gives us simulated results such as luminous flux, CRI, and CQS (Figure A3).

Step 4: double clicks on the components that need to see the results, such as CCT and spectral distribution as shown in Figures A4

Step 5: User materials card, concentrations for three types of particles in the mixture, including Y-P, G-P and SiO₂ (Figure A5 and Figure A6)

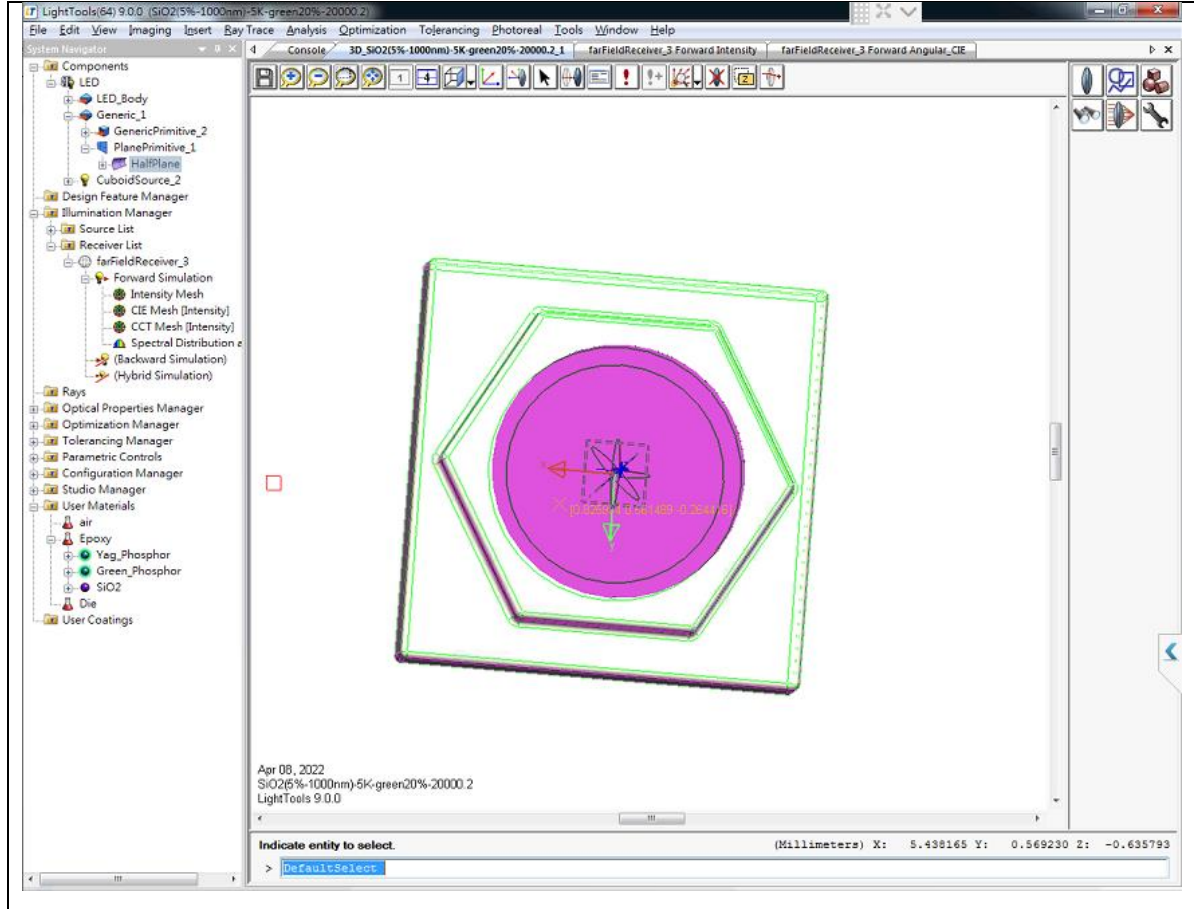


Figure A1: Single chip LED configuration built on LightTools 9.0 software.

Step 6: Put the concentration for the particles as shown in Figures A5 and Figure A6

Step 7: Check the running simulation A7

Step 8: Result luminous flux, color rendering index, color temperature, and spectrum as show in (Figure A8 to Figure A11)

Step 9: Get the data and then give it to Excel software to process and draw the chart as Figure A12.

Step 10: get the data and then give it to Excel software to process and draw the chart as Figure A12.

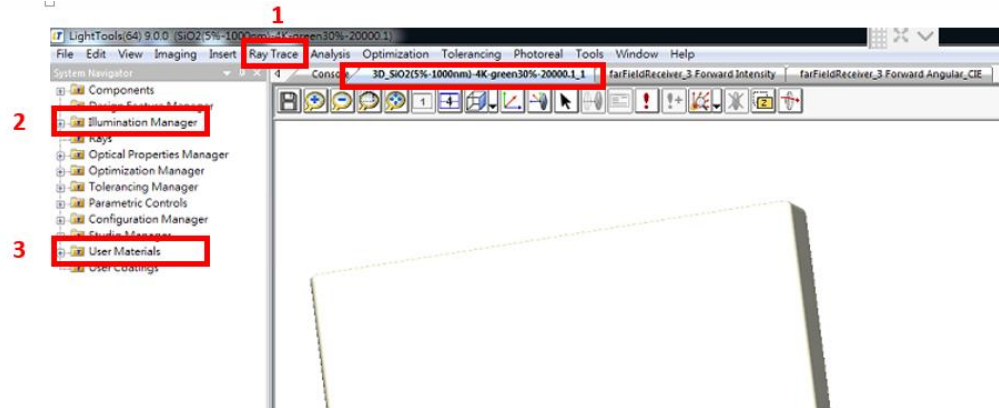


Figure A2: Tabs of interest to enter and retrieve data.

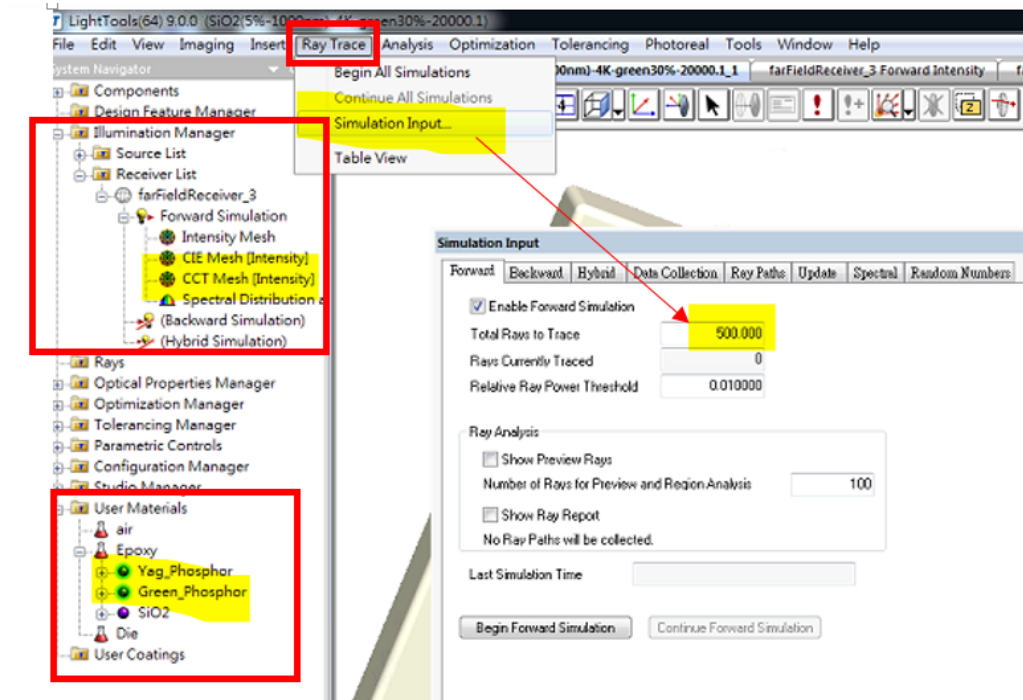


Figure A3: Uses of each tabs

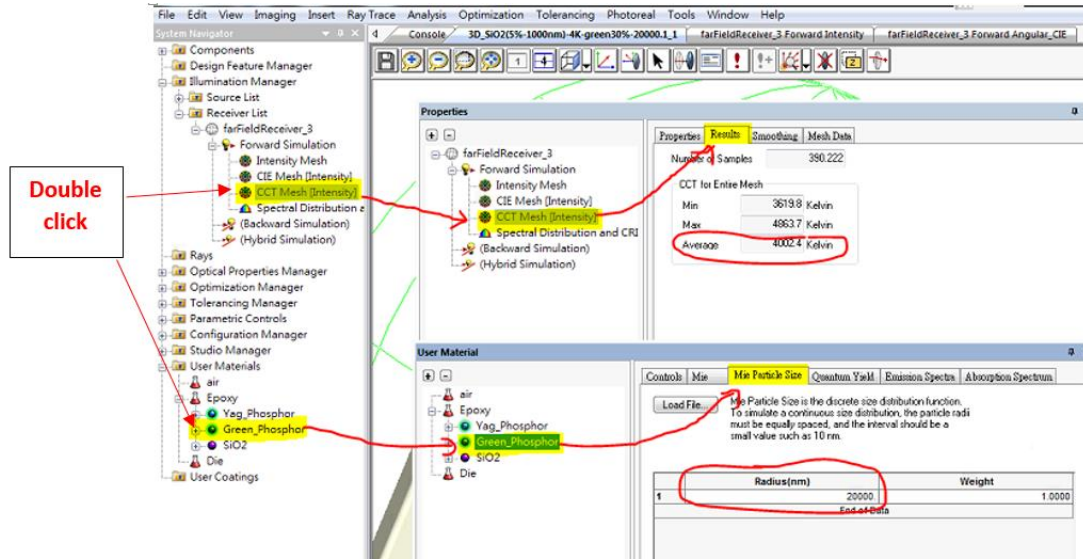


Figure A4: Properties and User material tabs

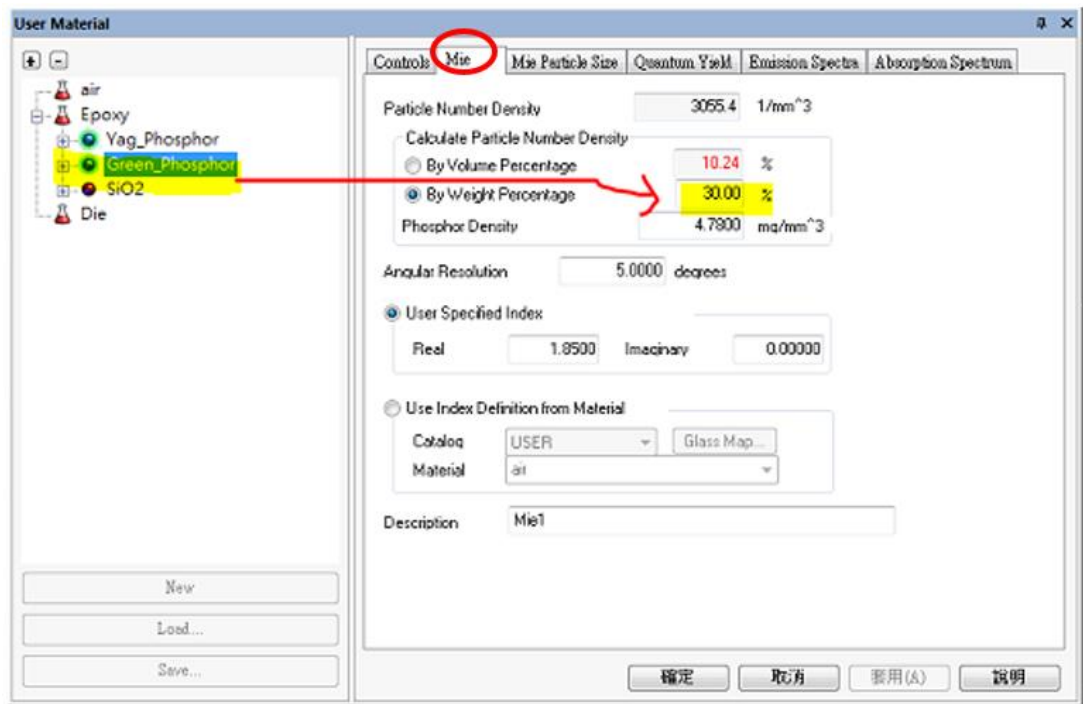


Figure A5: Enter the G-P concentration.

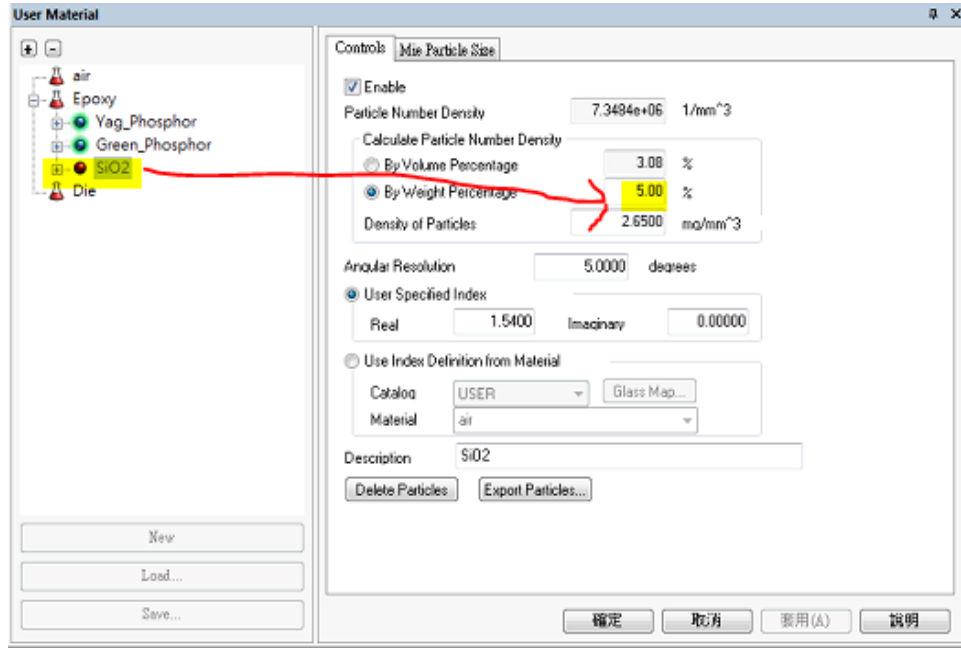


Figure A6: Enter the SiO₂ concentration

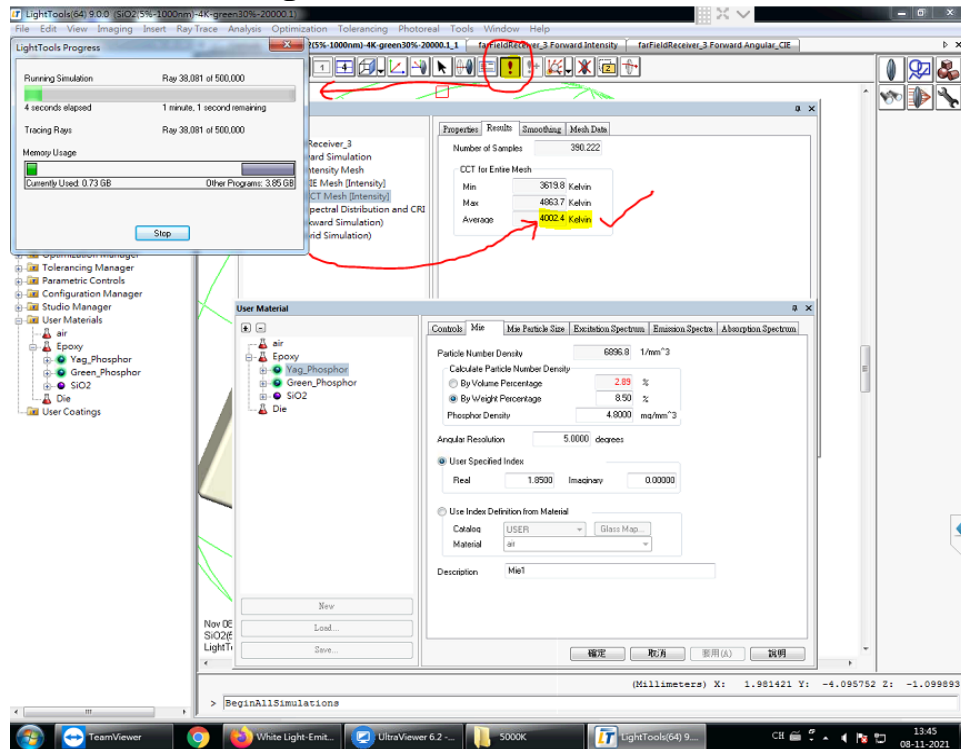


Figure A7: Run simulation

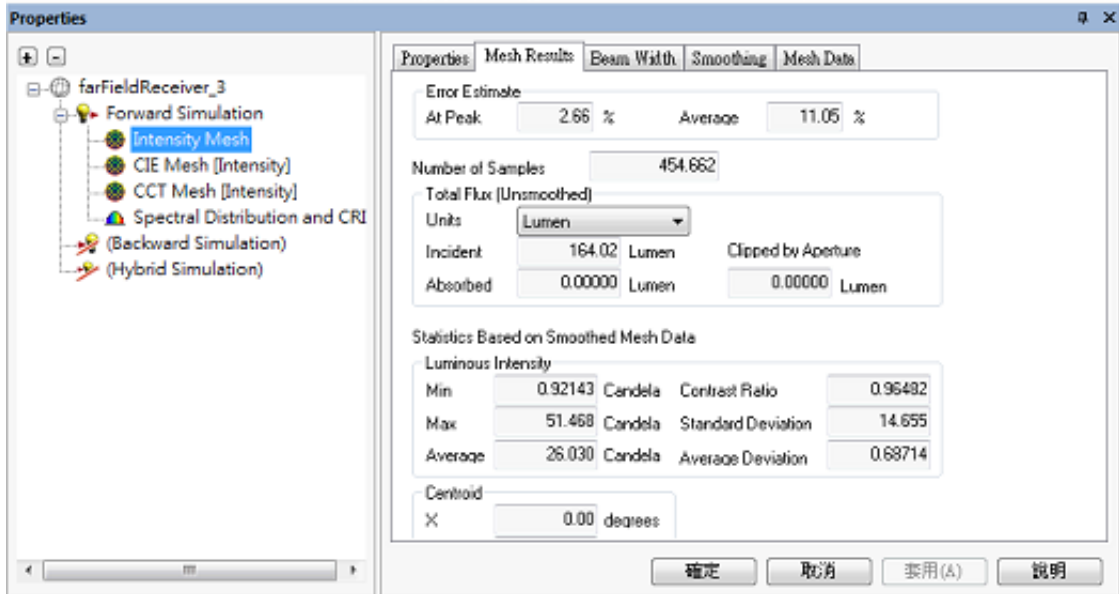


Figure A8: The result of luminous flux

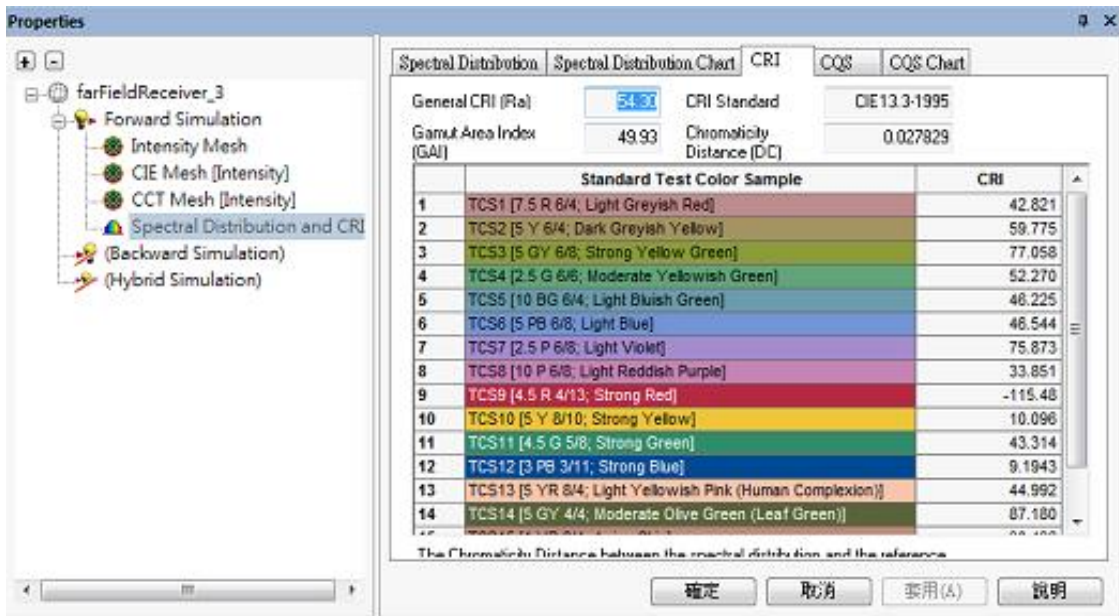


Figure A9: The result of CRI

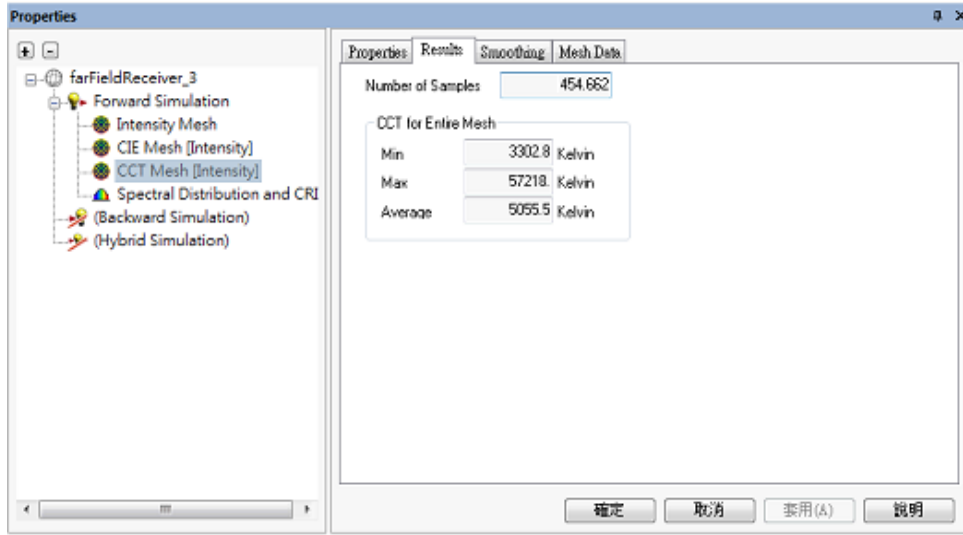


Figure A10: The result of CCT

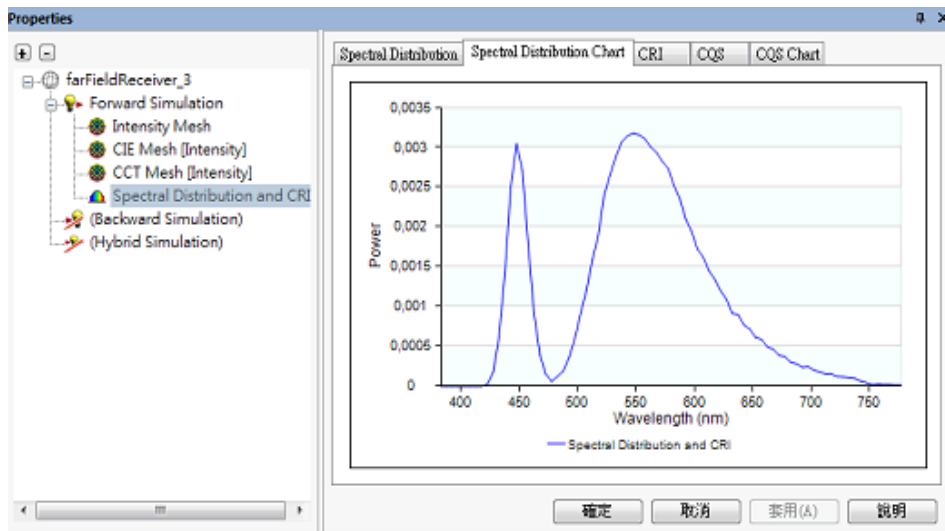


Figure A11: The result of spectrum

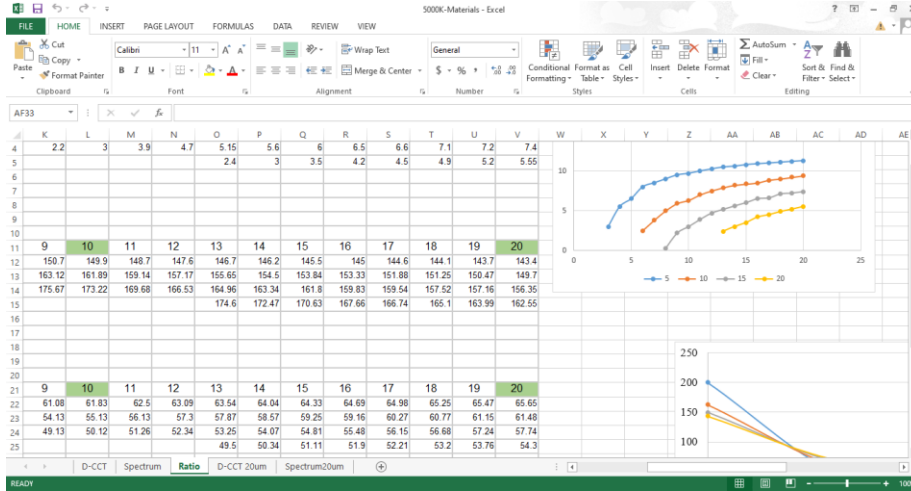


Figure A12: Data processing and charting